GEOLOGY AND GEOCHEMISTRY OF EARLY PROTEROZOIC GRANITOIDS FROM THE NORTHERN WET MOUNTAINS-SOUTHERN FRONT RANGE, SOUTH-CENTRAL COLORADO

by
R. Bruce Hallett

Submitted in Partial Fulfillment of the
Requirements for the Degree of
Master of Science in Geochemistry

New Mexico Institute of Mining and Technology
Socorro, New Mexico, USA
September, 1990

"One thing I have learned in a long life: that all our science, measured against reality is primitive and childlike--and yet is the most precious thing we have."

A. Einstein

Abstract

The Garrel Peak (1663 Ma), Phantom Canyon (1665 Ma), Twin Mountain (1706 Ma), and Crampton Mountain (1705 Ma), plutons intrude early Proterozoic amphibolite-grade supracrustal rocks in the Wet Mountains area near Canon City, Colorado. Contact zones are complex and range from 0.5 to 2.0 km wide. The Garrel Peak pluton is discordant and contains numerous large xenoliths of country rock along the southern margin. The other plutons have gradational contacts which include syn- to late syntectonic granitic sills and dikes, migmatites, and large K-feldspar porphyroblasts.

Granitization is locally important in country rocks adjacent to these pluton contacts. Three plutons appear to be compositionally zoned, becoming more felsic and porphyritic toward their centers. The exception is the Phantom Canyon pluton which becomes less felsic toward its center.

The plutons of the Wet Mountain area range from granodiorite to granite in composition and from peraluminous to slightly metaluminous. Ta-Nb depletion on chondrite normalized plots and light rare earth element-enriched patterns with variable negative Eu anomalies suggest geochemical characteristics similar to I-type granitoids. On Nb-Y, Ta-Yb, and related trace-element plots, the granitoids exhibit arc to within-plate characteristics.

High field strength element and rare earth element contents are greater and Eu anomalies are larger in the two younger plutons (Garrel Peak and Phantom Canyon).

Geochemical data require a two-stage model to explain the origin of the granitoid magmas. Initially, granodiorite magmas are produced by partial melting of a felsic granulite source, probably at low to mid-crustal depths. During the second stage, assimilation-fractional crystallization of these magmas produces more evolved compositions with the two younger plutons showing more fractionated geochemical trends than the two older ones.

Acknowledgments

Many individuals have contributed both directly and indirectly to the completion of this thesis. I extend a warm thanks to my advisor Dr. Kent C. Condie for his assistance in the field and knowledge in the classroom. A special thanks also goes to my two other committee members Drs. Philip R. Kyle and Antonius J. Budding.

Many hours of friendly discussion with M. Wilks, M. Boryta and M. Knoper have greatly contributed to my understanding of geochemistry and Precambrian geology. I thank J. and M. Boryta for their editorial skills in a version of this thesis. I appreciate the comradery of K. Panter and D. Caldwell and a special friend N. Langford, for "friendship is the wine of life" (Young).

This thesis is dedicated to my parents Martha and Robert who through my childhood and young adult years have provided financial and a great deal of moral support. I reserve a special thanks for my wife, Caroline, who takes the time to concern herself with my work.

Financial support for this project, in terms of research and teaching assistantships, were provided by New Mexico Tech. I thank the Graduate Student Association for providing field assistance in the summer of 1989. Partial presentation of this thesis at the Rocky Mountain Section of the Geological Society of America meeting in May of this year was made possible by generous and much appreciated financial contributions from the Antonius and Anita Budding

Graduate Research Fund and the Geological Society of America.

Contents

List of Figures

List of Tables

Introduction

This study examines the geology and geochemistry of four granitoid plutons located mainly in the northern Wet Mountains along the Arkansas River near Canon City, Colorado (Fig. 1). The Wet Mountains are a northwest-southeast-trending range, 80 km long and 25-30 km wide in south-central Colorado. One pluton, northeast of Canon City, is located in the southern Front Range. Rocks in the area of study range in age from Early Proterozoic to Quaternary and consist of sedimentary, metamorphic and igneous types.

Purpose of the Study

Since the Wet Mountains area was mapped by the USGS in the late 1970's and 1980's, an increasing number of U-Pb isotopic dates and other geological and geochemical data pertaining to Precambrian crustal evolution have become available. A majority of the data have been interpretated to represent a period of major crustal growth during the Early Proterozoic (1790-1660 Ma) by successive island arc accretions and/or arc magmatism (Condie, 1982; Reed et al., 1987; Bickford et al., 1989). This study contributes to an understanding of Proterozoic geology and geochemistry in south-central Colorado. Major geological and geochemical inconsistencies observed across this area may suggest different source regions, which in turn may imply more than one accreted terrain for the area. Now that sufficient

geologic mapping and isotopic dating are complete, the process of unraveling the crustal evolution for this area of Colorado is possible.

The objectives of this study are to gather and present lithologic, petrographic, and geochemical data for each pluton and to compare and contrast data within and between plutons. A tectonic interpretation and petrogenetic model is made from these findings. Finally, the Wet Mountains area is placed in an Early Proterozoic regional plate tectonic framework.

Ages of the Plutons

The Precambrian plutons of the Wet Mountains and southern Front Range are part of the Routt Plutonic Suite (Tweto, 1987), a group of plutonic bodies in Colorado dated at about 1700 Ma. These bodies are related in character, habit, structure, and tectonic setting. In general, the Routt Suite is synorogenic, foliated and concordant and predominantly granodiorite and quartz monzonite, although compositions range from granite to gabbro. Inclusions of early differentiates and various wall rocks are common and if the bodies are porphyritic, K-feldspars form tabular megacrysts (Tweto, 1987).

Recently, Bickford et al. (1989a; 1989b) dated Early Proterozoic plutons in central Colorado by the U-Pb zircon method. Ages obtained on the four Early Proterozoic plutons of this study indicate two periods of synchronous

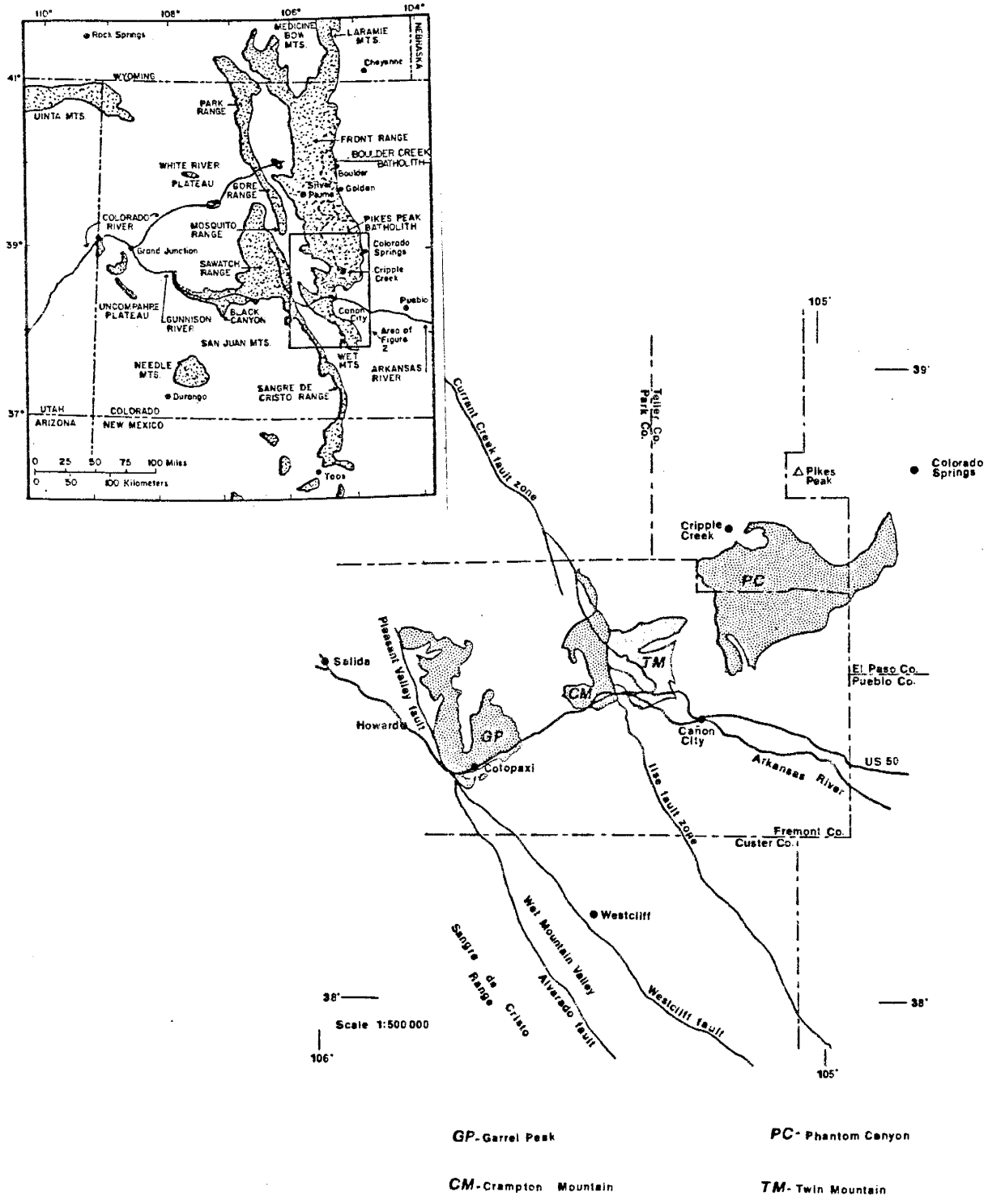

Figure 1. Generalized geologic map of study area. 1a shows exposed Precambrian rocks of the Southern Rocky Mountain region (after Cullers, 1986). 1b shows the locations of plutons included in this study.

crystallization. The Crampton Mountain and Twin Mountain plutons are dated at 1705 +/- 8 Ma and 1706 +/- 5 Ma respectively, whereas the Garrel Peak (1663 +/- 4 Ma) and Phantom Canyon (1665 +/- 5 Ma) plutons are about 40 Ma younger (Bickford et al., 1989).

Detailed metamorphic studies on the intruded country rocks are lacking; however, it is generally accepted that at least one period of metamorphism preceded granitoid intrusion (Bickford et al., 1989; Bickford, 1988; Noblett et al., 1987; Reed et al., 1987). The relative timing between metamorphism and intrusion is based on field relationships because no isotopic dates exist for surrounding metamorphosed country rocks. However, a minimum age of metamorphism can be constrained by the crystallization age of the Twin Mountain pluton (1705 Ma). Contact relationships, such as patterns of foliation within plutons and in juxtaposing wall rocks, suggest a syn-tectonic to late syn-tectonic emplacement, consistent with previous interpretations (Bickford, 1986; Noblett et al., 1987). Further west, in the volcano-plutonic terrane of the Gunnison and Salida areas, a similar deformational event between 1730 and 1710 Ma has been constrained by U-Pb dates (Bickford et al., 1989) and this event may be synchronous with the metamorphic event in the Wet Mountains area. Some workers (Bickford et al., 1989b; Condie and Knoper, 1986) suggest the Gunnison-Salida terrane, which lies about 100 km to the west of the Wet Mountains, represents an arc that

accreted at about 1770-1760 Ma and eventually evolved into a back-arc basin.

Previous Studies

Prior to the early 1890's, the Wet Mountains held little geologic interest. When gold was discovered in Late Proterozoic granites near Cripple Creek (Fig. 1), the Cripple Creek Mining District became the richest gold deposit in the U.S. during the late 1800's and early 1900's (Smith, 1977). Since the 1940's, mineralization in the Proterozoic granites has yielded Au, Ag, Cu, Pb and Zn in economic quantities.

Mapping of the Wet Mountains by the USGS had begun by the late 1800's. Additional detailed mapping during the 1950's and 1960's (Brock and Singewald, 1968; Christman and others, 1959) was conducted primarily for Th exploration and resulted in the distinction of 27 separate Proterozoic lithologic units, most of which are metamorphic rocks. In the past 15 years, all four plutons have been remapped by the USGS (Epis and others, 1979; Scott, 1977; Taylor and others, 1975a, 1975b and 1975c; Wobus and others, 1976, 1979, 1985a and 1985b).

Methods

Field work was initiated in the summer of 1988 with the collection of a representative suite of samples from each pluton. Observations were made on pluton/country rock contacts. Additional field work was conducted in the summer of 1989 for six weeks. In the fall and spring of 1988-1989 and summer and fall of 1989, 38 of the 55 collected samples were analyzed for 36 major and trace elements. Samples were irradiated at Sandia National Laboratory in Albuquerque, New Mexico, and trace element abundances were obtained by neutron activation analysis (NAA), using TEABAGS and the ND-6600 system at New Mexico Tech. Major and other trace elements were obtained by X-ray fluorescence (XRF), using a Rigaku XRF spectrometer at New Mexico Tech. Ten thin sections were made for petrographic analysis. Complete descriptions of sample preparation and analytical techniques are found in Appendices A and B.

General Geology

Similar to other mountain ranges in the Southern Rocky Mountain province, the present topographic expression and stratigraphic configuration of the Wet Mountains are the result of several major orogenic and erosional episodes dating back to at least Pennsylvanian time (Tweto, 1975). Most recently in the Wet Mountains, Neogene tectonism reactivated several subparallel fault systems (e.g. Ilse, Alvarado and Currant Creek faults, see Fig. 1 for locations) resulting in uplift of crustal blocks, which today form the fault-bounded, south-plunging anticlinorium of the Wet Mountains (Tweto, 1975).

The most spectacular fault system in the study area is the Ilse fault, a northwest-southeast-trending 600-m-wide fault zone (Fig. 1b). A thorough structural study of the Precambrian metamorphic rocks (Harper, 1976) shows two periods of Phanerozoic movement on this fault. The earliest was right-lateral, strike-slip displacement of about 16 km and most recently dip-slip movement of 120-180 m. Movement along other less continuous subparallel faults at similar times has also been documented (Scott et al., 1978). Although pre-Phanerozoic ancestry for faults in the Wet Mountains is difficult to prove, Proterozoic movement has been suggested for the Pleasant Valley, Alvarado and Westcliff faults to explain the rapid change in metamorphic grade from lower amphibolite facies near Salida to upper

amphibolite facies near Cotopaxi (Noblett et al., 1987).

Early Proterozoic rocks in the Wet Mountains consist of granitoids and supracrustal rocks of various compositions metamorphosed at low to high amphibolite facies (see Fig. 2 for detailed geologic map). The oldest metamorphic rocks were subjected to at least one period of deformation prior to emplacement of the four granitic plutons. Tweto (1987) reports a second period of metamorphism and deformation that accompanied intrusion of the Routt Suite throughout Colorado that peaked at about 1740 Ma. However, this metamorphic period is not everywhere synchronous. In the Wet Mountains, it appears that if there was a second period of deformation and metamorphism, it probably accompanied pluton emplacement at about 1705 Ma. Field evidence is inconclusive and timing relationships are somewhat ambiguous because no isotopic dates exist on the metamorphic rocks; a thorough regional field and geochronologic study of these rocks is required to accurately address the timing of deformation and metamorphism.

The metamorphosed country rocks consist mostly of mica schists, quartzo-feldspathic augen gneisses and both ortho- and paragneisses, all at amphibolite grade. Granulite-facies rocks are restricted to a smaller area in the central Wet Mountains south of the Royal Gorge area (Brock and Singewald, 1968; Lanzirotti, 1988). Rocks of similar composition but lower metamorphic facies (upper greenschist to lower amphibolite facies) are exposed in west-central

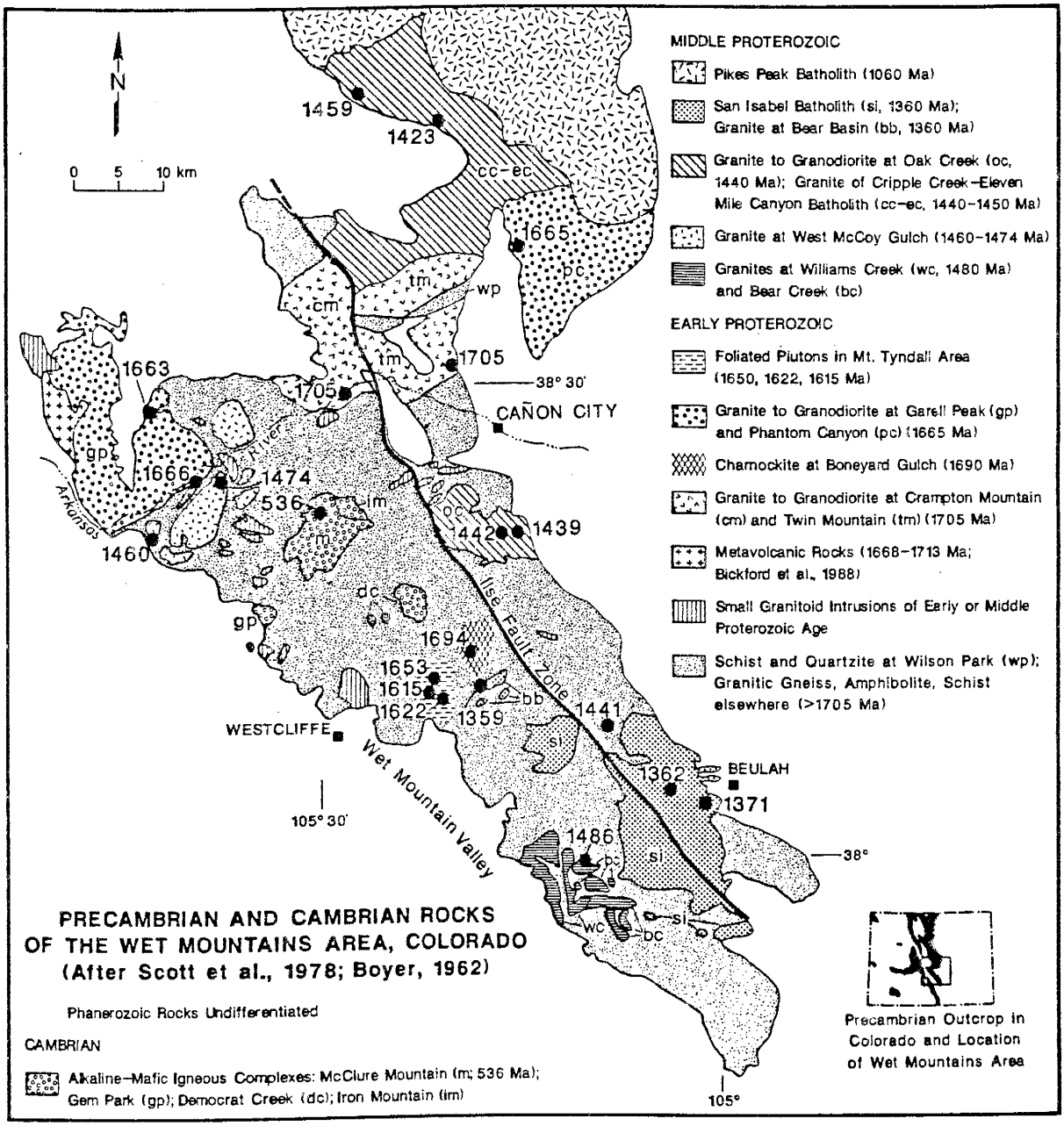

Figure 2. Geologic map of the Wet Mountains and southern Front Range, Colorado, with U-Pb zircon dates from Proterozoic and Cambrian rocks (after Boyer, 1962, Scott et al., 1978 and Bickford et al., 1989a).

Colorado near Gunnison and retain primary textures (Knoper and Condie, 1988; Knoper, 1990a). With the exception of metasedimentary and metavolcanic rocks near Howard and a small quartzite-schist unit (Blue Ridge quartzite-schist), metamorphic rocks in the northern Wet Mountains and southern Front Range lack original textures. Some investigators believe the rapid change from greenschist to amphibolite facies accompanied by the lack of primary textures may indicate that the Wet Mountains represent a deeper portion of the continental crust (Bickford et al., 1989a; Noblett et al., 1987).

Field Relations of the Plutons

General Characteristics

The four Early Proterozoic granitoids of the northern Wet Mountains and southern Front Range are surrounded by an older sequence of metavolcanic and metasedimentary gneisses. These rocks are feldspar and hornblende-bearing calc-silicate and sillimanite-garnet gneisses; most are fine-grained and generally well-foliated. When present, sillimanite coexisting with microcline indicates regional metamorphism to the upper amphibolite facies (Taylor and others, 1975a). Although muscovite is present in minor amounts, it commonly breaks down to form K-feldspar + quartz + sillimanite thus indicating muscovite is an unstable mineral phase at the observed metamorphic grade. Gneissic protoliths may be rhyodacites, intermediate flows and tuffs and mixed volcaniclastic-clastic sedimentary layers (Taylor and others, 1975a). Primary sedimentary or volcanic structures in this gneissic sequence have not been preserved.

The Blue Ridge quartzite-schist, a distinct lithostratigraphic unit, crops out in several locations in the Wilson Park area (Fig. 2). Volumetrically, this unit is insignificant; however, its presence has important paleoenvironmental and tectonic implications. The occurrence of abundant relict crossbeds and less abundant oscillation ripple marks in the quartzite favor deposition

in a shallow-water environment (Reuss, 1974). The dominant schists are muscovite-biotite schists with smaller amounts of schists containing garnet, sillimanite, andalusite, staurolite, cordierite and actinolite (Reuss, 1974). Exposed contacts in the Twin Mountain and Phantom Canyon plutons suggests the granitoids are intrusive into the quartzite-schist sequence (Cullers and Wobus, 1986; R.B. Chase, personal comm., 1989). Field descriptions and chemical analyses of the Blue Ridge sequence and the metavolcanic and metasedimentary rocks are found in Cullers and Wobus (1987), Noblett et al. (1987) and Lanzirotti (1988).

Early Proterozoic plutons of the southern Front Range and northern Wet Mountains are dominated by granodioritic to granitic compositions. Figure 3 shows CIPW normative mineral classification diagrams of each sample analyzed. The Garrel Peak pluton (Fig. 3a) is the most homogeneous whereas the others display a compositional range from granite to trondhjemite. Both Crampton Mountain and Twin Mountain plutons show compositional zonation with the least differentiated phases (granodiorite in Fig. 3b and granodiorite-quartz monzonite for Fig. 3c) occurring near pluton margins. The Phantom Canyon pluton (Fig. 3d) also is zoned and the most differentiated rocks (granite) form an outer augen gneiss, whereas the interior is quartz monzonite.

Near contacts, the plutons generally become finer

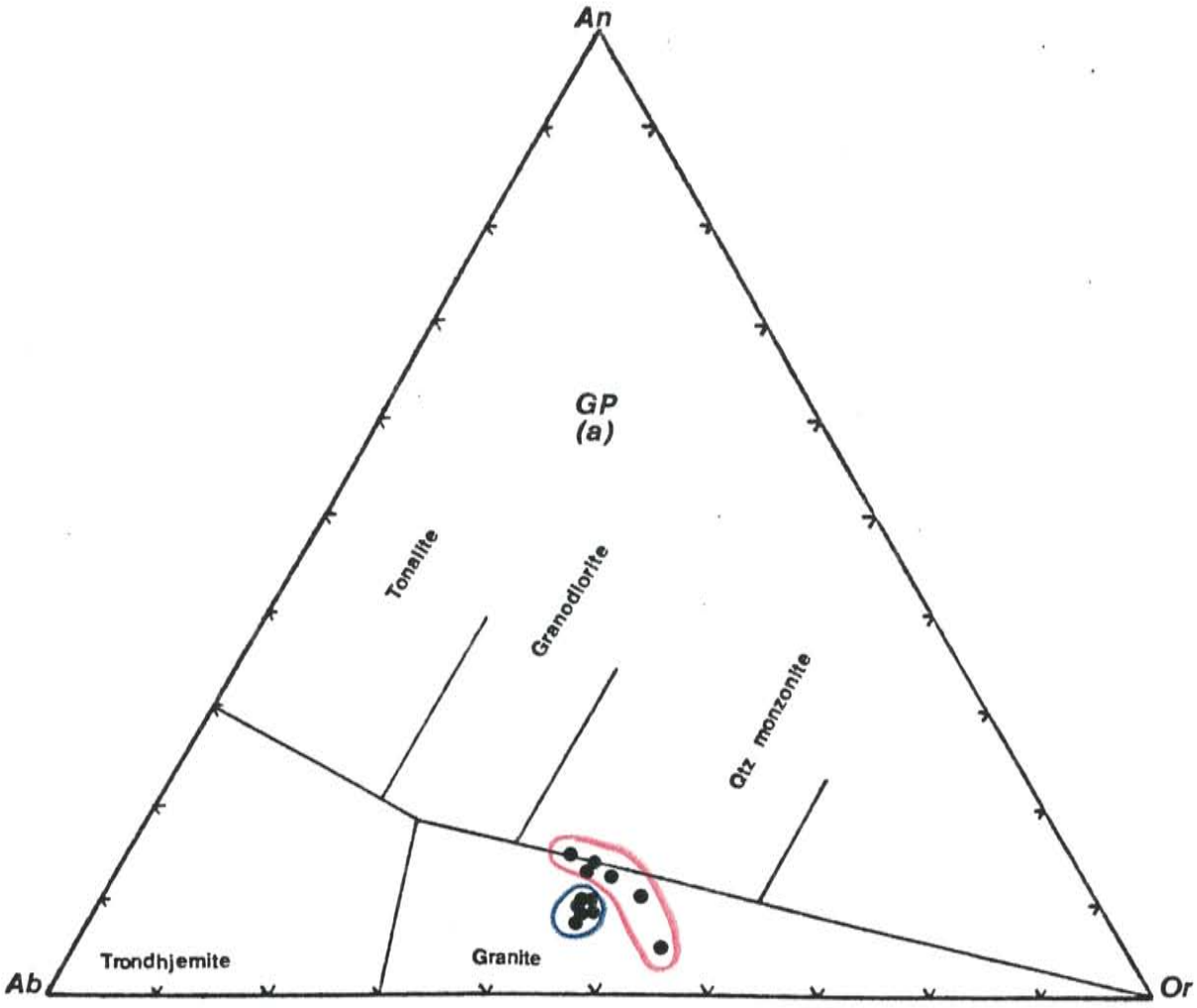

Figure 3a. An-Ab-Or, CIPW normative mineral classification (after Barker, 1979); GP--Garrel Peak pluton. Red —— indicates samples collected within 3 km of the contact, whereas blue —— indicates samples > 3 km from the contact.

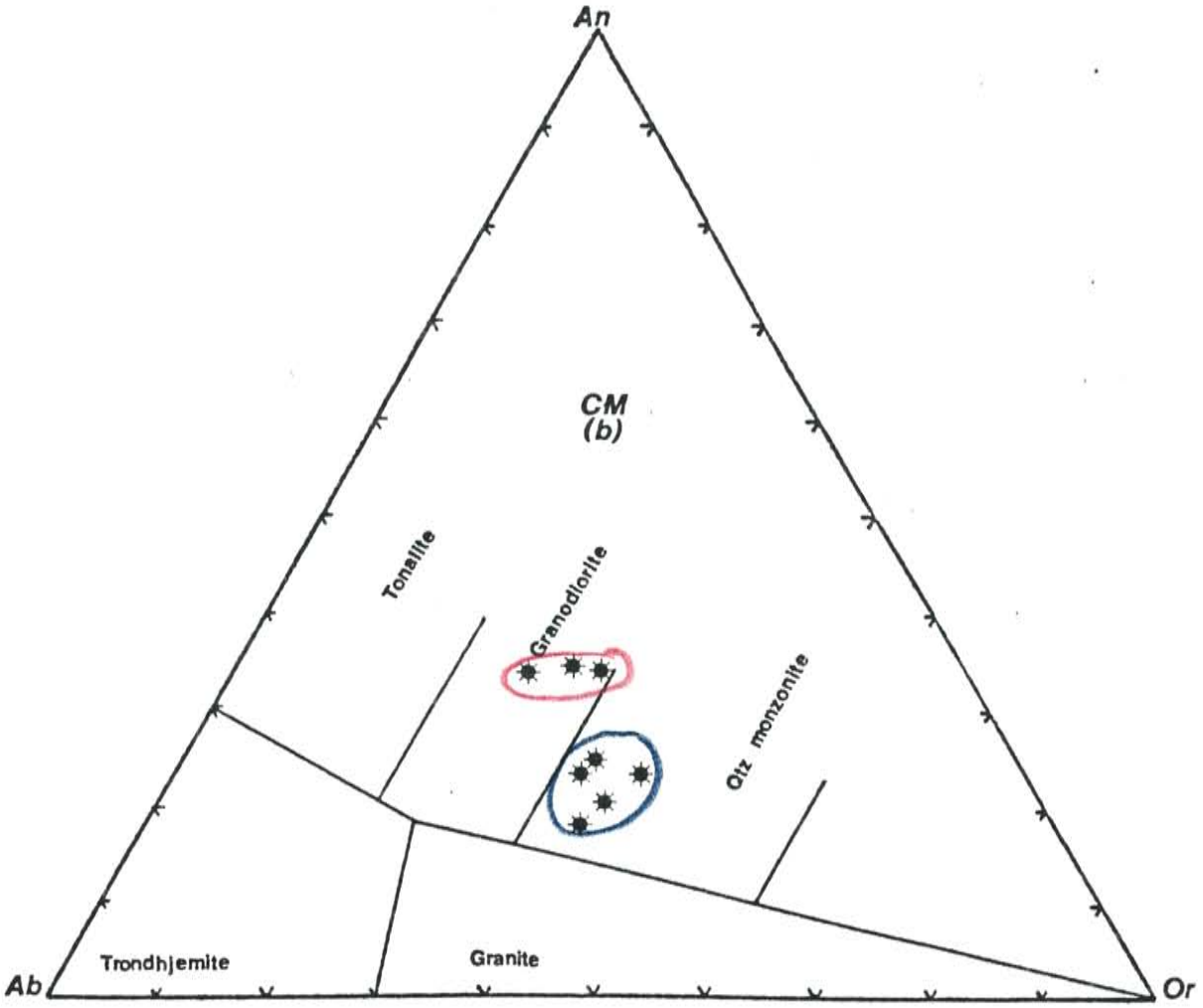

Figure 3b. An-Ab-Or, CIPW normative mineral classification (after Barker, 1979); CM--Crampton Mountain pluton. Red ▬ indicates samples collected within 3 km of the contact, whereas blue ▬ indicates samples > 3 km from the contact.

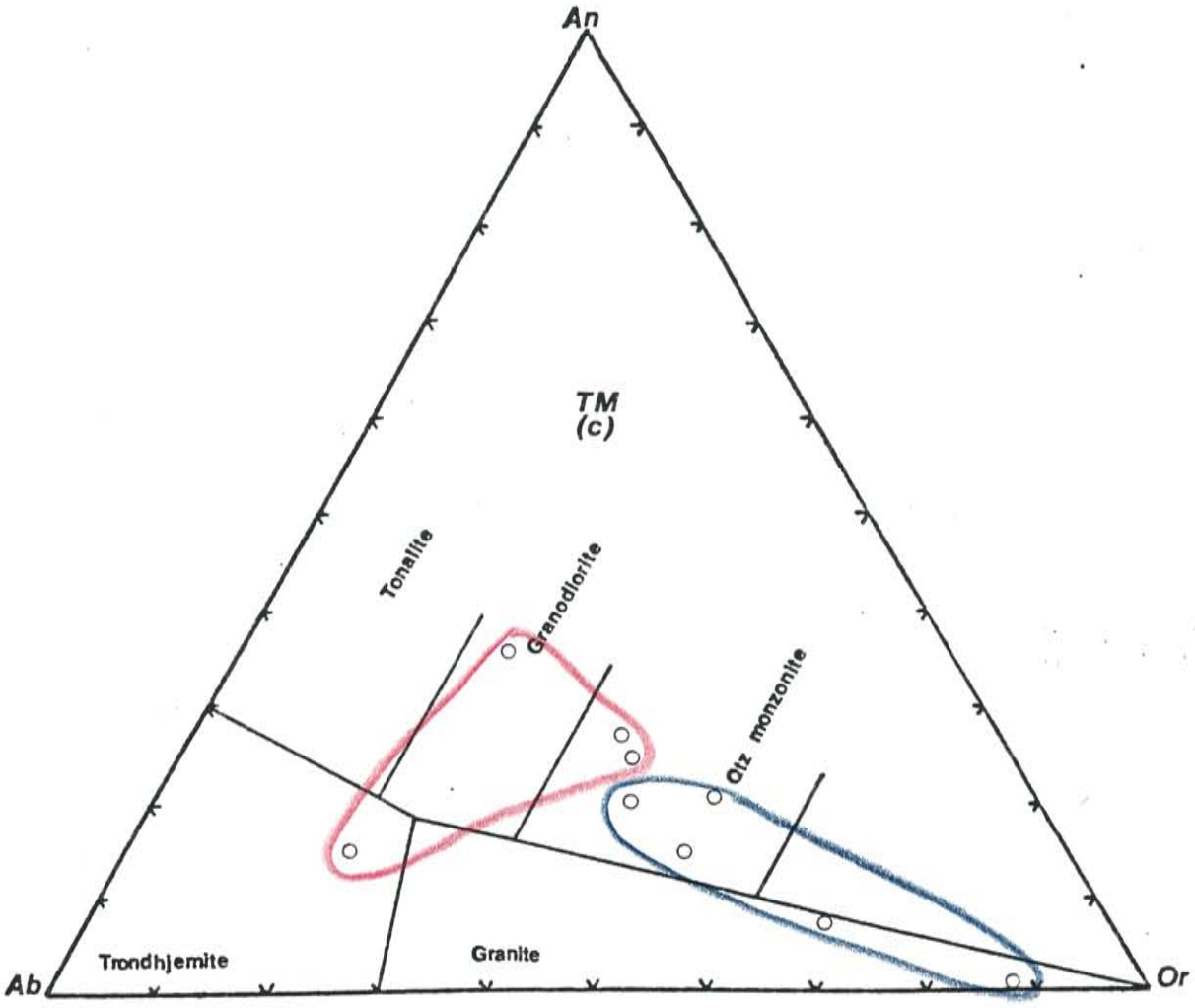

Figure 3c. An-Ab-Or, CIPW normative mineral classification (after Barker, 1979); TM--Twin Mountain pluton. Red —— indicates samples collected within 3 km of the contact, whereas blue —— indicates samples > 3 km from the contact.

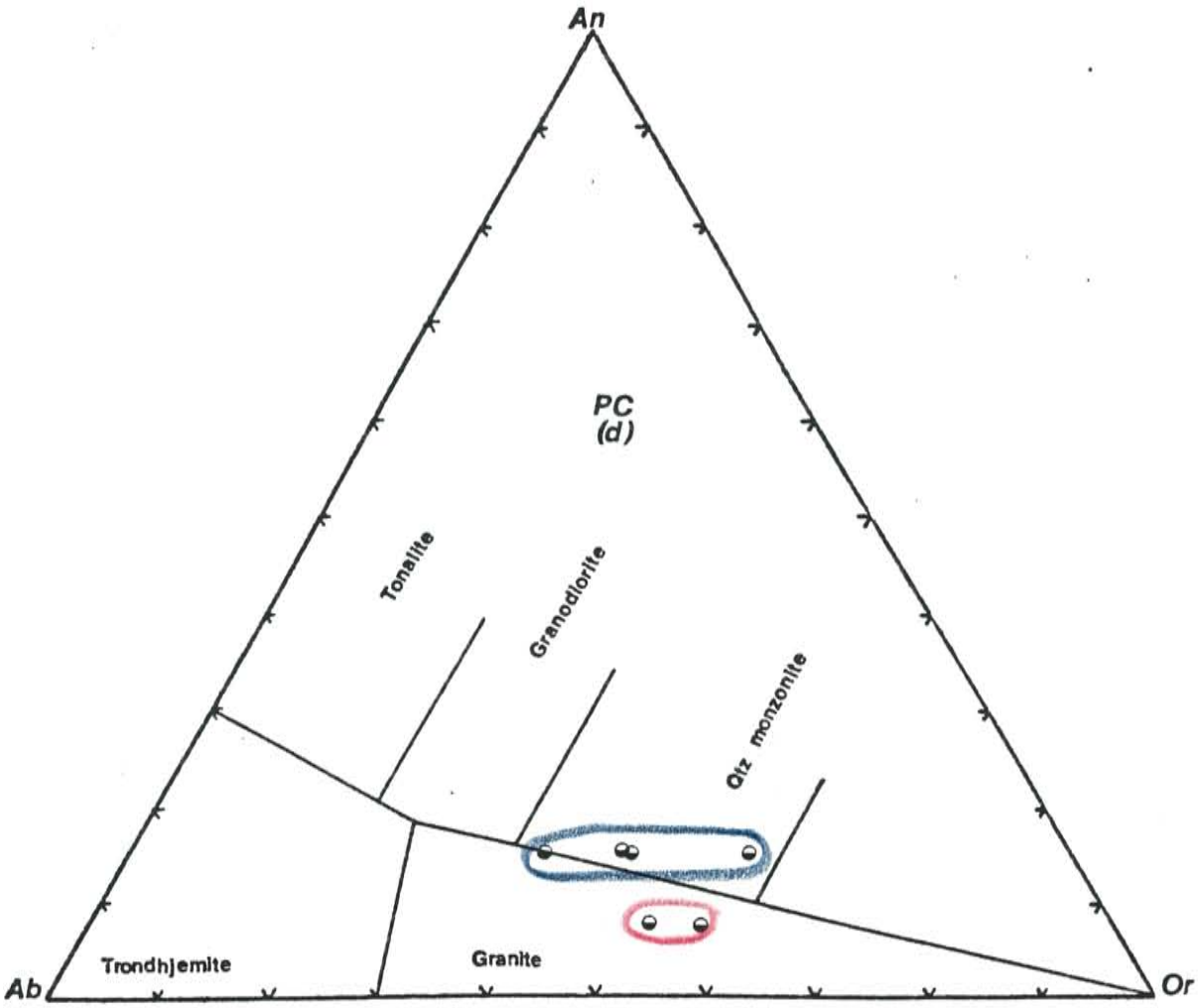

Figure 3d. An-Ab-Or, CIPW normative mineral classification (after Barker, 1979); PC--Phantom Canyon pluton. Red —— indicates samples collected within 3 km of the contact, whereas blue —— indicates samples > 3 km from the contact.

grained with foliated biotite and hornblende (when present) parallel to subparallel with country-rock foliation; also K-feldspar phenocrysts are smaller and subhedral. Figure 4 shows this finer grained texture in the Crampton Mountain pluton (sample is 1 km from mapped contact). In their interiors, all four plutons become coarse grained, some with tabular megacrysts 3.5 cm in length (e.g. Twin Mountain and Phantom Canyon plutons). Minor amounts of two-mica granite are present in the Garrel Peak, Twin Mountain, and Phantom Canyon plutons. Twin Mountain two-mica granite is a strikingly fine-grained, well-foliated leucogranite, whereas examples in the Garrel Peak pluton are medium-grained and unfoliated.

Detailed Contact Relations

Several similarities exist among the contact zones of each pluton (Table 1).

Table 1. Contact similarities among the plutons.

1) contact zone at least 0.75 km wide
2) injected granitic sills
3) deformed granitic dikes
4) migmatization
5) granitization
6) xenoliths

In the above list numbers 2-5 are generally restricted to the exterior portion of the contact while 6 (xenoliths) systematically decreases toward the interior of the pluton.

Figure 4. Characteristic border zone rocks in the Crampton Mountain pluton; foliated, medium-grained texture. Similar textures occur in border zones of the other plutons. Locally, the Crampton Mountain pluton shows rapakivi texture, although not easily seen in this photograph. Small xenoliths of country rock can be seen in the lower left of photograph. Photograph is taken near sample 1 in the Crampton Mountain pluton. See Fig. 11 for specific location.

Figure 5. Augen gneissic, two-mica granite from the outer edge of the Phantom Canyon pluton. Border zones are typically finer grained than interiors for all four plutons but only the Phantom Canyon pluton has an augen gneissic texture.

Figure 6. Layered appearance typical of pluton contact zones caused by injection of granitic sills subparallel to country rock foliation. Photograph of the Garrel Peak pluton near Texas Creek.

Each is at least 0.75 km wide and is characterized by alternating layers of granitic sills and metamorphic rocks. These sills were injected subparallel to foliation (possibly along original bedding) in the country rocks and have variable widths, as seen in Figure 6. Thin stringers of anatectic melt are common and often extend for greater than 5 or 10 m. In areas where structural deformation is evident, boudined anatectic dikes are prevalent. Migmatization is associated with all four plutons, although less frequently with the Phantom Canyon pluton. Granitization (Hyndman, 1985), a process by which fluids from the pluton, rich in K, Na and Si, metasomatize surrounding country rock, often makes metasediments adjacent to the pluton appear as fine-grained granitoids; a notable example is along the margins of the Phantom Canyon pluton. Xenoliths are common in both the inner contact zone and interior of this pluton with sizes varying from several centimeters to about half a meter. The xenoliths are typically foliated parallel to foliation in the surrounding rocks. However, inside the pluton they are often unfoliated and augen-shaped as shown in figure 7. Size and abundance of xenoliths decrease with increasing distance inward from the contact zone.

Pre-, syn-, and post-tectonic are used to label the relationship that exists between pluton emplacement of an and deformation. In the past this was based principally on field observations, for example, juxtaposing foliations and the orientation of kinematic porphyroblasts present in the

Figure 7. Xenolith of foliated gneiss within the Garrel Peak pluton. Such xenoliths are common both in contact zones and pluton interiors. The degree of foliation diminishes in xenoliths and eventually disappears inward from the pluton contact.

contact zone. More recent studies investigate, a) magmatic vs. tectonic foliations within the pluton; b) correlation of foliations in granitoids to those in the surrounding wall rocks; c) cleavage-porphyroblast relations in the wall rock; and d) U\Pb isotopic ages of plutons and surrounding metamorphic rocks (Blumenfeld and Bouchez, 1988; Paterson et al., 1989; Paterson and Tobisch, 1989). One concern with this study is to determine whether pluton emplacement is syn- or post-tectonic. However, this may depend more on its level of emplacement than on its time of emplacement relative to a regional tectonic event (Hamilton, 1981). No one contact is representative of an entire pluton in the Wet Mountains and therefore characteristic observations are compilations from several traverses, unless otherwise noted. For the purposes of this study, contacts are arbitrarily defined when country rocks contain less than 40% of the injected pluton.

Garrel Peak Pluton

The Garrel Peak pluton is located north of Cotopaxi, Colorado, along the Arkansas River (Fig. 8). The pluton intrudes two units of metamorphosed volcanic and sedimentary rocks. Along the west is a dominantly metavolcanic succession (Xvs) and along the east is a mixed metavolcaniclastic-metasedimentary succession (Xgn). In some places the pluton is unconformably overlain by

Paleozoic sedimentary rocks. The contact zone for this pluton is considerably narrower than those of the other plutons, on average slightly less than 1 km (see Fig. 14, discussed later in text). Near Texas Creek, granitic sill intrusions in the gneiss are common, like that shown in Figure 6. Foliation in the sills is parallel to that observed in country rocks supporting a syntectonic origin. Granitization of country rock is minor and anatectites derived from surrounding metamorphic rocks are exposed near Thorpe Falls just west of Cotopaxi. Figure 9 shows an outcrop of anatectites accompanied by brecciation of country rock.

Two populations of xenoliths are identified in the Garrel Peak pluton. Metavolcanic xenoliths are concentrated in the northwestern section between samples 3 and 4 on Figure 8 and metasedimentary-metavolcaniclastic xenoliths are found elsewhere. Both populations occur within 3 km of the contact. A well-defined transition from one type of xenolith to another is impossible due to lack of field evidence; however, an approximate boundary between the two xenolith populations is shown on the sample location map. Metasedimentary xenoliths are generally fine-grained and consist of K-feldspar, hornblende, biotite, quartz, plagioclase, Fe-Ti oxides and +/- muscovite. The metavolcanic xenoliths containing plagioclase, muscovite, quartz, cordierite and Mg-rich biotite have been interpreted

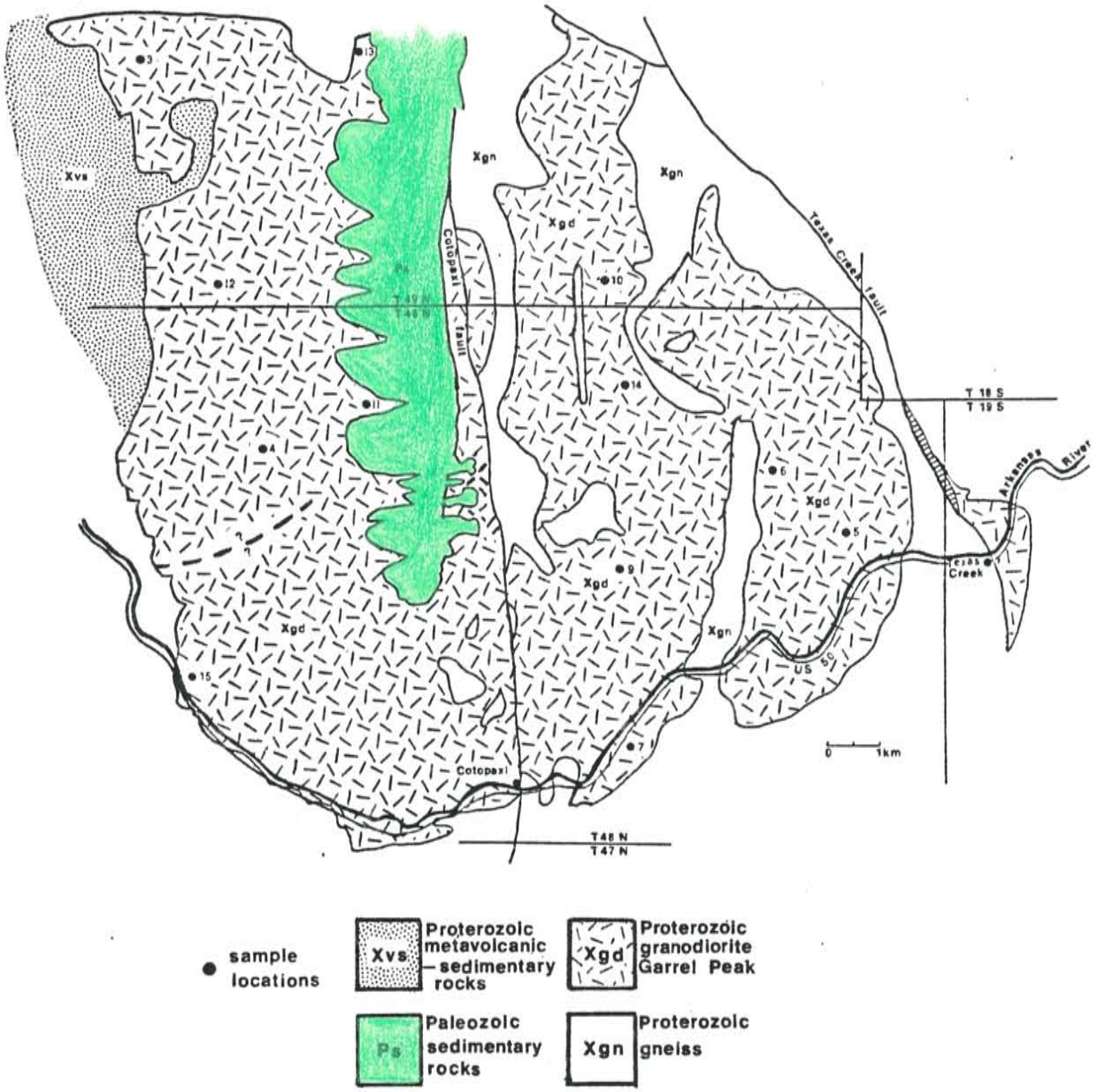

Figure 8. Generalized geologic and sample location map of the Garrel Peak pluton. Modified after Cullers and Wobus (1986). Dashed line on the west side of pluton indicates approximate boundary between xenoliths of Xvs and Xgn.

Figure 9. Brecciation of metasediments associated with anatectites in the Garrel Peak pluton, near U.S. 50 at Thorpe Falls.

as metatuffs (Taylor and others, 1975).

Numerous folded and unfolded granitic pegmatites and aplitic dikes crosscut the gneissic country rock. Although few can be traced back to the pluton, their presence suggests deformation both preceded and accompanied pluton emplacement. Based on the above field observations and criteria suggested by Paterson and Tobisch (1988) to date regional deformations, the Garrel Peak pluton appears to be late syntectonic.

Crampton Mountain-Twin Mountain Plutons

A generalized geologic and sample location map of the Crampton Mountain and Twin Mountain plutons is presented in Figure 10. The two plutons are separated by the Ilse fault and they intrude into the same gneiss-migmatite complex as the eastern part of the Garrel Peak pluton. Both bodies show compositional banding with the most differentiated rocks most widespread in the outer part of the plutons.

The contact relationships for both plutons are roughly the same as described for the Garrel Peak pluton with the exception of width, granitization, and migmatization. Although variable, the widths of the contact zones of these two plutons averages about 2 km, compared to 1 km for the Garrel Peak pluton (Fig. 14). Excellent exposures of the Twin Mountain contact can be seen in the Royal Gorge, whereas contacts of the Crampton Mountain pluton are less spectacular and generally not well exposed. Granitized

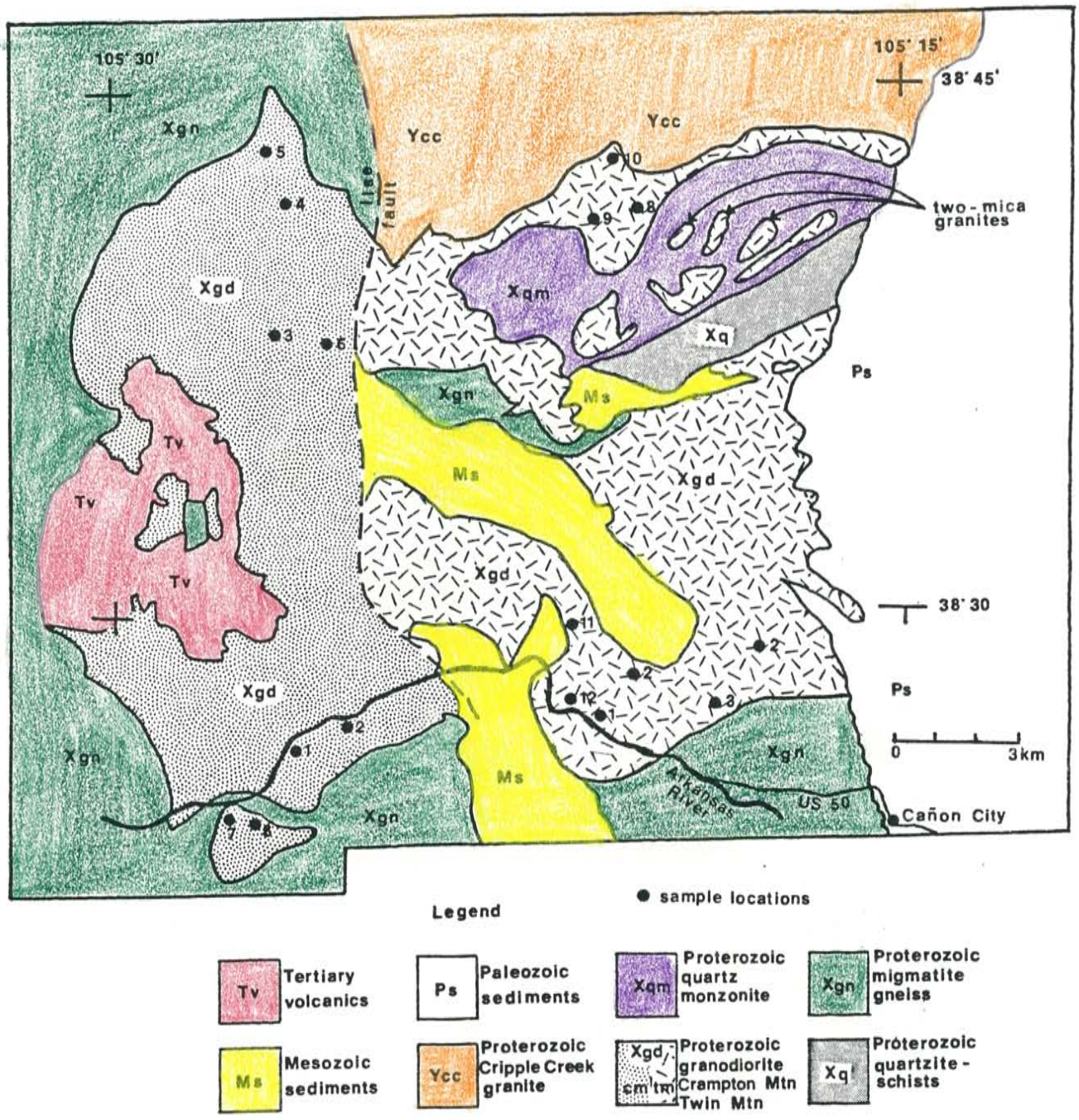

Figure 10. Generalized geologic and sample location map of the Twin and Crampton Mountain plutons. Modified after Cullers and Wobus (1986).

metasedimentary rocks penetrate more than 1 km inward from the mapped contact of both plutons. Migmatization is prevalent in both plutons' margins and is especially well exposed west of Canon City (Fig. 11) where precursor gneisses have been identified as metavolcanic rocks (Cullers and Wobus, 1986).

The Royal Gorge offers a well-exposed two-dimensional cut into the migmatite-gneiss complex and reveals a complex history of deformation. Three separate deformational events can be seen in the gorge walls: 1) deformation associated with metamorphism of the country rocks (pegmatite emplacement prior to deformation), 2) deformation associated with emplacement of the Twin Mountain pluton, and 3) injection and subtle folding of the 1450 Ma pegmatites. Two separate pegmatite intrusion events are recognized and the oldest pegmatites are associated with the emplacement of the Twin Mountain pluton. The youngest pegmatites are probably associated with the 1450 Ma anorogenic igneous event, crosscut older pegmatites and are generally more K-rich. The large number of early pegmatites may be related to a relatively wet Twin Mountain magma.

Phantom Canyon Pluton

The Phantom Canyon pluton is the largest of the four plutons. However, due to the large degree of alteration and weathering, it is the most difficult to sample and study. The southern contact of the pluton is located about 15 km northeast of Canon City and is accessible by Colorado State

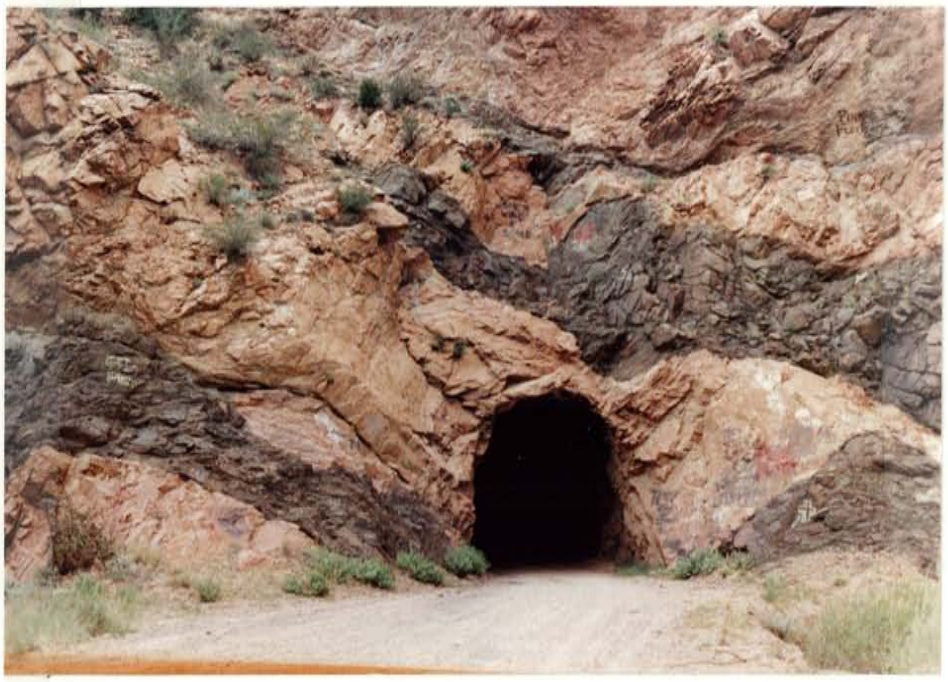

Figure 11. Migmatites exposed west of Canon City on Tunnel Drive. Precursor rocks have been identified as metavolcanic rocks by Cullers and Wobus (1986).

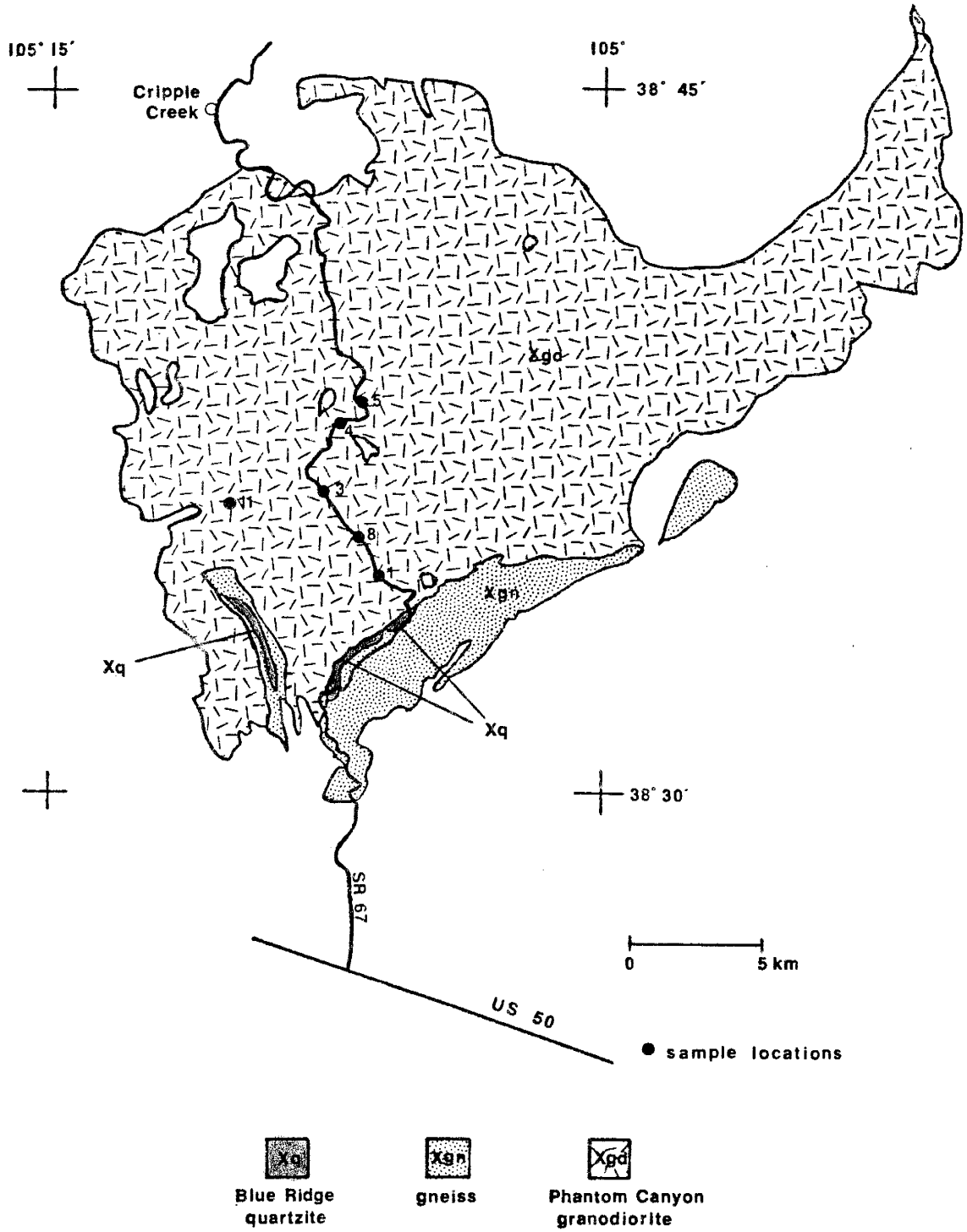

Figure 12. Generalized geologic and sample location map of the Phantom Canyon pluton. Modified after Scott et al. (1978).

Road 67 (Fig. 12). This road parallels Eightmile Creek through impressive switchbacks along Phantom Canyon. Very little exposed country rock remains (Xgn on the map), therefore, all contact relationships are from the southeastern contact zone. Similar to other plutons the Phantom Canyon pluton also is compositionally zoned; however, unlike the Twin and Crampton Mountain plutons its most differentiated rocks are near the contacts (granites of Fig. 3d). The most striking difference between this pluton and the others is the degree to which surrounding metasedimentary rocks have been granitized. Both the color and texture of the original gneisses are changed by granitization along the contact. Rocks near the pluton's margin are two-mica granites and represent the most extensive occurrence of two-mica granite in the four plutons. It is possible, although it was not fully investigated, that the occurrence of two-mica granite in the Twin Mountain and Phantom Canyon plutons is somehow associated with the Blue Ridge quartzite-schist sequence. Figure 13 is a typical granitized biotite-gneiss, and can be compared with an "ungranitized" exposure such as shown in Figure 9. Color change from gray to pink is likely due to K-rich fluids that came from the pluton and metasomatized the country rocks during pluton emplacement. Migmatites are also common and contribute to the augen texture in the rocks.

The pluton contact is a complex zone of migmatites,

Figure 13. Granitic-rich fluids have altered the appearance of metasedimentary rocks in the Phantom Canyon pluton; however, the original metamorphic fabric is preserved. Localized anatexis is probably responsible for the augen texture.

granitized metasedimentary rocks and foliated granitic sills roughly 1.5 km wide (Fig. 14). Sills are emplaced parallel to metamorphic fabric and vary in width from 0.5 to 5 m with their width and abundance increasing toward the pluton's interior.

Xenoliths are common, particularly near pluton contacts where metasedimentary rock is severely deformed and shows growth of late K-feldspar and muscovite porphyroblasts. These crystals are often obliquely oriented to foliation. The frequency of xenoliths decreases inward from the margins.

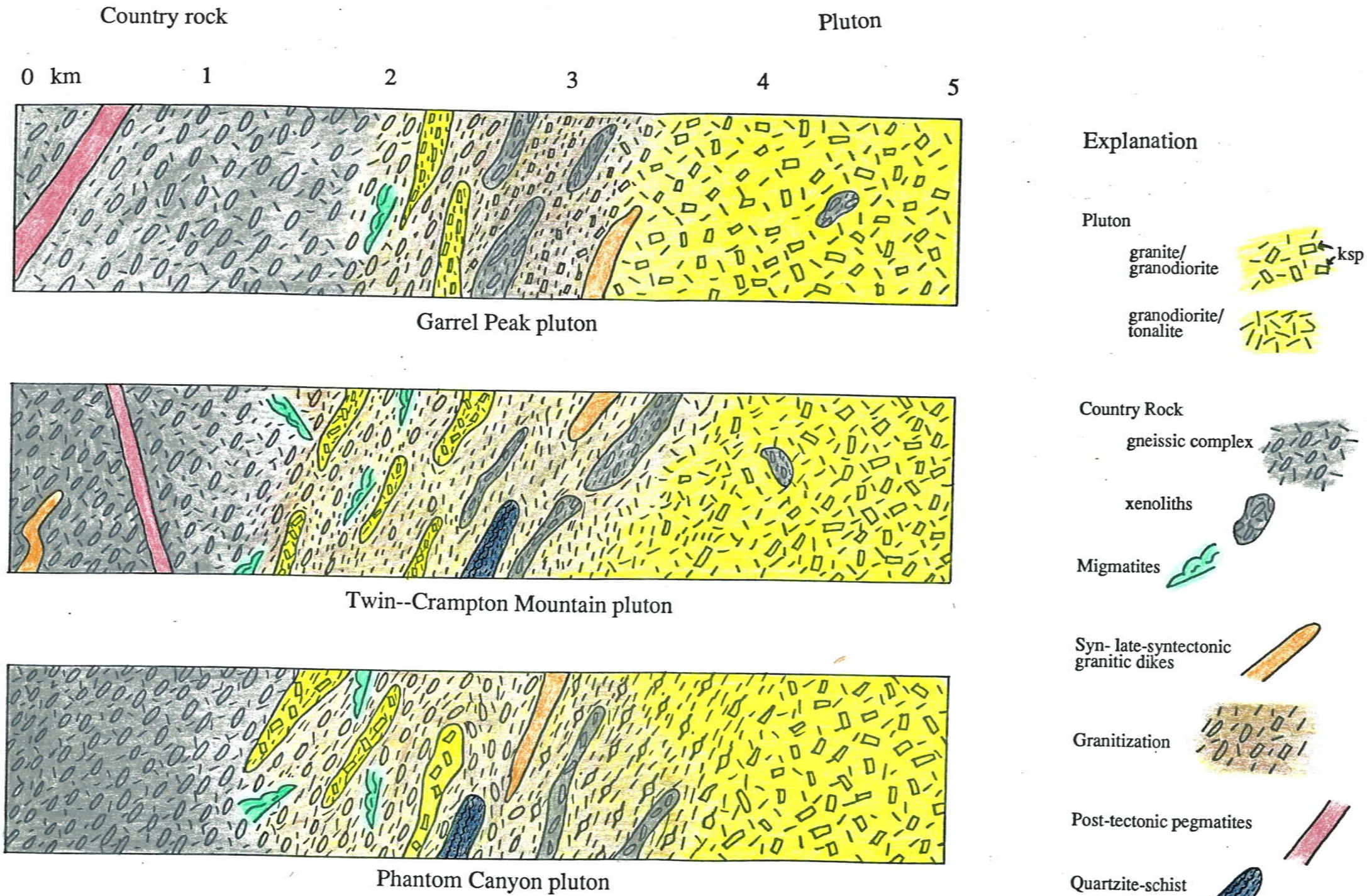

Figure 14. Diagrammatic cross-sections comparing the southern contact zones of four Early Proterozoic plutons from the Wet Mountains.

Petrography

The Garrel Peak pluton consists of a medium- to coarse-grained (1 to > 5mm) porphyritic quartz monzonite and granite with K-feldspar (35%), plagioclase (30%, An_{30-47}), quartz (20%) and small amounts of biotite and hornblende (7-9% and 1-6%, respectively). K-feldspar is the dominant megacryst and is commonly greater than 2 cm in length in the interior of the pluton. Plagioclase typically shows a myrmekitic texture with minor sericitization. Biotite and hornblende (Fig. 15) contain minor retrogressive chlorite along cleavage planes and tend to form a glomerophyric texture. Important trace-element bearing minerals for all plutons are sphene (often > 2%), Fe-Ti oxides, zircon, apatite, monazite and +/- allanite. These phases account for less than 4% of the total volume.

Figure 16 is the less differentiated granodiorite-tonalite phase of the Crampton Mountain pluton, which is composed of plagioclase (40-45%, An_{42}), quartz (20-25%), and biotite (30-35%) as major minerals. In thin section and outcrop there is a sparcity of K-feldspar (occasional trace of microcline seen in thin section). Minor mineral phases generally constitute < 2% by volume. The differentiated quartz monzonite phase contains K-feldspar (25-30%), plagioclase (25-30%, An_{35}), quartz (28-33%) and biotite (10-15%) as major minerals. Muscovite (1-2%) is a common minor mineral. Strained biotite cleavage and cataclastic

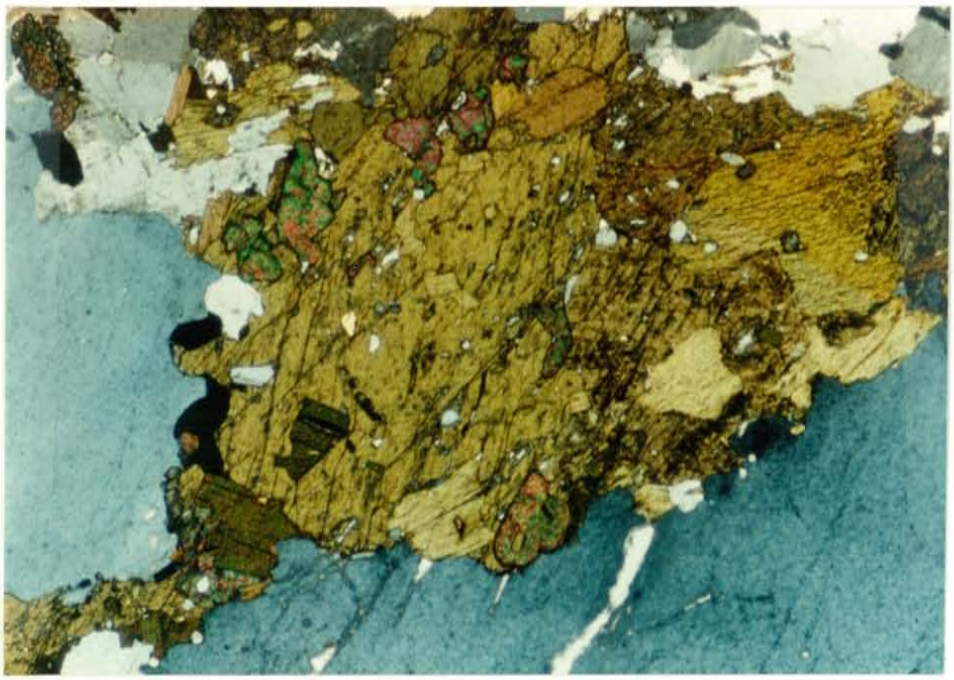

Figure 15. Photomicrograph in crossed polarized light (XPL) of glomerophyric mafic minerals, typical of each pluton. Brown hornblende shows 56° and 124° cleavage. Biotite, which is darker brown and has only one direction of cleavage, occurs in the lower left with minor retrograde chlorite. Also seen are small hexagonal apatite and sphene. Sample number GP-6. The grayish-blue mineral is quartz. Bottom length is 4.0 mm.

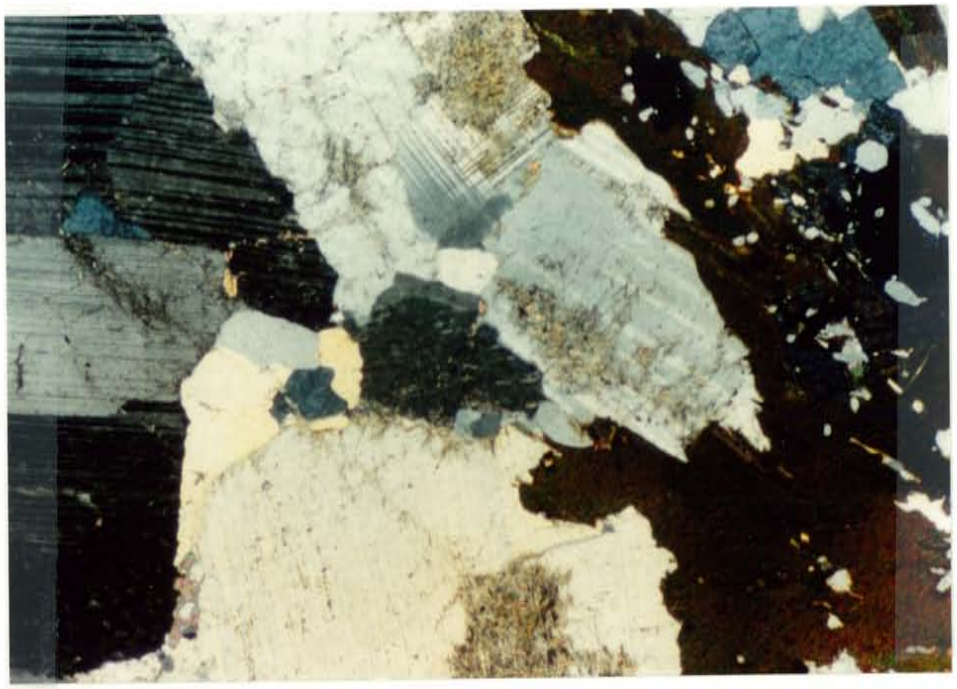

Figure 16. Photomicrograph in XPL of the granodiorite-tonalite phase of the Crampton Mountain pluton composed chiefly of plagioclase, quartz and biotite. Plagioclase is twinned and shows sericitization. Quartz appears slightly yellow and biotite is dark brown. Sample number CM-2. Bottom length is 4.0 mm.

plagioclase and quartz observed near the contacts suggests structural deformation.

The Twin Mountain pluton is the most compositionally complex pluton of the four in this study (Fig. 3). The border zone is chiefly granodiorite and the interior quartz monzonite to granite. This pluton is chiefly composed of plagioclase (30-40%, An_{40}), quartz (30-40%), K-feldspar (20-25%), and biotite (15-5%). A few isolated outcrops of fine-grained, two-mica leucogranite are seen in the northeast portion of the Twin Mountain area (Fig. 10); however, poor exposure and preservation prevents sampling and a detailed description of the relationship of these rocks to the rest of the pluton. Again minor phases constitute about 2% by volume with zircons showing growth zonation (Fig. 17).

Zircons for all plutons are typically subhedral, cloudy and fractured but only the Twin Mountain and Phantom Canyon plutons contain zoned crystals. In the Crampton Mountain pluton, minor alteration and metamorphism have produced chlorite and epidote, associated with the breakdown of biotite, muscovite (after K-feldspar) and sericite (after plagioclase). In general, a greater degree of mineral deformation, fracturing, and alteration occurs in the Twin Mountain and Crampton Mountain plutons. This could be the result of numerous movements on the Ilse fault and/or reheating of the pluton caused by emplacement of the anorogenic 1440-1450 Ma Cripple Creek-Eleven Mile Canyon batholith to the north (Fig. 2). The Phantom Canyon pluton

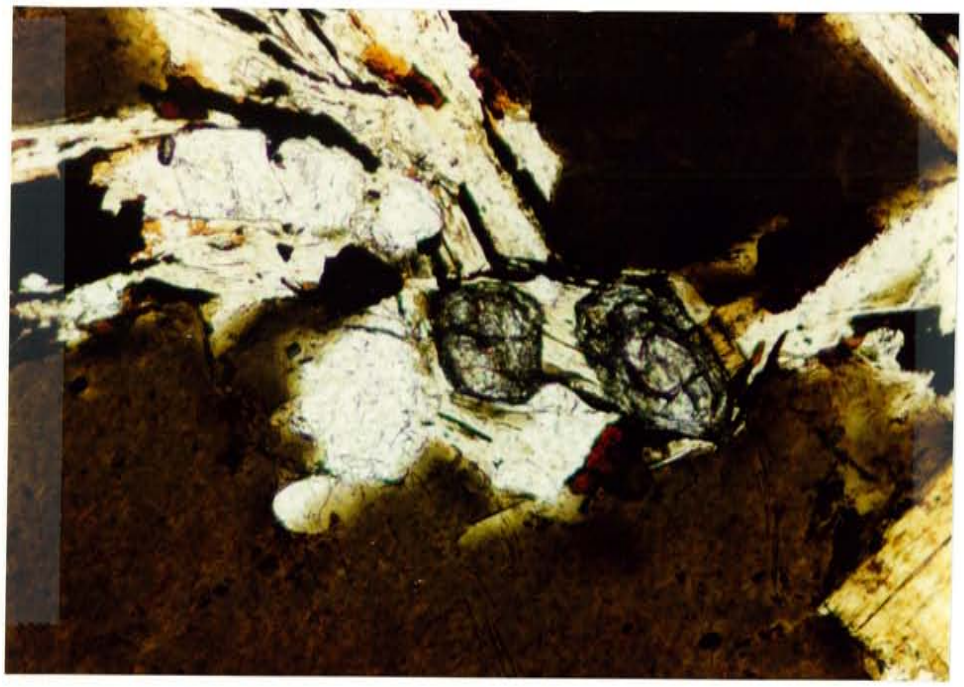

Figure 17. Photomicrograph in plane polarized light (PPL) of subhedral, zoned zircons characteristic of the Twin Mountain and Phantom Canyon plutons. Zircons for all plutons are generally subhedral, cloudy and fractured. Also shown are biotite (dark brown), stained K-feldspar (in upper left), clear, hexagonal apatite and minor allanite. Sample number TM-2. Bottom length is 0.8 mm.

has an inner and an outer facies which can be defined both by texture and composition. The outer augen gneiss facies, as previously mentioned, is the most differentiated and consists of quartz, plagioclase, and K-feldspar in sub-equal amounts (25-28%), with about 12% mica (biotite > muscovite). Alteration is less prevalent than that observed for the Twin and Crampton Mountain plutons; however, weathering of mica grains is common in outcrop.

In the inner quartz monzonite facies of the pluton K-feldspar is the dominant mineral (40-50%), followed by plagioclase (15-20%, An_{20-30}), quartz (10-20%) and biotite (6-8%). This rock is strikingly porphyritic with tabular K-feldspar megacrysts as large as 3 cm. Other textures in thin section include myrmekite and glomeroporphyritic mafic minerals. Alteration is minor and restricted to sericitization of plagioclase and chloritization of biotite.

Geochemistry

Tables 1 through 4 in Appendix A present major and trace element abundances and important elemental ratios in the four plutons studied along the Arkansas River. The Wet Mountains granitoids are dominantly peraluminous (Fig. 18), and only the two younger plutons (Garrel Peak and Phantom Canyon) show overlap into the metaluminous field. Samples that are slightly metaluminous correlate with low or absent normative corundum (Table D.1 in Append. D). None of the plutons is peralkaline.

As previously mentioned, these granitoids also show both a textural and mineralogical zonation from contact to interior, and as expected this zonation is also reflected in the chemical composition of each pluton. Figure 19 presents chondrite-normalized rare earth element (REE) patterns of individual plutons. Each pluton shows a light rare earth element (LREE) enrichment relative to the heavy rare earth elements (HREE). This is analogous to some of the REE patterns reported by Cullers and Graf (1984) in their compilation of REE data for granites (sensu stricto) and quartz monzonites from various parts of the world. Overall fractionation between the LREE and HREE is measured by $(La/Yb)_n$ ($_n$ = chondrite normalized). The average ratio is largest for the Twin Mountain pluton (11.7) and relatively constant for the Crampton Mountain, Garrel Peak and Phantom Canyon plutons (7.1, 8.6 and 8.0 respectively, see Append.

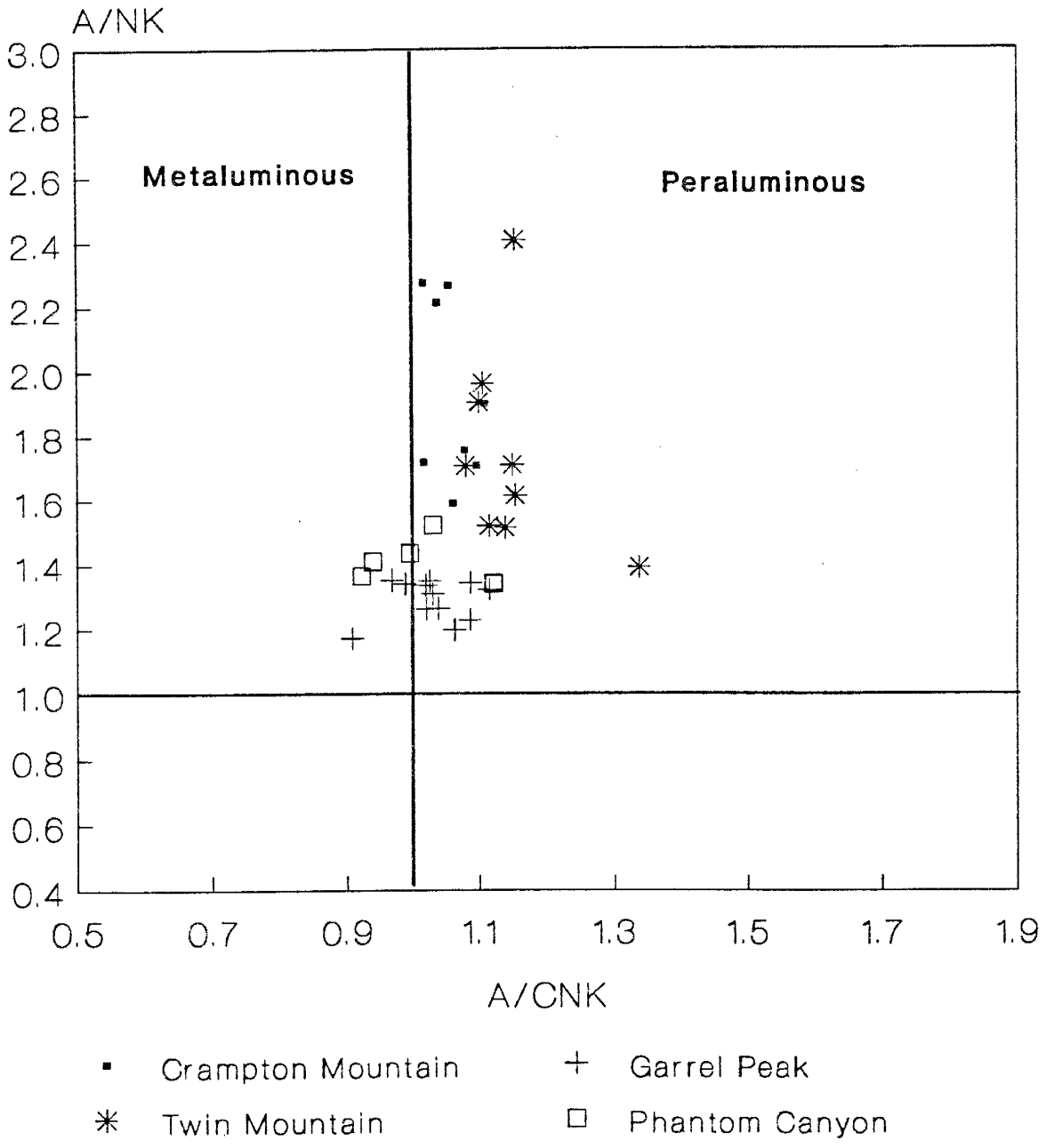

Figure 18. A/NK-A/CNK plot for Proterozoic granitoids of the northern Wet Mountains (after Shand, 1951). A/NK = $Al_2O_3/(Na_2O+K_2O)$ molar. A/CNK = $Al_2O_3/(CaO+Na_2O+K_2O)$ molar.

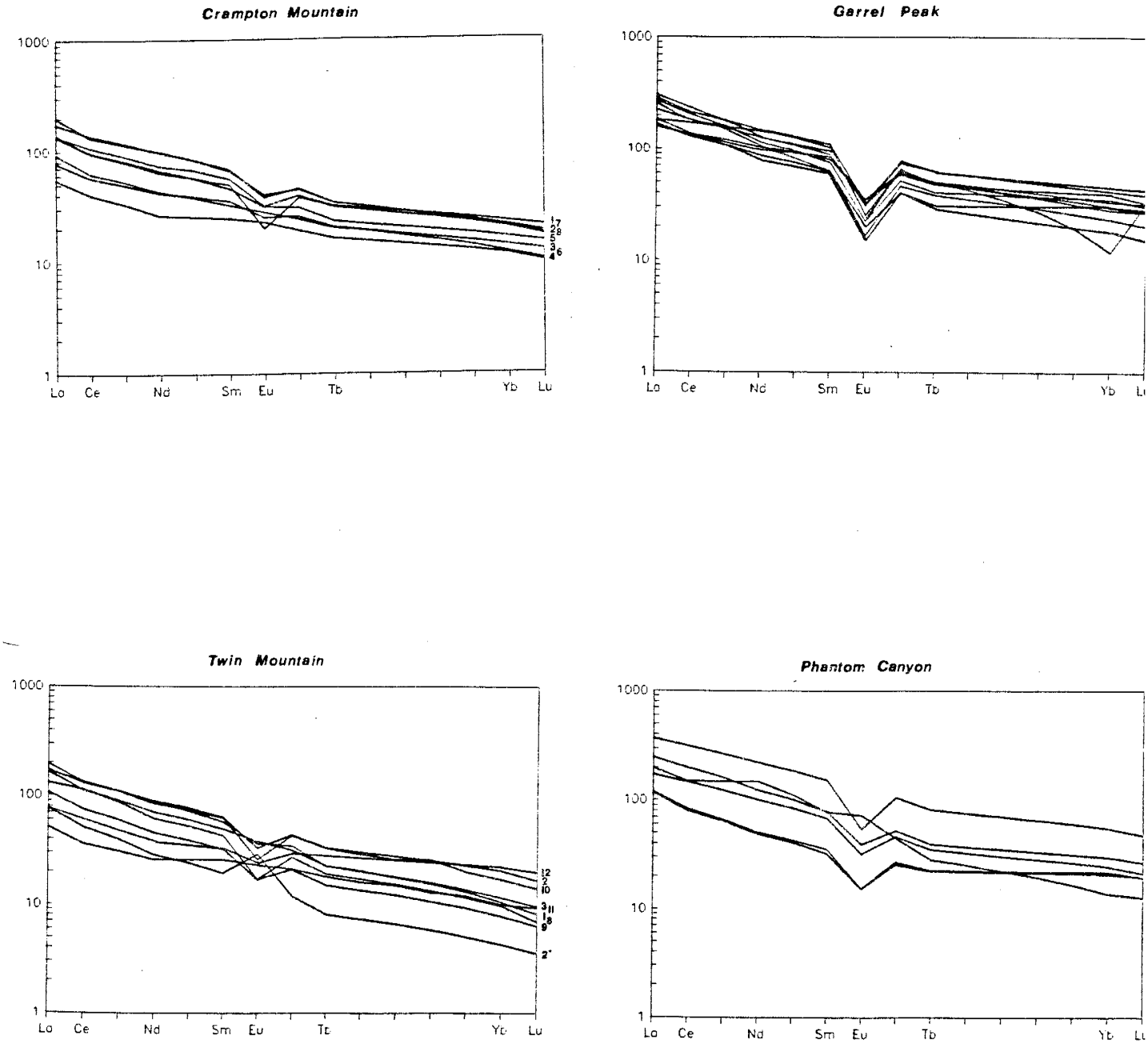

Figure 19. Chondrite-normalized REE diagrams of the Wet Mountain plutons. Each pluton characteristically shows LREE enrichment with variable Eu anomalies (except the Garrel Peak). The two younger plutons (Garrel Peak and Phantom Canyon) show greater LREE than the older plutons. Normalization values from Frey et al., 1968. 2* in (c) is sample TP-2.

C).

The Eu anomaly, Eu/Eu^*, is a measure of the degree of fractionation between the measured abundance of Eu and an interpolated value (Eu^*) on a chondrite normalized plot. $Eu/Eu^* > 1$ is a positive anomaly while $Eu/Eu^* < 1$ is a negative anomaly. One of the most striking features about the Garrel Peak pluton is the uniform REE patterns and invariable Eu/Eu^* ratios (about 0.35). The other plutons show a more varied Eu/Eu^* ratio (Table 1-4, Append. A) with less negative values corresponding to greater amounts of plagioclase accumulation and/or fractionation (Gromet and Silver, 1983).

Close examination of the REE data from the Twin and Crampton Mountain plutons reveals two types of REE patterns in terms of an Eu anomaly (Fig. 19). The flat REE patterns generally correlate with the less differentiated outer portion of these plutons, whereas the samples with the more pronounced negative Eu anomalies are typically located in the interiors. This type of spatial distribution favors plagioclase accumulation near the pluton contacts thereby depleting the residual liquid in Eu. Although the Eu anomaly in the Phantom Canyon pluton shows no relationship to zonation the most REE enriched patterns characterize the interior and less enriched patterns are more typical of the outer zone.

Tectonic Interpretation

Several techniques can be used to constrain tectonic setting. Tectonic discrimination diagrams will allow granites to be separated into four groups: ocean ridge granites, volcanic arc granites, within-plate granites, and collisional granites (Pearce et al., 1984). Granitoids may also be grouped according to their sources, such as I- S- M- and A-type granitoids (Chappell and White, 1974; White, 1979; Pitcher, 1983a). Although both approaches are effective as genetic classifications, the latter is sometimes difficult to apply to composite batholiths. For example, early intrusive phases may have I-type affinities whereas younger phases, associated with the same composite batholith, may have affinities to S-type sources (e.g. Brown et al, 1984; Brown, 1982; Pearce et al., 1984). In this section trace element discrimination diagrams, Harker diagrams, and spider diagrams are used to constrain tectonic setting.

Trace-element discrimination diagrams can be used to broadly constrain tectonic setting, particularly if very little geologic evidence (i.e. regional stratigraphy and intruded country rock) is preserved. Similar to other discrimination methods, these diagrams are based on chemical analyses of Phanerozoic granitoids, and they are assumed to be applicable to granitoids of other ages (Maniar and Piccoli, 1989; Brown et al., 1984; Pearce et al., 1984).

Discriminant boundaries, for these diagrams, are determined by petrographic, bulk chemistry and isotopic constraints (Pearce et al., 1984). Discrimination diagrams are generally restricted to those elements that behave incompatibly during fractional crystallization (Pearce et al, 1984). Therefore, such elements as Ti, Eu and Sr are not used since they behave compatibly in magnetite and ilmenite, plagioclase, and plagioclase and K-feldspar, respectively. Trace-element ratios also may be plotted against major elements which effectively monitors the degree of differentiation. For example, any trace-element/trace-element vs. SiO_2. The main advantage of this approach is that it allows elements of separate geochemical families (e.g. HFSE or LILE), that may behave differently in any given environment, to define a trend that is characteristic of a certain tectonic setting. For example, syn-collision granites can be differentiated from other types by the Rb/Zr ratio. This ratio is useful because Rb, which may be derived from a subducted sedimentary wedge, is often enriched in the volatile phase during partial melting, whereas Zr and other HFSE are concentrated in residual mineral phases of the subducting slab (Harris et al., 1986). Figure 20a presents the Rb/Zr ratio of the Wet Mountain granitoids plotted against SiO_2. All samples, with one exception, plot in the post-orogenic field, suggesting these granites are not syn-collision intrusions.

Based on similar geochemical principles, Ta/Nb ratios

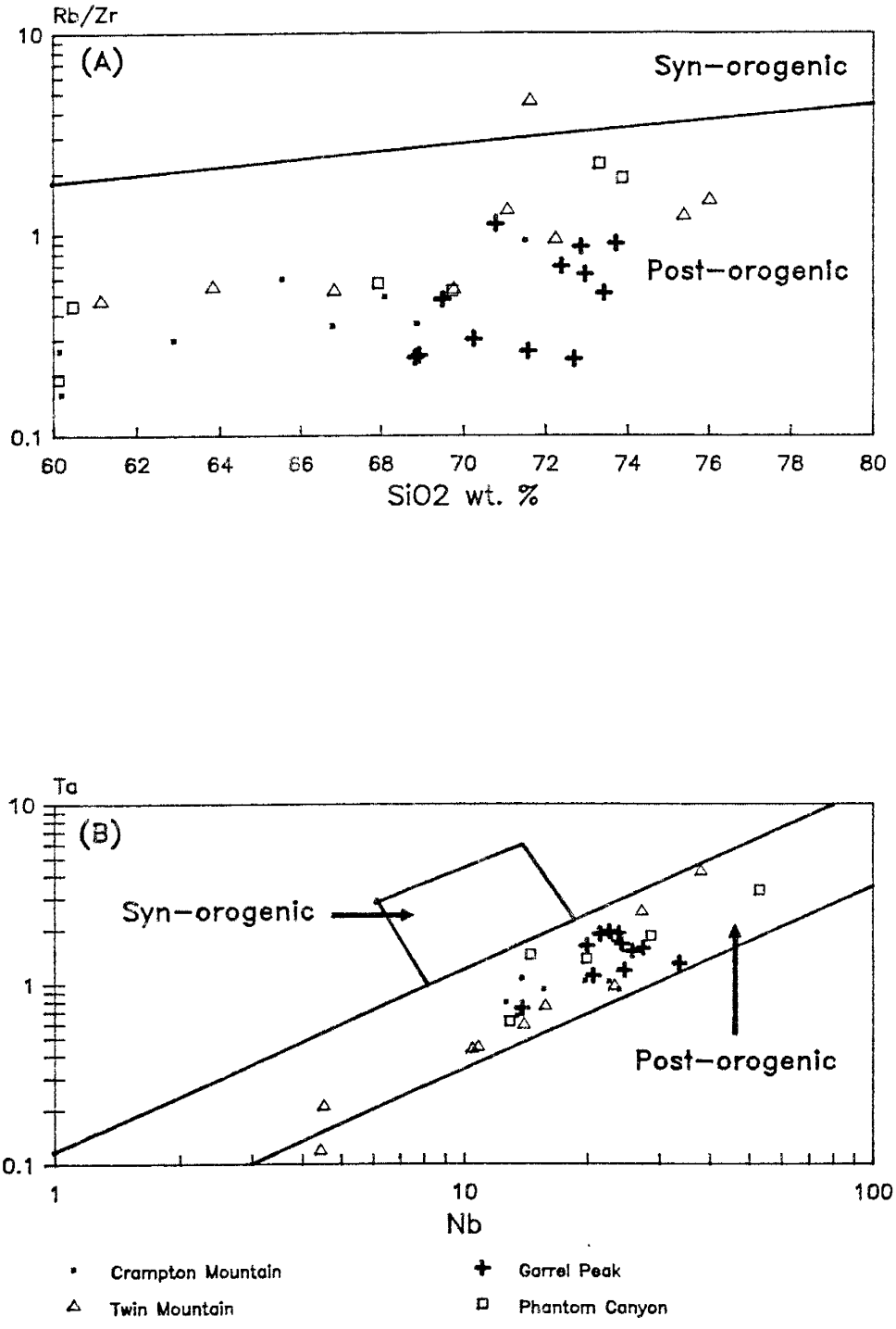

Figure 20. Trace element variation diagrams to determine the plutons' relationship to orogeny (after Harris et al., 1986). A) Rb/Zr (log) vs. SiO2 (wt. %). B) Ta (log) vs. Nb (log).

tend to show very little variation in non-collisional granites despite the large variation in the absolute abundances of the two elements (Harris et al., 1986). When plotted against each other (Fig. 20b) the volcanic-arc and within-plate granites define a narrow, post-orogenic band. In contrast, syn-orogenic granites typically lie above this band reflecting perhaps the presence of residual phases with low Ta/Nb ratios during melting in the source (e.g. cpx or opx) or by the introduction of volatiles with high Ta/Nb ratios (Harris et al, 1986).

Y and Yb are useful tectonic discriminants due to their greater abundance in ocean-ridge and within-plate granites compared to volcanic-arc granites, and also are reliable indicators for a wide SiO2 range (56-80%). Ta and Nb are equally useful for reasons discussed above.

Figure 21 presents the Wet Mountains samples in Ta vs. Yb space. The older plutons (Twin Mountain and Crampton Mountain) show a volcanic-arc affinity, whereas the two younger plutons overlap arc and within-plate fields. A similar trend is seen on Nb vs. Y plot (Fig. 22); all data, however, plot near the triple junction of the tectonic fields. Because of this grouping, the trace element discrimination diagrams (figures 21 and 22) for the four Wet Mountain plutons may not be conclusive in determining the correct tectonic setting.

If the Wet Mountains plutons are arc-related granites, how might their geochemical signatures compare to other

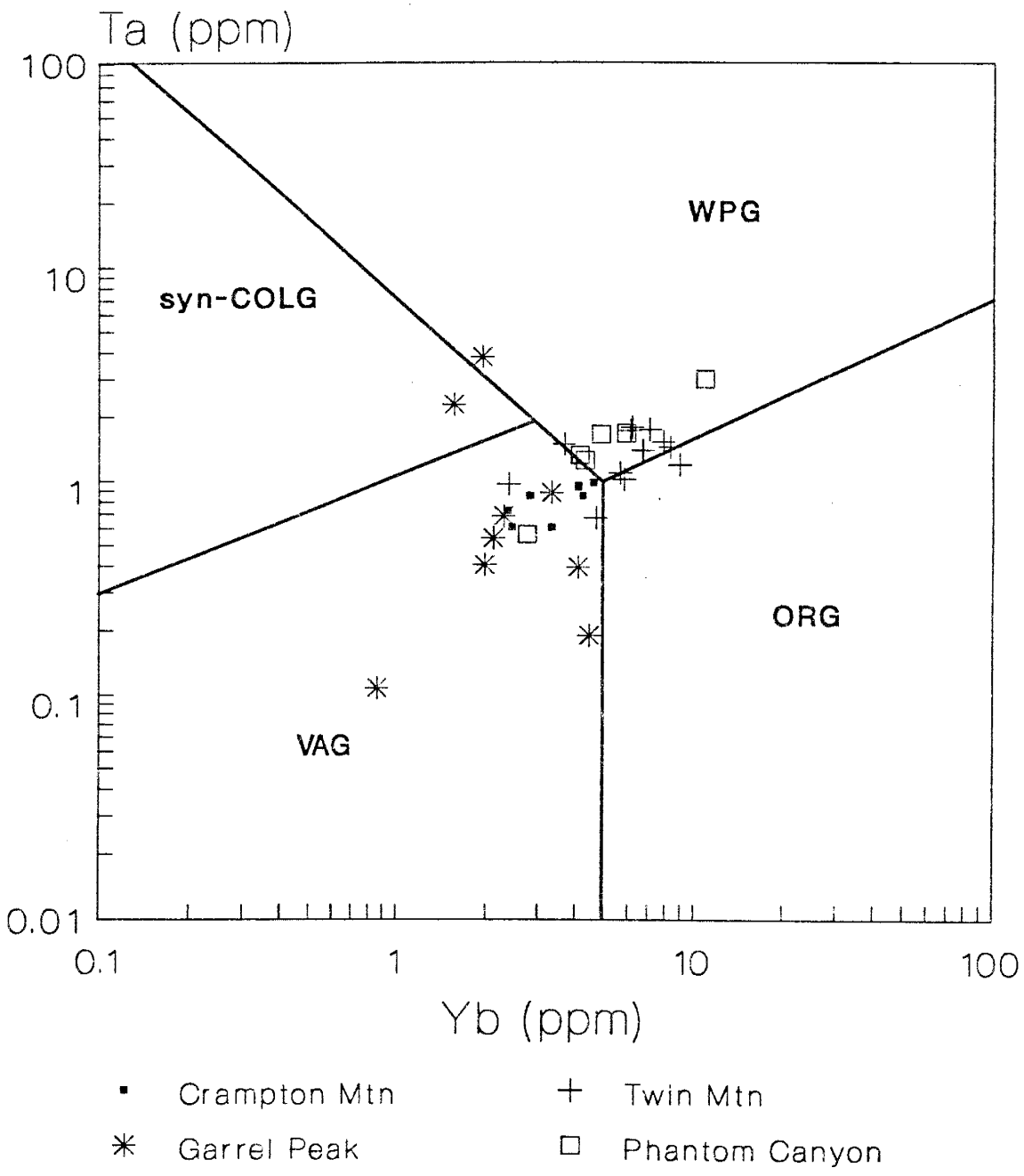

Figure 21. Log-log diagram of Ta vs. Yb (after Pearce et al., 1984). Fields are ORG = ocean-ridge granitoids, VAG = volcanic-arc granitoids, WPG = within-plate granitoids, and syn-COLG = syn-collision granitoids.

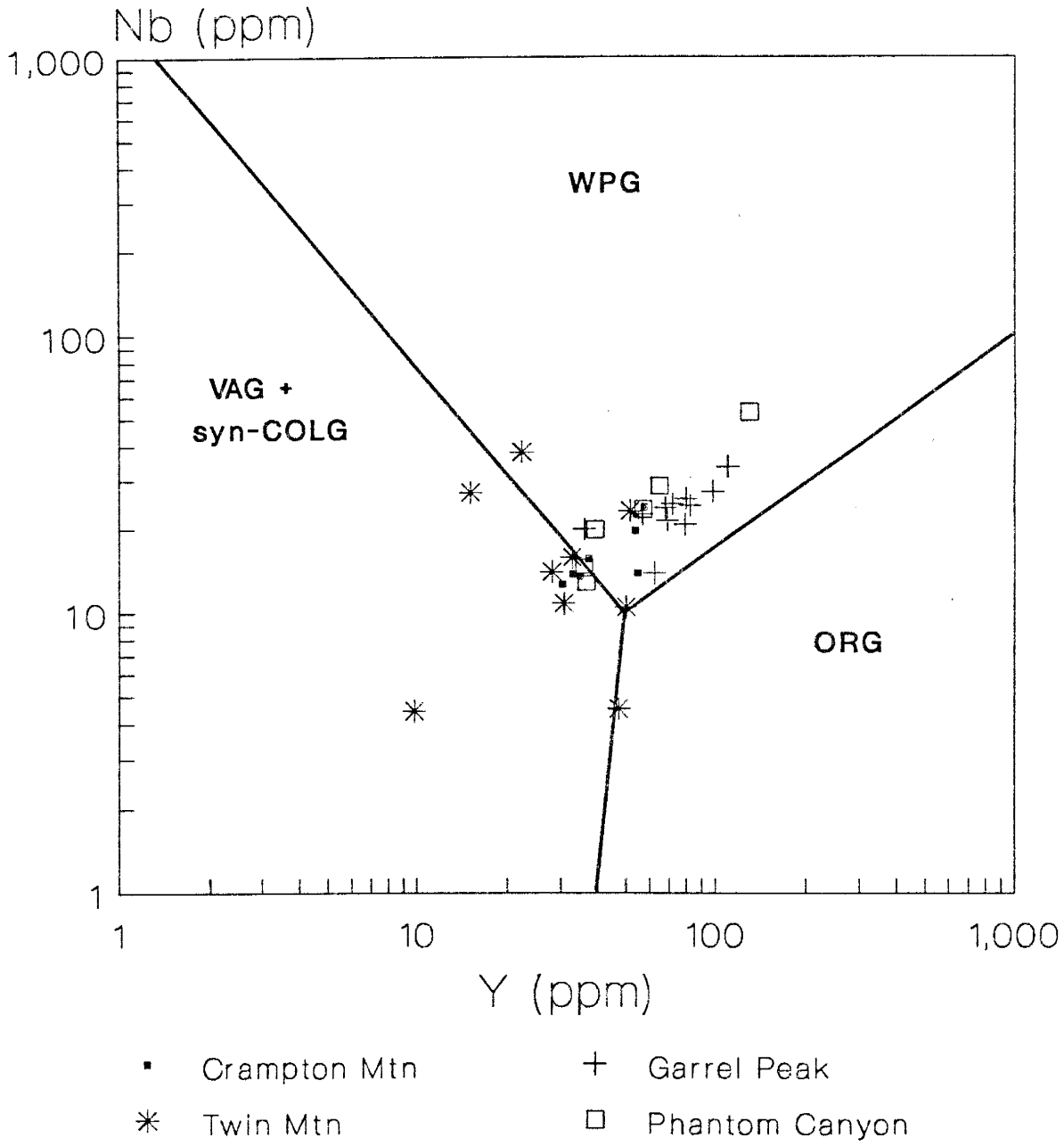

Figure 22. Log-log diagrams of Nb vs. Y (after Pearce et al., 1984). Fields are ORG = ocean-ridge granitoids, VAG = volcanic-arc granitoids, WPG = within-plate granitoids, and syn-COLG = syn-collision granitoids.

granitoids from known arc systems. Based on the studies of Brown et al. (1984), the geochemical characteristics that produce variations in modern subduction-related igneous suites are a function of arc maturity in time and space. This maturity is the result of two processes which control the natural variation in the parental magmas:

> "(a) subduction-zone enrichment of lithospheric mantle, locally coupled with crustal assimilation allied with fractional crystallization (AFC) in zones of thickened crust, all of which yield magmas with enhanced concentration of the LIL elements K, Rb, Th, U, LREE, etc; (b) with increasing distance from the active trench, contributions from within plate sub-continental lithosphere producing mantle-derived magmas, with enhanced levels of HFSE, among which Nb, Ta, Hf and Y are particularly distinctive." (Brown et al., 1984; p. 413).

Figure 23 is a primitive mantle-normalized spidergram where the individual Wet Mountain plutons are represented as averages. The overlay is a compilation from Brown et al. (1984) of contrasting arc types. Elements along the abscissa are arranged in order of increasing bulk partition coefficient (D) for mantle minerals (Wood, 1979). This figure is particularly useful to illustrate the basic trends observed from increasing arc maturity (denoted by arrows above the figure). In general, arcs become more mature and/or magmas are generated further inboard (i.e., continental side) from the active trench. Therefore, mature arcs have granitoids similar in trace element distributions to within-plate granitoids. The marked depletion of Ba, Sr, P and Ti in mature continental arcs can be explained by a greater degree of fractionation of feldspars, apatite and Fe-Ti oxides (Brown et al., 1984), and rocks with this type

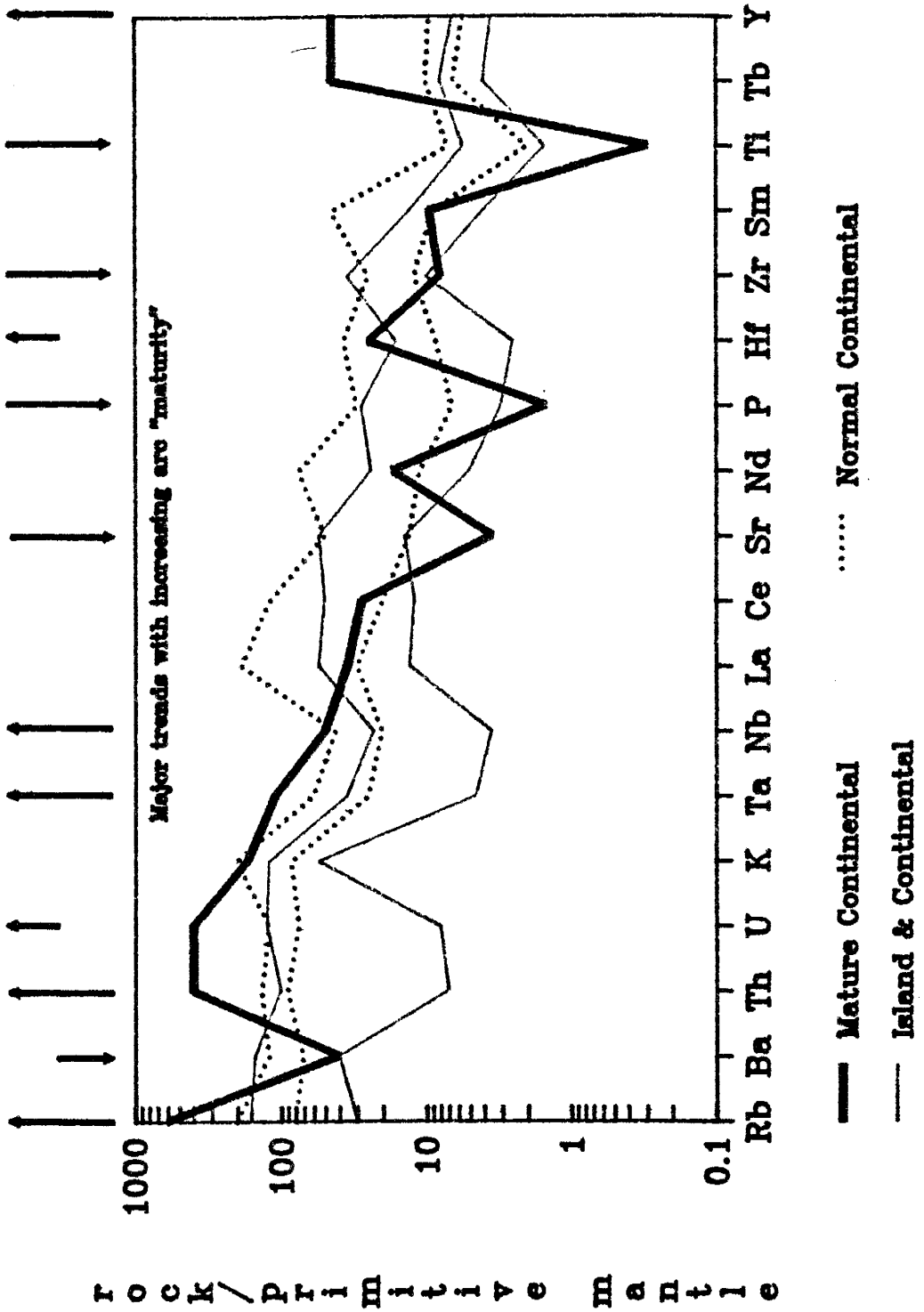

Figure 23. Primitive mantle-normalized trace-element patterns for granitoids from known Mesozoic and Cenozoic magmatic arcs (Brown et al., 1984). Overlay consists of normalized average abundances for each pluton. Normalization values: Rb=0.86; Ba=7.56; Th=0.096; U=0.027; K=252; Ta=0.043; Nb=0.62; La=0.71; Ce=1.90; Sr=2.3; Nd=1.29; P=90.4; Hf=0.35; Zr=11; Sm=0.385; Ti=1526; Tb=0.099; Y=4.87.

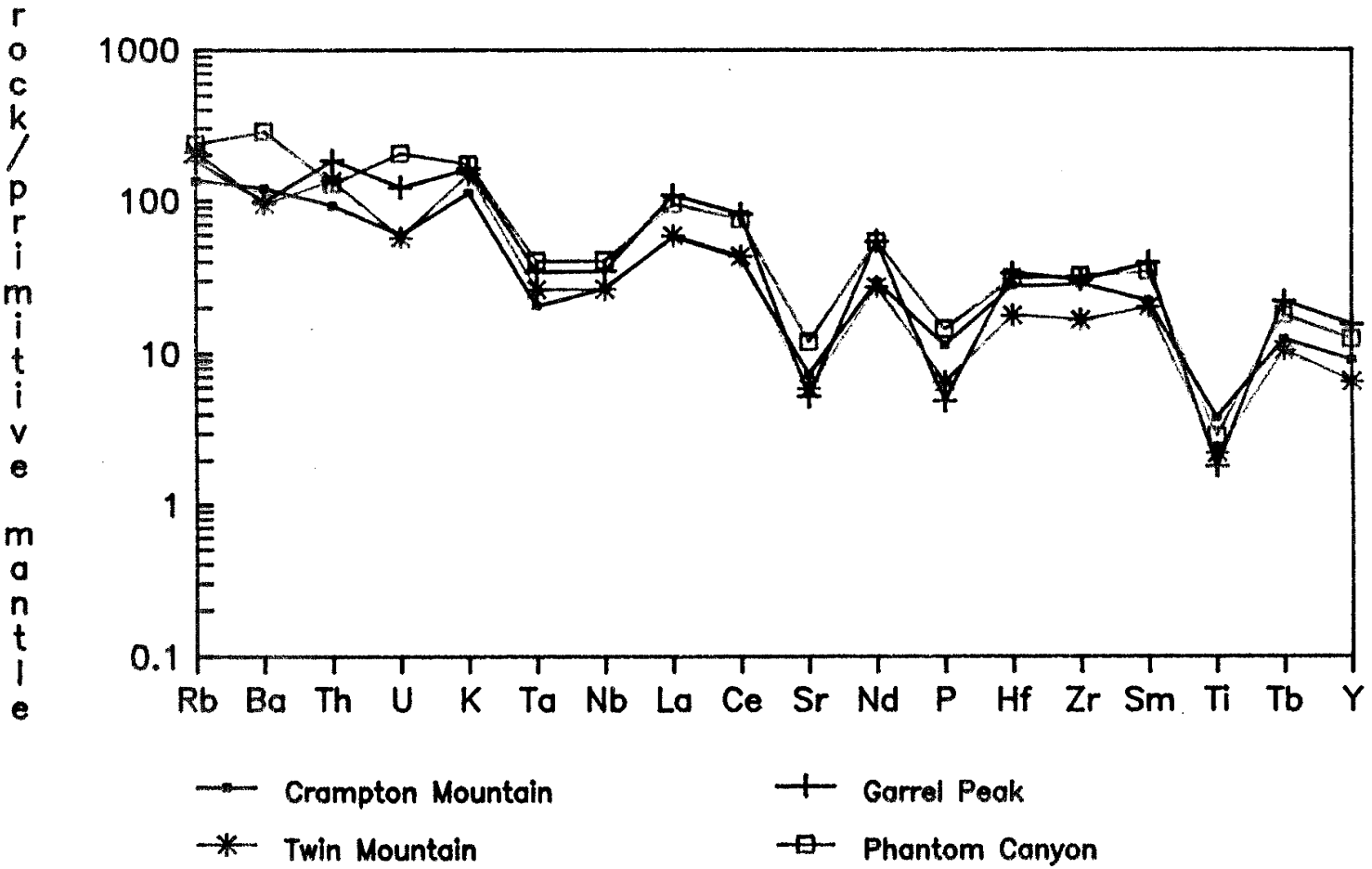
rock/primitive mantle
1000
100
10
1
0.1
Rb
Ba
Th
U
K
Ta
Nb
La
Ce
Sr
Nd
P
Hf
Zr
Sm
Ti
Tb
Y
Crampton Mountain
Garrel Peak
Twin Mountain
Phantom Canyon

of signature are often termed S-type granites. In effect, with increasing arc maturity these elements become increasing compatible. Rb, Th, U, Ta, Nb, Hf, and Y show an enrichment in magmas generated in mature arc systems. Granitoids formed in normal continental arcs are analogous to I-type, calc-alkaline, metaluminous to peraluminous granites, whereas oceanic island arcs and some young continental cordillera (Western pacific arcs) broadly correlate to the M-type calcic or metaluminous granitoids. The best fit of the Wet Mountain data suggests that the oldest plutons show an affinity to normal continental arcs, (I-type genesis), while the younger plutons show slightly more mature geochemical signatures characterized by relative enrichments in Ta and Nb, U, Hf and Y and relative depletions in Sr, P and Ti. It is possible, based on most elements, to produce the average differences observed among the Wet Mountain plutons by fractional crystallization, where the youngest plutons (Garrel Peak and Phantom Canyon) represent the most evolved liquids. For example, the Twin and Crampton Mountain plutons, on average, have lower trace element concentrations compared to the Garrel Peak and Phantom Canyon plutons at similar SiO_2 numbers.

Interpretation of the geochemical data suggest that granitic magma was initially produced in a setting similar to a normal continental volcanic arc. This interpretation, however, favors post-tectonic emplacement (Fig. 20), whereas, the geology of the contact zones favors a late syn-

tectonic emplacement. Perhaps the initial pulse of magmatism produces the early 1705 Ma-old plutons (Twin and Crampton Mountains) which have relatively low contents of LILE, REE, and HFSE. The later pulse of magmatism that produces the Garrel Peak and Phantom Canyon plutons is characterized by higher concentrations of LILE, REE, and HFSE suggesting evolution towards a mature continental arc setting. The Blue Ridge quartzite-schist sequence is a paleotectonic indicator of a shallow water environment (Reuss, 1974) and could possibly represent a back-arc basin deposit. This type of sedimentary deposit is characteristic, although not definitive of, a normal or mature continental arc.

Magma Origin and Source

In light of the past 40 years of experimental petrology, (e.g., Bowen and Tuttle, 1950; Tuttle and Bowen, 1958; Huang and Wyllie, 1975; Whitney, 1975; Maaloe and Wyllie, 1975; Wyllie, 1977; Anderson and Cullers, 1978; Hildreth, 1981; Sekine and Wyllie, 1982), temperature and water content are clearly the two most important parameters in the generation of granitic magma. A majority of experimental studies have dealt with synthetic granitic melts to ascertain the effect of water on the melting temperature. Other studies have concentrated on compositional parameters such as the Ab/An ratio of granitic magmas (von Platen, 1965; Winkler, 1979) as well as on the order of crystallization and its significance in terms of water content (Maaloe and Wyllie, 1975).

The phase relations for the granite system (Q-Ab-Or-An) at P_{H2O} ranging from 0.5-35 kb have been known for some time; however, application of this system to granite origin is difficult. If sufficient data exist to constrain the parental or most primitive composition, then an estimate of the depth of melting can be inferred provided the magma has not undergone significant changes since melt generation (Anderson, 1983). Such interpretations rely on numerous assumptions including whether or not the rock represents minimum or near minimum melt. Anderson (1983) reports that the effect of water saturation is minimized because the

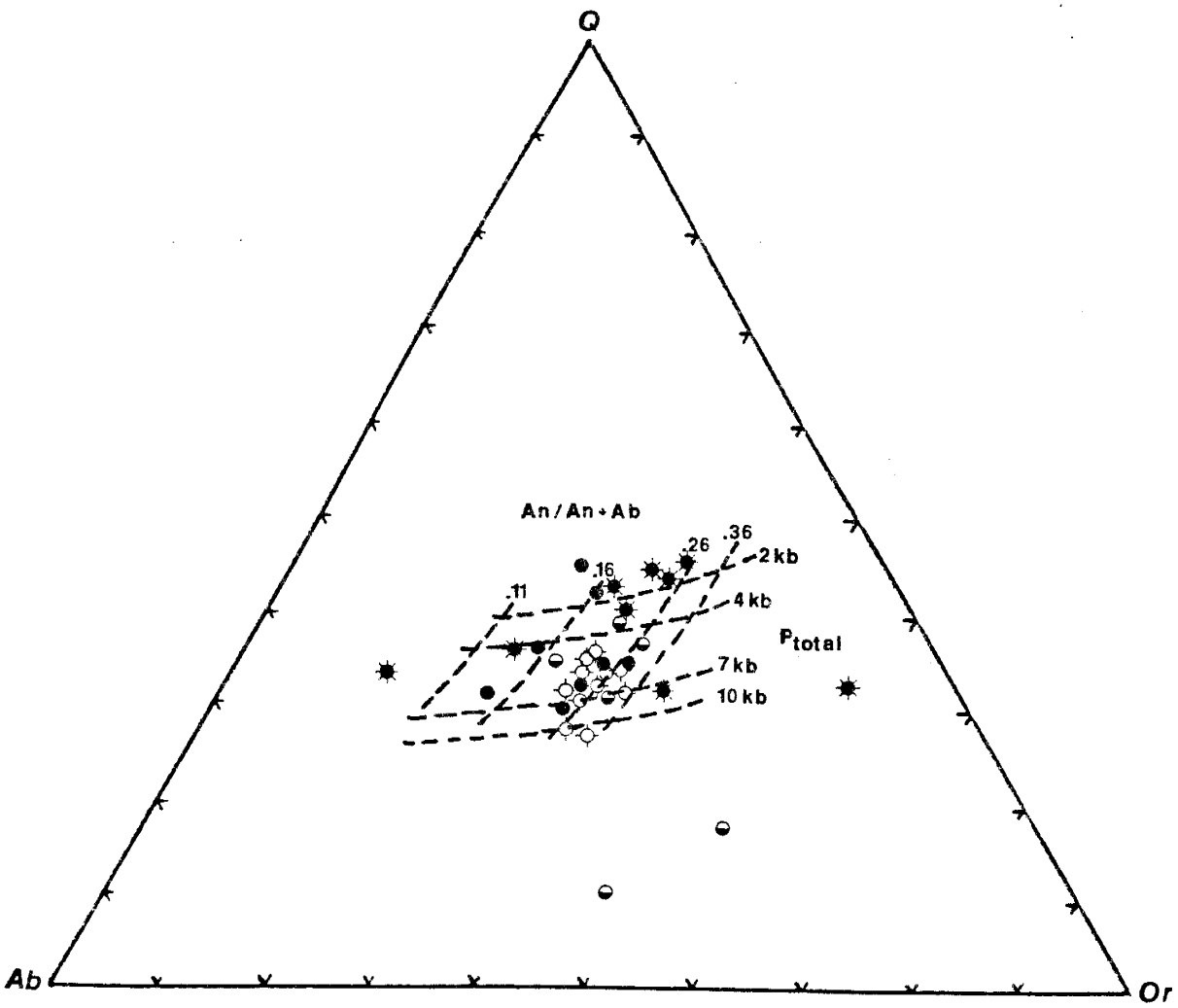

Figure 24. Q-Ab-Or normative diagram (after Anderson 1983). The subvertical hatched lines on the grid are normative An/An+Ab ratios while the sub-horizontal lines are total load pressure. Garrel Peak, ☼ ; Crampton Mountain, ● ; Twin Mountain, ✸ ; Phantom Canyon, ◒ .

lowering of P_{H2O} relative to P_{total} appears to shift minimum melts in a subparallel path to the isobars. The four Wet Mountain plutons are plotted on a Q-Ab-Or normative mineral triangle in Figure 24. A subvertical projection of normative An/An+Ab is superimposed over a subhorizontal projection of various pressures to form a grid. The Garrel Peak is the only pluton that yields consistent information about depth of magma generation, which is near the 5 to 7 kb minima, implying a middle to lower crustal source. The other plutons may have experienced more crystallization and/or assimilation of country rock.

The sequence of crystallization for granitic magmas is a function of water content. Because the phase boundary of biotite intersects those of quartz and K-feldspar, it can be used to place limits on possible water contents of parent magmas (Maaloe and Wyllie, 1975). During crystallization of magmas with water contents > 2.5 %, biotite crystallizes prior to K-feldspar and quartz (Maaloe and Wyllie, 1975). All four Wet Mountain plutons show either embayed K-feldspar (by biotite) or biotite grains wholly enclosed in K-feldspar. According to Maaloe and Wyllie (1975), this supports a water content > 1.2 %.

The probable source for water in many granitic magmas is through dehydration melting of mineral phases such as muscovite, biotite, and hornblende in the source. Melts generated by anatexis of these phases have distinctive chemical characteristics. Those melts in which biotite is a

major contributor tend to be peraluminous to metaluminous, form plutons that are granitic to granodioritic in composition, and have low K/Na ratios (Whitney, 1988). From the results shown in Figures 3 and 18, it would appear that the first and second conditions are consistent with the geochemical data. Figure 25 shows K/Na ratios plotted for each sample. With the exception of a few samples (TP-2 and TM-9) each pluton has low K/Na ratios (chiefly < 2) comparable to granitoids that are generated by dehydration melting of biotite (Whitney, 1988). The inconsistency for the few Twin Mountain samples may involve a muscovite component which would tend to increase the K/Na ratio. Genesis of the Wet Mountain granitoids by dehydration of muscovite or hornblende alone can be ruled out because the former produces strongly peraluminous magmas and the latter tends to produce peralkaline to metaluminous melts with lower K/Na ratios (Whitney, 1988).

The Wet Mountains plutons have similar elemental distributions which suggests that their compositional evolution is controlled by similar processes. These data suggest increased differentiation with time; i.e., the older plutons are generally less chemically evolved while the younger plutons are more evolved and show higher REE (except Eu), Rb, Th, U, Ta, Nb, Tb, and Y concentrations. Crystal accumulation, assimilation of continental crust, and crystallization of trace element-rich minor phases must be considered as possible processes contributing to the

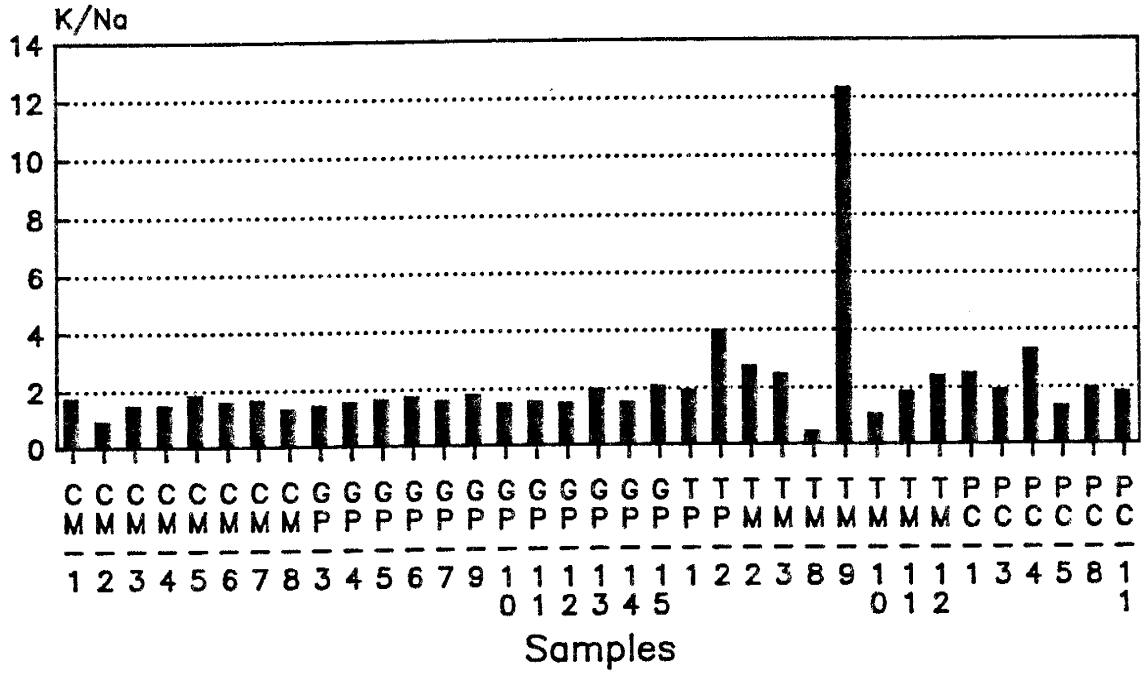

Figure 25. K/Na ratio of each Wet Mountain granitoid sample. These low ratios suggest source for water entrained in the parental melt was possibly derived from dehydration melting of biotite rich (with some minor muscovite) source rock (Whitney, 1988).

geochemical signatures of these felsic magmas. Most petrogenetic models call upon fractional crystallization (FXL) of basaltic magma, partial melting of crustal rocks, or a combination of assimilation and fractional crystallization (i.e. AFC) (Hanson, 1978). Subsequent modification may be caused by magma mixing and/or metasomatism.

In this study, computer programs were used to model both trace elements (MODULUS ver. 2.21 (Knoper, 1990b)) and major elements (MIXFRA (Bryan et al., 1969) (Knoper, 1990c)). Descriptions of these programs can be found in Appendix G. Numerous petrogenetic models were investigated involving several types of melting and crystallization. These models are inherently dependent on source and melt modes and crystallization modes or rate of assimilation if applicable. Experimentally determined Kds were obtained from the literature (Knoper, 1990b) and can be found in Appendix E.

Melting and Crystallization of Mantle Sources

One model tested is an I-type petrogenetic model (sensu stricto after Chappell and White, 1974). This model involves crystallization of a mantle-derived basaltic melt. Batch melting of either primordial mantle (Wood, 1979) or depleted mantle (Sun, 1980) followed by FXL produces granitic magma depleted in incompatible trace elements, particularly the HFSE, LILE, and REE, relative to the Wet

Mountains granitoids. An enriched mantle source is a way around this problem, although data are not available to test this possibility. What little isotopic data that are available for Wet Mountain rocks indicates Proterozoic continental crust was formed from a previously depleted (not enriched) source material (DePaolo, 1981).

FXL of N-MORB, E-MORB, island-arc tholeiite (Sun, 1980), within-plate tholeiite (Pearce, 1982) or back-arc tholeiite (Hawkesworth, 1979) produces granitic melts again too depleted in LILE and HFSE. Equilibrium crystallization of the same sources produces a depleted geochemical signature and a narrow geochemical range unlike the observed scatter in the four plutons.

Table 2. Summary of models tested for sources of the four Wet Mountain plutons. Dep = depleted with respect to Wet Mountain plutons. En = enriched with respect to Wet Mountain plutons. Com = comparable with respect to Wet Mountain plutons. Refer to text for explanation of models and Appendix F for mode and melt fractions, degree of melting, etc.

Model	Major	REE	LILE	HFSE
mantle source	com	dep	dep	dep
crustal source	com	en	en	en
AFC	com	com	com	com

Melting of Crustal Sources

Another model that involves batch melting of the upper, lower, or middle crust (Taylor and McClennan, 1985; Weaver and Tarney, 1984) produces trace element trends too enriched (especially in LILE) to explain the Wet Mountain granitoids. Fractional melting of the same sources produces melts enriched in Rb, Ba, and REE, and depleted in Sr and Ti.

Assimilation-Fractional Crystallization (AFC)

The preferred model for the production of the Wet Mountains granitoids is a two-stage process involving an initial batch melt followed by AFC. The parental source for the melt is an average post-Archean felsic granulite (Table H.1 in Append. H) involving both metasedimentary and metavolcanic protoliths, some with geochemical characteristics similar to granulites from Ivrea and Calabria (Maccarrone et al., 1983). The assimilant for AFC is an average paragneiss (collectively mapped as Xgn) seen in the surrounding country rock. Geochemical data for these rocks are from Lanzirotti (1988) and are listed in Table H.2 in Appendix H.

Two geochemical plots are used to trace the behavior of the LILE and REE in the proposed geochemical model. The LILE are represented in Figure 26 on a Ba vs. Sr plot. This type of compatible element-compatible element plot is preferred because major mineral phases such as K-feldspar have large distribution coefficients and are useful magma

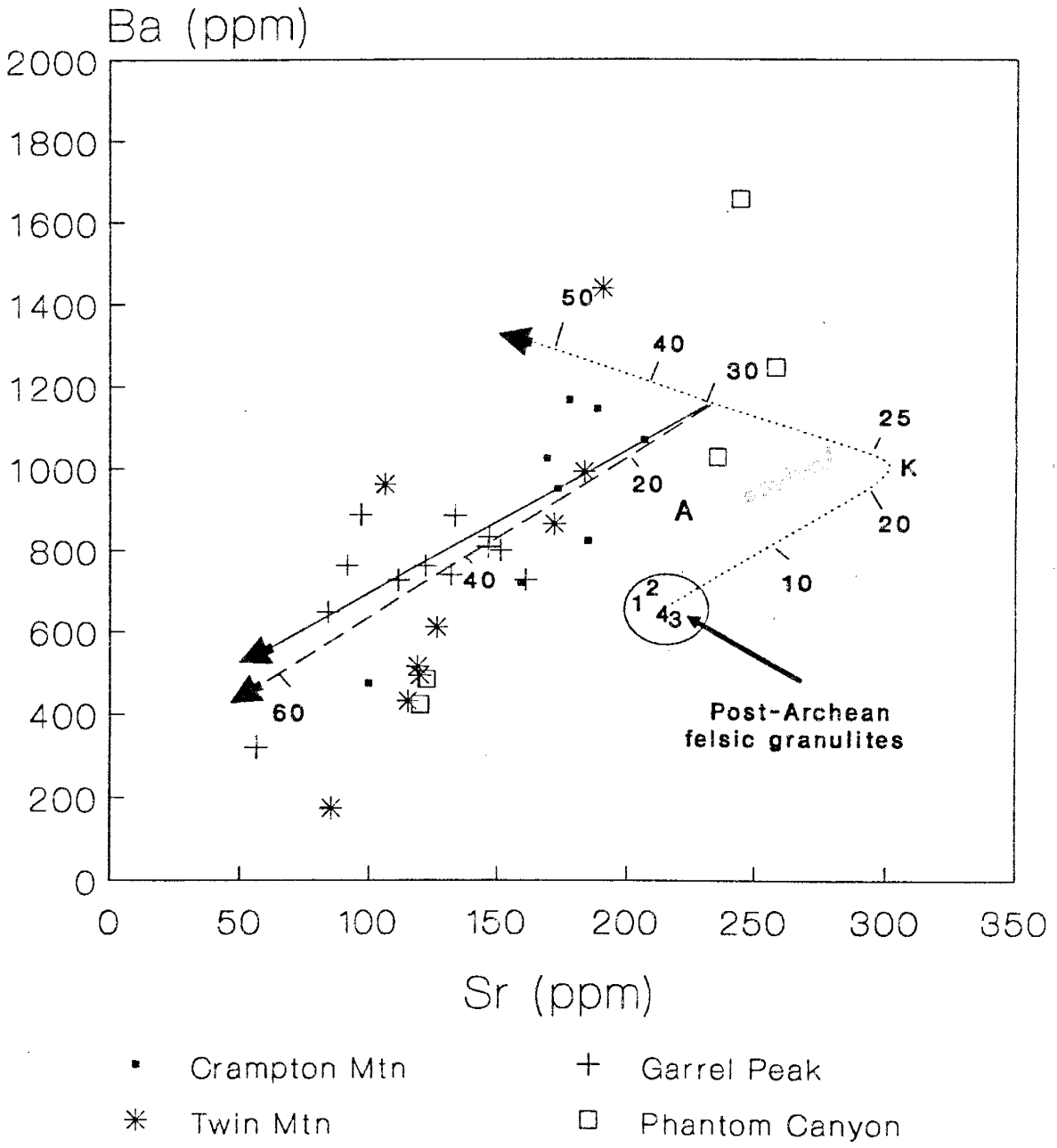

Figure 26. Ba vs. Sr petrogenetic model. Dotted line (·····) represents partial melting. The kink (K) in the trend is due to total melting of K-feldspar from the source. FXL is represented by the straight line (——) and AFC is represented by the dashed line (– – –). During AFC the ratio of assimilation/crystallization (R_a/R_c) is equal to 15%. The assimilant, A, is a weighted average of the intruded country rocks. Each crystallization path represents a total of 60% crystallization. The references 1-4 in the felsic granulite source area are found in Appendix H.

composition monitors during crystallization processes. The behavior of Ba is primarily controlled by K-feldspar, biotite, and plagioclase (minerals listed by decreasing K_ds) while Sr is controlled chiefly by plagioclase (K_ds are found in Append. E). During batch melting both, Ba and Sr are partitioned into the liquid resulting in a curved batch melting trend. Once K-feldspar has melted from the source (at about 22% melting) the batch melting curve has a negative slope where the trace element behavior is controlled by biotite and plagioclase. Granodiorite magma is produced between 25-30% melting (Fig. 26). This initial batch melt is low compared to the critical melt fraction (40-50%) of Wickham (1987) and may be a limiting factor on the model. Source and melt modes are given in appendix F.

In the second stage, the liquid undergoes fractional crystallization accompanied by about 15% assimilation of country rock. Anywhere from 15-60% fractional crystallization is needed to produce rocks that range from granodiorite to granite in major element composition. A FXL trend is compared to the AFC trend on Figure 26, but shows little deviation from the AFC trajectory because the assimilant (A) is similar to the granitoids in Ba and Sr concentrations. On similar LILE plots involving Rb and K, significant scatter of the data supports field evidence for granitization and suggests mobility of these ions particularly in the Phantom Canyon pluton. This is a minor

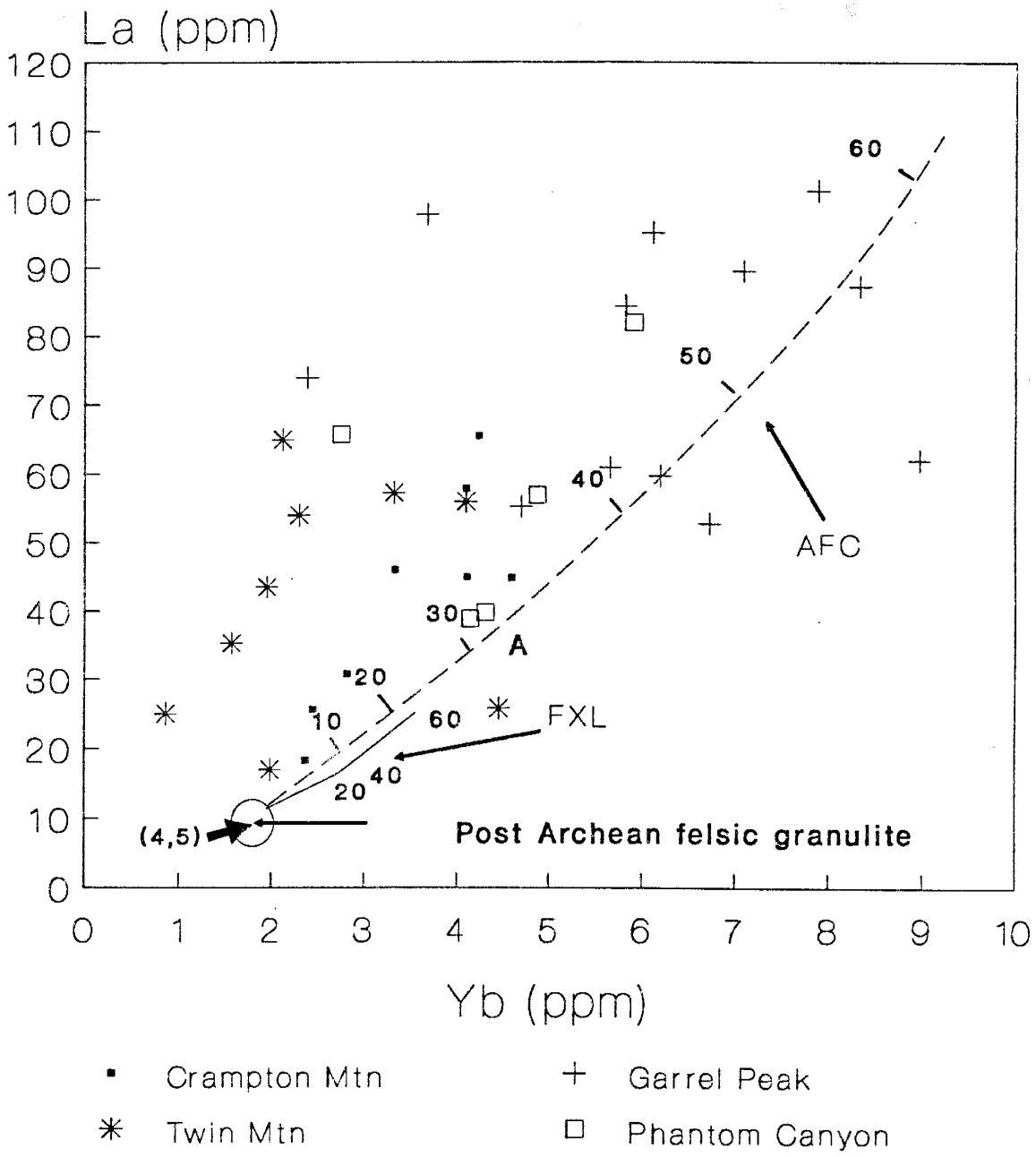

Figure 27. La vs. Yb petrogenetic model. Labels are given in Figure 26. Batch melting of 25-30% barely changes from the initial granulite composition, therefore, to avoid complexity, is not shown in the figure.

process but not uncommon during emplacement and regional metamorphism accompanying pluton emplacement (Pearce, 1975; Winchester and Floyd, 1976; Hyndman, 1985). Figure 27 is the same petrogenetic model presented in the previous figure but illustrates the behavior of REE by plotting La versus Yb. During 25-30% batch melting of the granulitic source very little enrichment of the REE occurs due to the low distribution coefficients (Append. E) for plagioclase, K-feldspar, quartz, and biotite. As a result, the concentrations of La and Yb in the liquid are similar to the starting composition. During crystallization, REE abundances are controlled by the formation of minor mineral phases such as zircon (concentrates the HREE), sphene (concentrates all REE), and apatite (concentrates all REE but not to the extent of sphene) (Condie, 1978; Miller and Mittlefehldt, 1982; Gromet and Silver, 1983). Figure 27 demonstrates that assimilation is needed to explain the REE enrichments, particularly in the Garrel Peak pluton. FXL alone (60%) is inadequate to explain the geochemical variation. In contrast with the Ba-Sr distributions (Fig. 26), the La-Yb data for the Phantom Canyon pluton shows better agreement with the proposed model suggesting the relative immobility of REE compared to LILE.

During crystallization, the HFSE, like the REE are controlled by minor mineral phases such as zircon (Zr and Hf) and sphene (Nb and Yb) (Pearce et al., 1984; Hanson, 1978). Kds are typically large (see Append. E) and there-

fore strongly partitioned into the solid phase. The two-stage petrogenetic model applied to the HFSE shows similar positive slope FXL and AFC trajectories compared to those in Figure 27.

Major-element modelling, presented in Append. G, agrees with the trace-element model during the initial batch melting stage. The "goodness" of fit is measured by the squared residuals; the lower the residuals the better the fit. For melting the squared residuals are < 0.9. During crystallization the fit is not as low but squared residuals are less than 2.0.

The proposed model described above is similar to that published by Noblett et al. (1987) for the Twin and Crampton Mountain and Garrel Peak plutons which are produced by partial melting of a low-K crustal source with residual plagioclase, followed by FXL. However, this study emphasizes the importance of AFC over FXL based on other geological and geochemical evidence.

Plate Tectonic Model

Over the past 15 years many different interpretations of the Early Proterozoic history for the Southwest have been published (Condie and Budding, 1979; DePaolo, 1981; Van Schmus and Bickford, 1981; Condie, 1982; Bickford, 1988; Hoffman, 1988). It is a widely held theory that during the Early Proterozoic, successive, essentially juvenile, volcanogenic terranes were added to the southern margin of the Archean craton (Wyoming Province). This type of accretion was episodic and spanned the period between 1790 and 1630 m.y. ago (Bickford, 1988). Isotopic data ($^{143}Nd/^{144}Nd$, $^{87}Sr/^{86}Sr$ and $^{206}Pb/^{204}Pb$) strengthen the argument that these terranes were juvenile additions to the crust (DePaolo, 1981; Nelson and DePaolo, 1985; Stacey and Hedlund, 1983, respectively).

In the northern Wet Mountains and southern Front Range, the plate tectonic setting appears to involve two different settings (Reed et al., 1987). In general, the metamorphosed volcanic rocks decrease in abundance from west to east in the study area whereas metasedimentary rocks increase. However, the two groups are complexly interlayered and interfingered in the vicinity of the Crampton and Twin Mountains plutons.

The westernmost pluton (Garrel Peak) intrudes a metavolcanic sequence on its west side and a metamorphosed volcanic-volcaniclastic-sedimentary sequence on the south,

north and east (Taylor and others, 1975). Further to the east the Twin Mountain and Crampton Mountain plutons intrude the same metamorphosed volcanic and sedimentary sequence. Here, the Twin Mountain pluton intrudes into the Blue Ridge quartzite and shale. This unit has important bearing on the interpretations of tectonic setting because its lithologies and textures are suggestive of deposition in a stable, shallow water environment (Noblett et al., 1987; Reuss, 1974). This same sedimentary unit is exposed further east near the Phantom Canyon pluton.

At present, the most widely accepted model explaining amalgamation of the Colorado province is by accretion of magmatic arcs (Condie, 1982; Reed et al., 1987) and is adequate to explain the plate tectonic evolution. In the proposed model, a southeastward migrating, juvenile continental-margin arc system overrides a northwest-dipping subduction zone and bimodal volcanic successions are erupted adjacent to the arc (Fig. 28). A small back-arc basin or a shallow, oceanic basin not closed by successive collisions develops and a quartzite-shale succession accumulates in the basin (Fig. 28a). The basin closes as a result of Andean style orogeny, accompanied by metamorphism of upper amphibolite to lower granulite facies (figure 28b). A thickened continental crust results and partial melting of a felsic granulitic source begins in the lower or middle crust. The magmas begin to fractionate and rise into the upper crust where anatectic melts from the surrounding

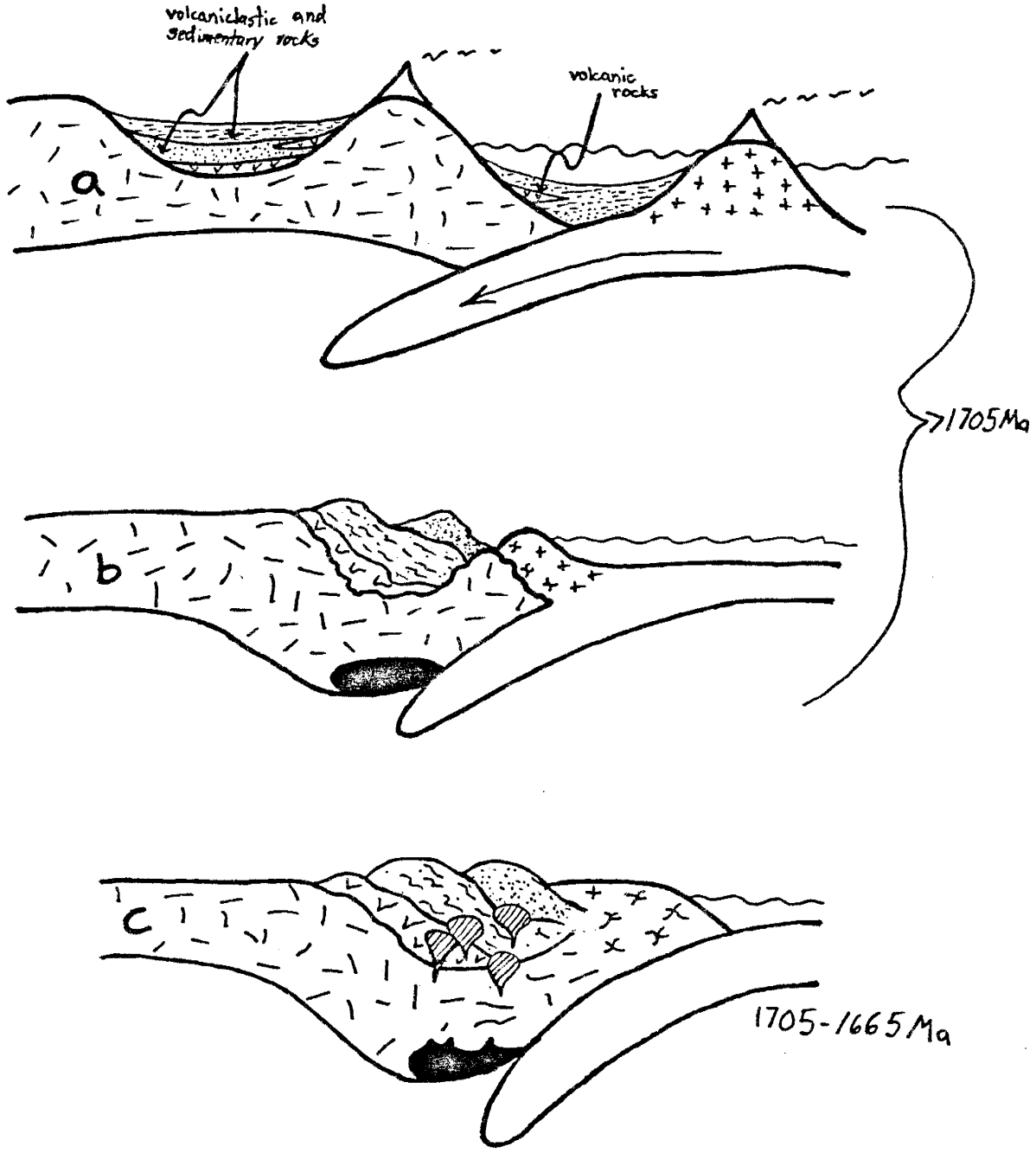

Figure 28. Plate-tectonic model for the evolution of the Wet Mountain plutons (modified after Condie, 1982). A) subduction from the south produces volcanic and volcaniclastic rocks derived from the arc proper. B) Continued subduction and collision induces melting at depth. C) from 1705-1665 Ma granitic plutons are emplaced at mid- to upper crustal depths.

country rock mix with the magmas (figure 28c). Mixing need not be homogeneous, with the exception of the Garrel Peak pluton.

This model is consistent with the absence of Archean crust south of the Wyoming province (Condie, 1981; Condie, 1982). Short crustal-residence times and $^{143}Nd/^{144}Nd$ ratios indicate that the Wet Mountains and southern Front Range plutons were formed from a homogeneous and previously depleted source in the upper mantle 1.8 Ga ago with no identifiable component of older crust (DePaolo, 1981) and thus also appear to favor this model. The stratigraphic relationships between the intruded supracrustal successions (Condie, 1982; Bickford, 1988) and the geologic and geochemical evidence presented in this study suggest that the northern Wet Mountains and southern Front Range plutons were emplaced during the waning stages of arc magmatism.

Conclusions

The following is a summary of the major conclusions:

1) Detailed traverses indicate contact zones 0.75 to 2 km wide which contain migmatites and granitic material injected subparallel to country rock foliation. These zones are typically fine-grained, rich in country rock xenoliths, and show variable degrees of granitization.

2) The Wet Mountain plutons are peraluminous to slightly metaluminous, range in composition from granodiorite to granite, and have geochemical characteristics similar to I-type granitoids. With the exception of the Garrel Peak, the plutons show both a chemical and textural zonation from contact to interior.

3) The tectonic setting changed from a dominantly volcanic arc to a within-plate setting with time.

4) Geochemical data are consistent with a two-stage petrogenetic model. A granodioritic melt is produced by 25-30% batch melting of a felsic granulite, followed by fractional crystallization and about 15% assimilation of surrounding country rock.

Appendix A
Sampling and Sample Preparation

A.1 Sampling

Approximately 55 samples were collected during the two field seasons. One piece was kept for reference and hand sample study, another for thin section study, and the rest used for chemical analysis. The geochemical sample was reduced to small fist sized cobbles at the outcrop to reduce sample contamination. Care was taken to avoid collection of samples with weathered surfaces and those close to pegmatitic or aplitic dikes and xenoliths. Of the samples collected, 37 were used for chemical analysis and of those, 8 for thin section study.

A.2 Sample Preparation

The geochemical sample was first crushed by a large electrical jaw crusher to 1-2 cm. The first few kilograms of each sample were discarded in order to reduce the possibility of contamination from a previous sample. The sample was then rechecked for any oxidized surfaces and/or metal fragments. The above fraction was then reduced to less than 200 mesh by a Bico pulverizer, using porcelain grinding plates followed by a high-speed agate grinder. After each sample was powdered, pure quartz sand was run through the pulverizer to "clean" the grinding plates. These techniques are designed to avoid sample contamination during successive sample preparation.

Appendix B
Analytical Methods

B.1 Instrumental Neutron Activation Analysis

a) Analytical Technique

The trace element abundances of Cs, Ba, Th, U, Ta, Hf, La, Ce, Nd, Sm, Eu, Tb, Yb, Lu, Sc, Cr and Co were determined by instrumental neutron activation analysis (INAA). Approximately 300 mg of each sample powder was sealed in polyethylene vials and irradiated at the Annular Core Research Reactor at Sandia National Laboratory, Albuquerque, New Mexico. All samples were irradiated on 11-11-88 for 10^4 seconds at a power level of 1MW and total deposited energy of 10,000 MJ. Air blowing into the irradiation chamber assures that a constant neutron flux of 2.7×10^{13} passes through each sample. Two counts of released gamma rays were made 7 and 40 days after irradiation using coaxial high purity Ge detectors along with a Nuclear Data 6600 multichannel analyzer and LSI-11 computer. Data for the elements Ba, U, La, Ce, Nd, Sm, Yb, and Lu were taken off the short (7 day) count, Eu, Hf, Ta, and Th were taken off the long (40 day) count, and Sc, Cr, Co, Cs, and Tb were averaged between the long and short counts. Reference samples of fly ash standard NBS-1633 were irradiated in triplicate; two were used as calibrating standards and one was run as an unknown. Other standards analyzed as unknowns were W-2 (USGS), GS-N (ANRT), AN-G (GIT-IWG), and MA-N (GIT-IWG). The data were reduced using

TEABAGS (Trace Element Analysis By Automated Gamma-ray Spectrometry, Lindstom and Korotev, 1982) software.

The Fe measured from INAA was compared with the Fe measured from XRF to further insure each sample saw the same flux gradient. If:

$$[(Fe_{XRF} - Fe_{INAA}) / Fe_{XRF}] > 0.05$$

then the ratio was used as a correction factor and multiplied by each trace-element abundance determined by INAA.

b) Detection Limits

A list of parent nuclides, daughter nuclides, decay energies, detection limits and lower limits of determination are presented in table B.1-1.

c) Accuracy

Tables B.1-2 through B.1-5 present means for standards run as unknown samples. Each standard was counted twice. Calculated accuracy is determined from multiple analyses of standards W-2, GS-N, AN-G, and MA-N.

Table B.1-1 Pertinent information for neutron activation

Parent Nuclide	Daughter Nuclide	KeV	Count Time in days	Detection Limit-ppm	Determination Limit-ppm
Ba-130	Ba-131	373 496*	7	2.0	25.0
Ce-140	Ce-141	145*	7	0.12	1.5
Co-59	Co-60	1173* 1332	7,40	0.05	1.0
Cr-50	Cr-51	320*	7,40	0.3	1.0
Cs-133	Cs-134	605 796	7,40	0.04	0.5
Eu-151	Eu-152	245 344* 779 1408*	40	0.02	0.15
Hf-180	Hf-181	482*	40	0.02	0.1
La-139	La-140	329* 487* 816 1596	7	-	0.9
Lu-176	Lu-177	208*	7	-	0.04
Nd-146	Nd-147	91 531	7		2.5
Sc-45	Sc-46	889* 1121*	40	0.20	0.5
Sm-152	Sm-153	103*	7	-	0.5
Ta-181	Ta-182	1189* 1221* 1231	40	0.002	0.04
Tb-159	Tb-160	299* 879 966* 1178	7,40	0.01	0.05
Th-232	Pa-232	312*	40	0.04	0.1
U-238	Np-239	228 278*	7	0.017	0.020
Yb-174	Yb-175	177* 198	7	0.017	0.020

* = preferred KeV

Table B.1-2 INAA Accuracy, W-2 (Diabase), n=2

Element	Mean	Accepted*	Accuracy (%)@
Ba~	174.0	173.6	0.2
Cs	0.94	1.01	6.9
Th	2.23	2.41	7.5
U	0.47	0.49	4.1
Sc	38.90	35.7	8.9
Cr	100.12	91.51	8.4
Co	49.15	43.15	13.9
Hf	2.8	2.6	7.7
Ta	0.50	0.52	3.8
La~	12.56	10.36	21.2
Ce~	22.69	23.37	2.9
Nd~	12.00	14.0	14.3
Sm	3.72	3.31	12.4
Eu	1.15	1.12	2.7
Tb	0.66	0.66	0.0
Yb	1.91	2.14	10.7
Lu	0.32	0.33	3.0

All values in ppm
n = number of samples analyzed
* = accepted value from Govindaraju (1989)
@ = accuracy = [(mean-accepted)/accepted]x100
~ = abundances are corrected for fission of U
irradiation date: 11/18/88

Table B.1-3 INAA Accuracy, GS-N, n=2

Element	Mean	Accepted*	Accuracy (%)@
Ba~	1540	1400	10.0
Cs	6.5	5.7	14.0
Th	46.36	44.00	5.4
U	9.6	8.0	20.0
Sc	7.8	7.0	11.4
Cr	65.0	55.0	18.2
Co	76.0	65.0	17.0
Hf	7.7	5.9	30.5
Ta	2.8	2.6	7.7
La~	88.3	75.0	17.7
Ce~	149.5	140.0	6.8
Nd~	53.8	50.0	7.6
Sm	8.4	8.2	2.4
Eu	1.8	1.7	5.9
Tb	0.7	0.6	16.6
Yb	2.4	1.7	41.1
Lu	0.20	0.20	0.0

All values in ppm
n = number of samples analyzed
* = accepted value from Govindaraju (1989)
@ = accuracy = [(mean-accepted)/accepted]x100
~ = abundances are corrected for fission of U
irradiation date: 11/18/88

Table B.1-4 INAA Accuracy, AN-G, n=2

Element	Mean	Accepted*	Accuracy (%)@
Ba~	36.9	34.0	8.5
Cs	ND	ND	
Th	ND	ND	
U	ND	ND	
Sc	11.0	10.0	10.0
Cr	55.0	50.0	10.0
Co	30.0	25.0	20.0
Hf	0.47	0.38	23.7
Ta	0.2	0.2	0.0
La~	2.5	2.0	25.0
Ce~	5.7	4.7	21.3
Nd~	2.6	2.4	8.3
Sm	0.9	0.7	28.5
Eu	0.38	0.37	2.7
Tb	0.2	0.2	0.0
Yb	0.82	0.85	3.5
Lu	0.13	0.12	8.3

All values in ppm
n = number of samples analyzed
* = accepted value from Govindaraju (1989)
@ = accuracy = [(mean-accepted)/accepted]x100
~ = abundances are corrected for fission of U
irradiation date: 11/18/88

Table B.1-5 INAA Accuracy, MA-N, n=2

Element	Mean	Accepted*	Accuracy (%)@
Ba~	58	42	38.1
Cs	528	640	17.5
Th	1.0	1.0	0.0
U	9.52	12.0	20.6
Sc	ND	0.23	
Cr	28.1	3.0	>100.0
Co	3.75	1.0	>100.0
Hf	4.0	4.5	11.1
Ta	275.0	290.0	5.2
La~	5.2	0.4	>100.0
Ce~	ND	1.0	
Nd~	ND	ND	
Sm	ND	ND	
Eu	ND	ND	
Tb	0.06	ND	
Yb	ND	ND	
Lu	0.07	ND	

All values in ppm
n = number of samples analyzed
* = accepted value from Govindaraju (1989)
@ = accuracy = [(mean-accepted)/accepted]x100
~ = abundances are corrected for fission of U
irradiation date: 11/18/88

B.2 X-Ray Fluorescence

a) Sample Preparation and Analytical Techniques

Major and trace elements Rb, Ba, Sr, Y, Nb, Ni, Zr, Ga, Pb, and V were determined by X-ray fluorescence (XRF) using the New Mexico Bureau of Mines and Mineral Resources' X-ray lab. The abundances were collected by an automated Rigaku 3064 XRF spectrometer and PDP-11 computer and associated software. Fused disks were prepared (following the methods of Norrish and Hutton, 1969) in order to analyze for major elements (SiO_2, TiO_2, Al_2O_3, Fe_2O_3-T, MgO, Cao, Na_2O, K_2O, MnO, and P_2O_5). These were made from approximately 0.5 grams of powdered sample, about 2.7 grams of Spectroflux-105, and several beads of NH_4NO_3 (oxidizing agent). The mixture was then melted and heated in a Pt crucible for ten minutes and then molded and cooled on a mechanical heated press. Pressed pellets were made (following the methods of Norrish and Chappel, 1977) to analyze for the trace elements Zr, Rb, Ba, Sr, Y, Nb, Cu, Ni, Zn, Ga, and Pb. The pellets were prepared from about 8 grams of powdered sample containing 5 drops of polyvinyl alcohol (binding agent) and presses with a boric acid backing. The mixture was then subjected to 10 tons of pressure under a hydrolic press for five minutes.

b) Detection Limits

A list of measured energies, detection limits and lower limits of determination are given in table B.2-1. Detection

limits give the excited electron shells, minimum concentration of an element needed for qualitative analytical detection. Lower limit of determination describes the minimum concentration of an element needed for quantitative analytical determination.

Table B.2-1 Pertinent information for X-Ray fluorescence analyses

Element	Electron Shell	* KeV Measured	Lower Limit Detection (ppm)	Lower Limit Determination (ppm)
Si	Ka 1,2	1.739	-	100
Ti	Ka 1,2	4.508	-	100
Al	Ka 1,2	1.486	-	100
Fe	Ka 1,2	6.398	-	20
Mg	Ka 1,2	1.253	-	100
Ca	Ka 1,2	3.690	-	100
Na	Ka 1,2	1.041	-	100
K	Ka 1,2	3.312	-	100
Mn	Ka 1,2	5.874	7.0	22
P	Ka 1,2	2.013	-	100
Rb	Ka 1,2	13.373	1.02	3.0
Sr	Ka 1,2	14.140	0.94	3.0
Pb	Ka 1,2	10.550	3.28	9.8
V	Ka 1,2	4.949	-	-
Ni	Ka 1,2	7.471	0.68	2.0
Y	Ka 1,2	14.931	1.08	3.2
Zr	Ka 1,2	15.744	0.78	2.5
Nb	Ka 1,2	16.581	2.0	3.0

* = from White and Johnson (1970)
- = not determined

Appendix C

Table C.1. Chemical analyses of samples from the Garrel Peak pluton.

Table C.1

SAMPLE	GP-3	GP-4	GP-5	GP-6	GP-7	GP-9
SiO2	71.58	68.85	72.87	72.96	73.43	70.25
TiO2	0.37	0.63	0.29	0.37	0.36	0.53
Al2O3	13.62	13.97	13.96	13.56	13.62	13.75
Fe2O3-T	3.30	4.87	2.78	3.14	3.47	4.43
MgO	0.53	0.70	0.49	0.54	0.34	0.55
CaO	1.35	2.04	1.32	1.31	1.40	1.77
Na2O	3.64	3.30	3.41	3.03	3.39	3.01
K2O	4.70	4.61	5.02	4.71	4.82	4.83
MnO	0.06	0.12	0.06	0.07	0.09	0.11
P2O5	0.06	0.15	0.07	0.09	0.09	0.11
LOI	0.52	0.41	0.40	0.44	0.29	0.49
TOTAL	99.73	99.65	100.66	100.22	101.30	99.82
Rb	92	113	203	158	182	137
Ba	763	809	727	728	648	761
Cs	0.6	2.8	3.1	2.2	2.2	0.7
Sr	92	147	112	161	84	122
Pb	9	14	18	23	24	51
Th	12.1	9.3	24.8	24.7	32.9	17.4
U	3.4	3.5	4.7	3.4	2.6	2.5
Ga	22	22	22	17	19	19
Sc	5	13	5	4	7	12
V	62	28	21	21	8	16
Cr	15	8	2	6	6	4
Co	4	5	3	4	2	3
Ni	8	1	ND	2	4	5
Y	79	111	57	36	82	98
Zr	348	459	232	249	354	449
Nb	21	34	23	20	24	27
Hf	10.9	14.1	8.3	9.1	12.1	13.9
Ta	1.1	1.3	2.0	1.6	1.7	1.6
La	84	62	60	98	101	87
Ce	163	152	122	163	206	165
Nd	78	88	48	62	78	73
Sm	17.1	20.0	10.7	11.6	15.5	17.9
Eu	1.63	2.29	1.06	1.39	1.79	2.24
Tb	2.30	2.88	1.46	1.36	2.21	2.89
Yb	5.8	9.0	6.2	3.7	7.9	8.3
Lu	0.94	1.47	0.96	0.53	1.16	1.33

Table C.1

SAMPLE	GP-3	GP-4	GP-5	GP-6	GP-7	GP-9
Mg Number	26.5	24.3	28.4	28.0	18.1	21.9
K2O/Na2O	1.29	1.39	1.47	1.56	1.42	1.60
K2O+Na2O	8.3	7.9	8.4	7.7	8.2	7.8
K2O/MgO	8.9	6.6	10.2	8.7	14.1	8.7
FeO-T/MgO	5.60	6.30	5.10	5.20	9.20	7.20
Rb/Sr	1.01	0.77	1.81	0.99	2.17	1.12
Ba/Sr	8.33	5.53	6.51	4.52	7.71	6.22
Rb/Zr	0.3	0.2	0.9	0.6	0.5	0.3
Ba/La	9.0	13.0	12.1	7.4	6.4	8.7
K/Na	1.4	1.6	1.6	1.7	1.6	1.8
K/Rb	424	339	206	247	220	293
Eu/Sm	0.1	0.1	0.1	0.1	0.1	0.1
(Eu/Eu*)n	0.3	0.4	0.3	0.4	0.4	0.4
(La/Yb)n	8.8	4.2	5.9	16.1	7.8	6.4
A/CNK	1.0	1.0	1.0	1.1	1.0	1.0
A/NK	1.2	1.3	1.3	1.3	1.3	1.4

FeO-T = Fe2O3-T * 0.899
(Eu/Eu*)n = (Eu/.087)/[(Sm/.231)-(((Sm/.231)-(Tb/.058))/3)]
(La/Yb)n = (La/.367)/(Yb/.248)
A/CNK = Al2O3/(CaO+Na2O+K2O) molar
A/NK = Al2O3/(Na2O+K2O) molar
Total Fe reported as Fe2O3
ND = not detected
MAJOR ELEMENTS reported in wt. %
TRACE ELEMENTS reported in parts per million (ppm)

Table C.1

SAMPLE	GP-10	GP-11	GP-12	GP-13	GP-14	GP-15
SiO2	72.70	70.79	68.94	69.51	72.39	73.72
TiO2	0.37	0.55	0.78	0.60	0.42	0.25
Al2O3	16.08	13.74	13.73	14.04	14.23	13.20
Fe2O3-T	3.45	4.27	5.53	4.58	3.22	2.31
MgO	0.49	0.77	0.78	0.70	0.57	0.25
CaO	1.25	1.87	2.21	1.61	1.82	0.77
Na2O	3.95	3.74	3.30	3.03	3.43	3.03
K2O	5.22	5.15	4.37	5.30	4.62	5.58
MnO	0.07	0.10	0.15	0.10	0.08	0.06
P2O5	0.06	0.14	0.18	0.14	0.09	0.04
LOI	0.42	0.39	0.30	0.47	0.34	0.29
TOTAL	104.04	101.51	100.27	100.07	101.20	99.50
Rb	92	185	127	181	173	216
Ba	887	833	799	886	740	321
Cs	1.4	2.7	3.1	5.5	2.7	2.5
Sr	97	147	151	134	132	56
Pb	6	51	16	52	21	25
Th	13.4	10.7	10.4	12.2	28.3	13.8
U	3.3	2.1	3.2	3.8	4.6	2.6
Ga	22	18	22	21	18	19
Sc	4	11	15	12	6	5
V	19	25	28	28	27	8
Cr	4	8	5	7	8	3
Co	3	4	5	4	4	2
Ni	ND	ND	ND	5	5	ND
Y	69	88	80	72	68	63
Zr	381	163	503	379	248	238
Nb	21	ND	26	25	24	14
Hf	12.9	12.9	16.0	12.4	9.4	8.3
Ta	1.9	1.1	1.5	1.2	1.9	0.7
La	95	74	53	61	89	55
Ce	188	160	117	121	180	114
Nd	89	76	58	62	69	52
Sm	18.5	15.8	15.2	14.4	13.5	11.3
Eu	1.75	2.15	2.44	2.42	1.56	1.15
Tb	2.26	2.34	2.34	2.25	1.90	1.79
Yb	6.1	2.4	6.7	5.7	7.1	4.7
Lu	0.98	1.13	1.08	0.92	1.03	0.69

Table C.1

SAMPLE	GP-10	GP-11	GP-12	GP-13	GP-14	GP-15
Mg Number	24.1	28.8	24.1	25.4	28.5	19.7
K2O/Na2O	1.32	1.38	1.33	1.75	1.35	1.85
K2O+Na2O	9.2	8.9	7.7	8.3	8.0	8.6
K2O/MgO	10.7	6.7	5.6	7.6	8.1	22.2
FeO-T/MgO	6.40	5.00	6.40	5.90	5.10	8.20
Rb/Sr	0.95	1.26	0.84	1.35	1.31	3.82
Ba/Sr	9.16	5.67	5.28	6.61	5.59	5.69
Rb/Zr	0.2	1.1	0.3	0.5	0.7	0.9
Ba/La	9.3	11.3	15.1	14.5	8.3	5.8
K/Na	1.5	1.5	1.5	2.0	1.5	2.1
K/Rb	470	231	286	243	221	215
Eu/Sm	0.1	0.1	0.2	0.2	0.1	0.1
(Eu/Eu*)n	0.3	0.4	0.5	0.5	0.4	0.3
(La/Yb)n	9.4	18.8	4.8	6.5	7.7	7.1
A/CNK	1.1	0.9	1.0	1.0	1.0	1.1
A/NK	1.3	1.2	1.4	1.3	1.3	1.2

Table C.2. Chemical analyses of samples from the Crampton Mountain pluton.

Table C.2

SAMPLE	CM-1	CM-2	CM-3	CM-4	CM-5	CM-6
SiO2	71.50	60.20	65.55	68.10	66.81	68.90
TiO2	0.57	1.49	0.83	0.64	0.78	0.74
Al2O3	14.04	16.40	16.08	15.62	15.22	14.10
Fe2O3-T	3.73	9.82	5.30	3.92	5.39	4.89
MgO	0.90	2.30	1.29	1.02	1.32	1.24
CaO	2.52	4.89	3.54	2.70	2.99	2.91
Na2O	2.47	2.84	3.04	3.20	2.52	2.32
K2O	3.85	2.34	4.02	4.21	4.17	3.33
MnO	0.09	0.16	0.11	0.08	0.09	0.10
P2O5	0.08	0.37	0.21	0.17	0.20	0.19
LOI	0.55	0.59	0.48	0.36	0.71	0.93
TOTAL	100.29	101.42	100.44	100.02	100.20	99.64
Rb	158	81	153	110	101	98
Ba	474	1070	1168	1025	1146	720
Cs	4.7	3.5	7.6	3.2	3.5	2.3
Sr	100	207	178	169	189	159
Pb	26	20	21	23	19	20
Th	15.8	10.7	3.7	4.8	9.4	6.0
U	1.7	1.8	1.9	1.1	2.0	1.2
Ga	19	24	21	16	20	19
Sc	12	26	14	11	16	13
V	38	118	59	42	66	50
Cr	18	27	14	6	12	12
Co	7	20	11	8	11	9
Ni	8	19	20	5	7	10
Y	55	54	37	31	35	33
Zr	169	500	253	224	288	271
Nb	14	23	16	13	13	14
Hf	6.2	14.4	8.2	7.3	8.9	8.8
Ta	1.1	1.0	0.9	0.8	0.7	0.7
La	45	58	31	18	46	26
Ce	85	122	56	36	85	51
Nd	38	59	26	16	40	25
Sm	9.1	12.4	6.0	4.5	8.4	6.5
Eu	1.39	2.63	1.96	1.58	2.18	1.76
Tb	1.49	1.60	0.95	0.77	1.09	0.97
Yb	4.6	4.1	2.8	2.4	3.3	2.5
Lu	0.72	0.61	0.44	0.35	0.52	0.36

Table C.2

SAMPLE	CM-1	CM-2	CM-3	CM-4	CM-5	CM-6
Mg Number	35.2	34.5	35.4	36.8	35.6	36.3
K2O/Na2O	1.56	0.82	1.32	1.32	1.66	1.43
K2O+Na2O	6.3	5.2	7.1	7.4	6.7	5.6
K2O/MgO	4.3	1.0	3.1	4.1	3.2	2.7
FeO-T/MgO	3.7	3.8	3.7	3.5	3.7	3.6
P2O5/Th	0.0	0.0	0.1	0.0	0.0	0.0
Rb/Sr	1.58	0.39	0.86	0.65	0.54	0.61
Ba/Sr	4.74	5.17	6.57	6.06	6.08	4.52
Rb/Zr	0.9	0.2	0.6	0.5	0.4	0.4
Ba/La	10.6	18.5	37.9	56.0	24.9	28.1
K/Na	1.7	0.9	1.5	1.5	1.9	1.6
K/Rb	203	240	218	319	343	283
Eu/Sm	0.2	0.2	0.3	0.4	0.3	0.3
(Eu/Eu*)n	0.5	0.7	1.0	1.0	0.8	0.8
(La/Yb)n	5.9	8.6	6.6	4.7	8.4	6.3
A/CNK	1.1	1.0	1.0	1.1	1.1	1.1
A/NK	1.7	2.3	1.7	1.6	1.8	1.9

FeO-T = Fe2O3-T * 0.899
Eu/Eu* = (Eu/.087)/[(Sm/.231) - (((Sm/.231)-(Tb/.058))/3)]
A/CNK = Al2O3/(CaO+Na2O+K2O) molar
A/NK = Al2O3/(Na2O+K2O) molar
(La/Yb)n = (La/.367)/(Yb/.248)
Total Fe reported as Fe2O3
ND = not detected
MAJOR ELEMENTS reported as wt. %
TRACE ELEMENTS reported in parts per million (ppm)

Table C.2

SAMPLE	CM-7	CM-8
SiO2	60.15	62.89
TiO2	1.53	1.26
Al2O3	15.18	15.86
Fe2O3-T	10.08	8.29
MgO	2.40	2.01
CaO	4.27	4.42
Na2O	2.11	2.38
K2O	3.13	2.85
MnO	0.16	0.13
P2O5	0.38	0.30
LOI	0.45	0.49
TOTAL	99.82	100.88
Rb	125	114
Ba	950	824
Cs	6.7	4.9
Sr	173	185
Pb	18	21
Th	11.4	10.2
U	1.6	1.7
Ga	20	20
Sc	27	22
V	126	105
Cr	30	27
Co	21	17
Ni	19	14
Y	58	54
Zr	469	383
Nb	24	20
Hf	14.0	11.4
Ta	0.9	1.0
La	66	45
Ce	117	95
Nd	59	44
Sm	12.0	10.2
Eu	2.80	2.22
Tb	1.59	1.46
Yb	4.2	4.1
Lu	0.64	0.59

Table C.2

SAMPLE	CM-7	CM-8
Mg Number	34.8	35.3
K2O/Na2O	1.48	1.20
K2O+Na2O	5.2	5.2
K2O/MgO	1.3	1.4
FeO-T/MgO	3.8	3.7
P2O5/Th	0.0	0.0
Rb/Sr	0.72	0.62
Ba/Sr	5.49	4.45
Rb/Zr	0.3	0.3
Ba/La	14.5	18.3
K/Na	1.7	1.3
K/Rb	208	207
Eu/Sm	0.2	0.2
(Eu/Eu*)n	0.7	0.7
(La/Yb)n	9.4	6.6
A/CNK	1.0	1.1
A/NK	2.2	2.3

Table C.3. Chemical analyses of samples from the Twin Mountain pluton.

Table C.3

SAMPLE	TP-1	TP-2	TM-2	TM-3	TM-8	TM-9
SiO2	66.85	76.03	72.25	63.84	71.08	71.63
TiO2	0.82	0.15	0.40	0.91	0.48	0.29
Al2O3	15.41	12.69	14.44	16.43	16.83	15.45
Fe2O3-T	4.87	1.32	2.64	5.64	2.98	1.86
MgO	1.38	0.38	0.77	1.45	0.80	0.53
CaO	3.35	1.52	2.26	3.47	2.29	0.25
Na2O	2.25	1.53	1.97	2.14	5.02	0.82
K2O	3.84	5.42	4.81	4.72	1.99	9.01
MnO	0.08	0.04	0.05	0.09	0.08	0.05
P2O5	0.18	0.02	0.09	0.21	0.13	0.13
LOI	0.88	0.56	0.62	0.75	0.71	0.65
TOTAL	99.90	99.65	100.28	99.64	102.39	100.67
Rb	124	119	133	143	210	511
Ba	993	432	495	1440	175	961
Cs	3.9	1.2	3.1	4.1	21.0	26.9
Sr	183	116	120	191	85	106
Pb	22	28	27	22	21	38
Th	17.4	6.9	20.9	14.1	16.1	12.3
U	1.2	0.8	1.5	1.2	2.2	2.2
Ga	19	12	15	24	20	13
Sc	14	3	9	16	11	8
V	55	11	25	72	34	25
Cr	21	8	7	17	12	6
Co	10	2	5	11	5	4
Ni	8	4	3	7	6	3
Y	28	10	50	33	22	15
Zr	237	81	142	261	160	112
Nb	14	4	10	16	38	27
Hf	7.4	3.3	5.5	9.4	4.9	4.1
Ta	0.6	0.1	0.4	0.8	4.2	2.5
La	65	25	56	55	44	35
Ce	118	45	119	97	100	66
Nd	52	17	51	42	37	27
Sm	10.4	3.5	11.3	9.0	7.8	5.9
Eu	2.49	1.99	1.78	2.62	1.17	1.17
Tb	1.07	0.38	1.54	1.06	0.89	0.71
Yb	2.1	0.9	4.1	2.3	1.9	1.6
Lu	0.28	0.12	0.57	0.33	0.24	0.21

Table C.3

SAMPLE	TP-1	TP-2	TM-2	TM-3	TM-8	TM-9
Mg Number	38.9	39.6	39.8	36.6	37.5	39.1
K2O/Na2O	1.71	3.55	2.45	2.20	0.40	11.01
K2O+Na2O	6.1	6.9	6.8	6.9	7.0	9.8
K2O/MgO	2.8	14.1	6.2	3.3	2.5	16.9
FeO-T/MgO	3.200	3.100	3.100	3.500	3.400	3.100
Rb/Sr	0.7	1.0	1.1	0.7	2.5	4.8
Ba/Sr	5.41	3.74	4.11	7.56	2.06	9.04
Rb/Zr	0.524	1.473	0.939	0.547	1.313	4.572
Ba/La	15.3	17.2	8.9	26.4	4.0	27.3
K/Na	1.9	4.0	2.7	2.5	0.4	12.3
K/Rb	257.0	377.0	300.0	274.0	79.0	146.0
Eu/Sm	0.2	0.6	0.2	0.3	0.1	0.2
(Eu/Eu*)n	0.8	1.8	0.5	0.9	0.5	0.6
(La/Yb)n	18.6	17.7	8.3	14.4	13.6	13.7
A/CNK	1.1	1.1	1.2	1.1	1.2	1.3
A/NK	12.0	1.5	1.7	1.9	1.6	1.4

FeO-T = Fe2O3-T * 0.899
(Eu/Eu*)n = (Eu/.087)/[(Sm/.231)+(((Sm/.231)-(Tb/.058))/3)]
(La/Yb)n = (La/.367)/(Yb/.248)
A/CNK = Al2O3/(CaO+Na2O+K2O) molar
A/NK = Al2O3/(Na2O+K2O) molar
Total Fe reported as Fe2O3
ND = not detected
MAJOR ELEMENTS reported in wt %
TRACE ELEMENTS reported in parts per million (ppm)

Table C.3

SAMPLE	TM-10	TM-11	TM-12
SiO2	61.15	69.78	75.40
TiO2	1.33	0.57	0.20
Al2O3	16.46	13.97	13.53
Fe2O3-T	8.93	3.71	1.29
MgO	2.21	0.87	0.35
CaO	4.08	2.61	1.78
Na2O	2.56	2.39	2.24
K2O	2.43	3.93	4.81
MnO	0.13	0.06	0.03
P2O5	0.30	0.14	0.03
LOI	0.58	1.17	0.64
TOTAL	100.16	99.20	100.29
Rb	163	119	106
Ba	865	611	516
Cs	10.7	4.1	1.8
Sr	172	127	119
Pb	18	18	32
Th	15.3	4.8	10.0
U	1.5	2.0	1.3
Ga	23	20	13
Sc	25	10	5
V	122	42	10
Cr	36	12	7
Co	18	7	2
Ni	12	4	5
Y	52	31	47
Zr	350	224	86
Nb	23	11	5
Hf	11.0	7.3	3.5
Ta	1.0	0.4	0.2
La	57	17	26
Ce	116	32	54
Nd	54	16	23
Sm	11.6	4.7	6.1
Eu	2.31	1.61	1.68
Tb	1.56	0.85	1.32
Yb	3.3	2.0	4.5
Lu	0.47	0.32	0.67

Table C.3

SAMPLE	TM-10	TM-11	TM-12
Mg Number	35.7	34.5	37.9
K2O/Na2O	0.95	1.65	2.15
K2O+Na2O	5.0	6.3	7.1
K2O/MgO	1.1	4.5	13.8
FeO-T/MgO	3.600	3.800	3.300
Rb/Sr	0.9	0.9	0.9
Ba/Sr	5.04	4.82	4.32
Rb/Zr	0.467	0.532	1.233
Ba/La	15.1	36.0	20.0
K/Na	1.1	1.8	2.4
K/Rb	123.0	274.0	377.0
Eu/Sm	0.2	0.3	0.3
(Eu/Eu*)n	0.6	1.0	0.8
(La/Yb)n	10.5	5.2	3.5
A/CNK	1.2	1.1	1.1
A/NK	2.4	1.7	1.5

Table C.4

SAMPLE	PC-1	PC-3	PC-4	PC-5	PC-8	PC-11
SiO2	73.31	67.93	60.47	69.73	73.87	60.12
TiO2	0.21	0.85	1.48	0.69	0.23	0.98
Al2O3	13.97	14.41	14.34	13.31	13.60	18.39
Fe2O3-T	1.46	4.93	8.79	4.13	1.77	5.16
MgO	0.34	1.23	2.88	0.96	0.40	1.38
CaO	1.12	2.45	2.80	2.57	1.11	3.17
Na2O	2.58	2.87	2.10	3.33	2.85	3.54
K2O	5.71	4.90	6.20	3.95	5.02	5.77
MnO	0.04	0.11	0.17	0.08	0.04	0.09
P2O5	0.11	0.33	0.57	0.27	0.11	0.41
LOI	0.48	0.53	0.69	0.35	0.52	0.53
TOTAL	99.33	100.54	100.50	99.37	99.52	99.56
Rb	245	197	288	155	225	118
Ba	484	1247	1657	1030	423	8202
Cs	5.8	4.3	8.3	4.7	3.7	2.2
Sr	123	258	245	236	120	665
Pb	36	24	31	20	35	28
Th	13.6	12.4	20.1	10.8	14.7	2.8
U	11.0	4.1	8.0	3.4	5.3	1.4
Ga	13	15	19	15	18	24
Sc	6	14	26	11	9	15
V	15	49	94	40	16	73
Cr	8	6	11	8	5	ND
Co	2	8	12	6	2	5
Ni	8	5	ND	ND	ND	ND
Y	36	65	131	57	39	37
Zr	110	345	651	298	119	617
Nb	15	29	53	23	20	13
Hf	3.7	11.1	19.7	9.0	4.3	18.2
Ta	1.5	1.9	3.3	1.8	1.4	0.6
La	39	82	123	57	40	66
Ce	71	177	279	130	73	133
Nd	30	75	135	61	30	89
Sm	5.8	14.2	27.6	12.3	6.4	13.9
Eu	1.05	2.69	3.69	2.19	1.04	4.97
Tb	1.04	1.83	3.79	1.63	1.06	1.32
Yb	4.1	5.9	10.9	4.9	4.3	2.8
Lu	0.66	0.90	1.60	0.72	0.66	0.43

Table C.4

SAMPLE	PC-1	PC-3	PC-4	PC-5	PC-8	PC-11
Mg Number	34.6	36.0	42.4	34.4	33.9	37.6
K2O/Na2O	2.21	1.71	2.95	1.19	1.76	1.63
K2O+Na2O	8.3	7.8	8.3	7.3	7.9	9.3
K2O/MgO	16.6	4.0	2.2	4.1	12.4	4.2
FeO-T/MgO	3.800	3.600	2.700	3.900	3.900	3.400
Rb/Sr	2.00	0.76	1.18	0.66	1.86	0.18
Ba/Sr	3.943	4.829	6.774	4.367	3.516	12.331
Rb/Zr	2.2	0.6	0.4	0.5	1.9	0.2
Ba/La	12.4	15.2	13.5	18.1	10.6	124.8
K/Na	2.5	1.9	3.3	1.3	2.0	1.8
K/Rb	193.0	207.0	179.0	211.0	185.0	404.0
Eu/Sm	0.2	0.2	0.1	0.2	0.2	0.4
(Eu/Eu*)n	0.5	0.6	0.4	0.6	0.5	1.2
(La/Yb)n	5.7	8.4	6.8	7.1	5.6	14.4
A/CNK	1.1	1.0	0.9	0.9	1.1	1.0
A/NK	1.3	1.4	1.4	1.4	1.3	1.5

FeO-T = Fe2O3-T * 0.899
(Eu/Eu*)n = (Eu/.087)/[(Sm/.231)-(((Sm/.231)-(Tb/.058))/3)]
(La/Yb)n = (La/.367)/(Yb/.248)
A/CNK = Al2O3/(CaO+Na2O+K2O) molar
A/NK = Al2O3/(Na2O+K2O) molar
Toltal Fe reported as Fe2O3
ND = not detected
MAJOR ELEMENTS reported as %
TRACE ELEMENTS reported in part per million (ppm)

Table C.4. Chemical analyses of samples from the Phantom Canyon pluton.

Appendix D
CIPW Normative Minerals
(in weight percent)

Fe2O3-T determined by XRF.
Fe2O3 = 0.135 * Fe2O3-T
FeO = 0.778 * Fe2O3-T

Table D.1 Garrel Peak pluton

	GP-3	GP-4	GP-5	GP-6	GP-7	GP-9	GP-10
quartz	27.43	24.79	28.98	32.44	29.93	27.88	23.85
corundum	0.23	0.22	0.70	1.30	0.49	0.61	1.73
orthoclase	28.08	27.54	29.65	27.99	28.25	28.83	29.85
albite	31.16	28.28	28.83	25.74	28.47	25.76	32.37
anorthite	6.37	9.21	6.06	5.98	6.33	8.18	5.65
diopside	0.00	0.00	0.00	0.00	0.00	0.00	0.00
hypersthene	5.22	7.42	4.53	5.02	4.96	6.60	5.10
magnetite	0.65	0.96	0.54	0.62	0.67	0.88	0.65
ilmenite	0.71	1.22	0.55	0.70	0.69	1.03	0.67
apatite	0.15	0.36	0.16	0.20	0.21	0.24	0.13
TOTAL	100.00	100.00	100.00	100.00	100.00	100.00	100.00

	GP-11	GP-12	GP-13	GP-14	GP-15
quartz	22.81	24.95	25.34	28.44	31.92
corundum	0.00	0.01	0.74	0.49	0.89
orthoclase	30.19	24.97	31.59	27.14	33.32
albite	31.40	28.02	25.80	28.82	25.86
anorthite	5.46	9.79	7.14	8.40	3.59
diopside	2.44	0.00	0.00	0.00	0.00
hypersthene	5.52	8.26	7.02	5.09	3.39
magnetite	0.83	1.09	0.90	0.63	0.46
ilmenite	1.04	1.49	1.15	0.78	0.48
apatite	0.31	0.42	0.32	0.21	0.09
TOTAL	100.00	100.00	100.00	100.00	100.00

Table D.2 Twin Mountain pluton

	TM-2	TM-3	TM-8	TM-9	TM-10	TM-11	TM-12
quartz	35.51	21.90	26.64	30.53	21.55	33.27	39.23
corundum	2.10	2.01	2.52	4.20	2.95	1.41	1.47
orthoclase	28.60	28.31	11.62	53.30	14.52	23.78	28.57
albite	16.74	18.41	41.89	6.93	21.96	20.67	19.03
anorthite	10.71	16.15	10.37	0.43	18.52	12.31	8.69
diopside	0.00	0.00	0.00	0.00	0.00	0.00	0.00
hypersthene	4.86	9.86	5.19	3.40	15.49	6.37	2.31
magnetite	0.52	1.12	0.58	0.36	1.77	0.74	0.26
ilmenite	0.76	1.75	0.91	0.56	2.55	1.11	0.38
apatite	0.20	0.49	0.28	0.29	0.71	0.34	0.06
TOTAL	100.00	100.00	100.00	100.00	100.00	100.00	100.00

	TP-1	TP-2
quartz	28.41	42.39
corundum	1.94	1.62
orthoclase	23.00	32.35
albite	19.27	13.04
anorthite	15.65	7.47
diopside	0.00	0.00
hypersthene	8.77	2.54
magnetite	0.97	0.26
ilmenite	1.57	0.28
apatite	0.42	0.05
TOTAL	100.00	100.00

Table D.3 Phantom Canyon pluton

	PC-1	PC-3	PC-4	PC-5	PC-8	PC-11
quartz	33.56	24.03	11.65	27.73	34.89	7.43
corundum	1.81	0.73	0.45	0.00	1.74	1.56
orthoclase	34.15	29.07	36.98	23.63	29.98	34.56
albite	22.12	24.40	17.94	28.52	24.42	30.40
anorthite	4.85	10.02	10.28	9.86	4.85	13.24
diopside	0.00	0.00	0.00	1.06	0.00	0.00
hypersthene	2.54	8.40	16.79	6.42	3.07	8.91
magnetite	0.29	0.96	1.74	0.82	0.35	1.03
ilmenite	0.41	1.62	2.84	1.32	0.45	1.90
apatite	0.27	0.77	1.33	0.64	0.25	0.97
TOTAL	100.00	100.00	100.00	100.00	100.00	100.00

Table D.4 Crampton Mountain pluton

	CM-1	CM-2	CM-3	CM-4	CM-5	CM-6	CM-7
quartz	34.35	16.94	21.01	24.80	25.90	33.23	19.51
corundum	1.45	1.18	0.79	1.31	1.62	1.88	1.48
orthoclase	22.88	13.84	23.85	25.07	24.91	20.00	18.75
albite	20.98	24.04	25.86	27.23	21.54	19.98	18.15
anorthite	12.02	21.86	16.29	12.38	13.63	13.43	19.00
diopside	0.00	0.00	0.00	0.00	0.00	0.00	0.00
hypersthene	6.41	16.52	9.09	6.83	9.36	8.64	17.29
magnetite	0.74	1.92	1.04	0.77	1.07	0.97	2.00
ilmenite	1.09	2.84	1.58	1.22	1.50	1.43	2.94
apatite	0.18	0.86	0.49	0.39	0.47	0.44	0.88
TOTAL	100.00	100.00	100.00	100.00	100.00	100.00	100.00

	CM-8
quartz	22.47
corundum	1.55
orthoclase	16.87
albite	20.21
anorthite	20.04
diopside	0.00
hypersthene	14.13
magnetite	1.63
ilmenite	2.40
apatite	0.70
TOTAL	100.00

Appendix E
Distribution Coefficients

Intermediate Kds are used for batch melting of a felsic granulite source and felsic Kds are used for AFC of the Wet Mountain granitoids. Kds are compiled from Dostal et al. (1983), Drake and Weill (1975), Fujimaki and Tatsumoto (1984), Irving and Frey (1984), Nash and Crecraft (1985), and Watson (1980).

Table E.1 Felsic Kds (solid/liquid)

	Plag	Biot	Ksp	Zir	Sph	Apt	Aln
Rb	0.04	2.2	0.35	0	0	0	0
Ba	0.3	6.0	6.0	0	1	2	50
Sr	4.0	0.12	4.0	0	0	2	100
Y	0.1	0.03	0.1	60	0	40	100
Zr	0.1	2.0	0.1	100	65	0.1	2
Nb	0.06	5.0	0.05	50	0	0.1	2
Ta	0.05	1.5	0.05	50	0	0.1	2
La	0.3	0.11	0.05	2	32	20	2500
Ce	0.25	0.32	0.04	2.5	60	35	2000
Nd	0.2	0.3	0.025	2.2	0	57	1700
Sm	0.13	0.25	0.02	3.1	0	63	1300
Eu	1.5	0.25	1.1	3.5	0	30	800
Tb	0.6	0.35	0.006	100	0	20	500
Yb	0.05	0.44	0.01	200	0	25	100
Lu	0.05	0.3	0.006	200	0	25	100

Table E.2 Intermediate Kds (solid/liquid)

	Ksp	Plag	Biot	Zir	Sph	Apt	Aln
Rb	0.35	0.05	3.3	0	0	0	0
Ba	5.0	0.4	10	0	1	0	0
Sr	4.0	2.0	0.12	0	100	0	0
Y	0.1	0.03	0.03	60	30	20	100
Zr	0.03	0.03	1.2	100	65	0.1	2
Nb	0.05	0.03	5	50	6	0.1	2
Ta	0.05	0.08	1	50	17	0.1	2
La	0.05	0.15	0.03	2	32	20	2500
Ce	0.04	0.12	0.04	2.5	60	35	2000
Nd	0.025	0.08	0.04	2.2	180	57	1700
Sm	0.02	0.067	0.06	3.1	200	63	1300
Eu	1.1	0.8	0.15	3.5	120	30	800
Tb	0.006	0.06	0.16	100	210	20	500
Yb	0.01	0.07	0.18	200	190	25	100
Lu	0.006	0.06	0.2	200	115	25	100

Appendix F
Modes, Melting, and Crystallization Proportions

Table F.1 Modes and melting proportions

Felsic Granulite

	Mode %	Melt %
Biotite	5	4
K-feldspar	8	34
Plagioclase (An_{35})	57	31
Quartz	19	30
Orthopyroxene	5	-
Clinopyroxene	4	-
Magnetite	2	1

Tonalite

	Mode %	Melt %
Plagioclase (An_{35})	57	31
Biotite	10	4
K-feldspar	8	34
Quartz	22	30
Magnetite	2	1
Zircon	0.1	0.1
Allanite	0.005	0.005
Apatite	0.6	0.1
Sphene	0.05	0.1

Lherzolite

	Mode %	Melt %
Olivine	60	25
Orthopyroxene	25	20
Clinopyroxene	15	55

Table F.2 Crystallization mineral proportions

Basalt to dacite (F=0.3)

	proportion %
Plagioclase	65
Olivine	5
Clinopyroxene	25
Magnetite	5

Dacite to rhyolite (F=0.4)

	proportion %
Plagioclase	71
Clinopyroxene	10
Orthopyroxene	10
Quartz	5
Magnetite	4
Zircon	0-0.2
Apatite	0.1-0.3

Modes and melt percentages compiled by Condie (unpublished data).

Appendix G
Computer Programs

G.1 Major Elements

Major element modelling was preformed on MIXFRA, a major element mixing program written by M.W. Knoper at New Mexico Tech. This program utilizes the least-squares approximation set forth by Bryan et al., (1969). The example used is the first stage of the proposed two-stage petrogenetic model which involves batch melting of a felsic granulite to produce a granodioritic melt. GD is an average granodiorite from Hyndman (1985), QTZ=quartz, BIO=biotite mica-Fe from Govindaraju (1989), PLAG=plagioclase JF-1 from Govindaraju (1989), KSP=K-feldspar NBS570a from Govindaraju (1989), MGT=magnetite from Govindaraju (1989), GRAN is the average felsic granulite from Calabria, Italy Maccarrone et al. (1983). Complete description of this least-squares mixing process can be found in Bryan et al., (1969).

Table G.1 [MIXFRA]:Least-squares mixing (Bryan et al., 1969)

--> BATCH MELT OF FELSIC GRANULITE

Attempt: 1

Input data:

	GD	QTZ	BIO	PLAG	KSP	MG	GRAN
SiO2	66.86	%100	35.51	65.63	67.39	0.00	64.02
TiO2	0.53	0.00	2.58	0.00	0.01	25.00	1.09
Al2O3	16.02	0.00	20.13	18.55	18.01	0.00	15.38
Fe2O3	4.78	0.00	26.48	0.06	0.07	75.00	9.46
MnO	0.08	0.00	0.36	0.00	0.00	0.00	0.14
MgO	1.67	0.00	4.70	0.00	0.00	0.00	3.18
CaO	3.44	0.00	0.44	0.09	0.11	0.00	1.98
Na2O	3.54	0.00	0.31	2.48	2.54	0.00	2.08
K2O	2.93	0.00	9.03	13.19	11.87	0.00	2.58
P2O5	0.15	0.00	0.46	0.00	0.00	0.00	0.09
Total	100.00	100.00	100.00	100.00	100.00	100.00	100.00

Table G.1 continued

Output data:

	Y Obs.	Y Est.	Residuals	Components	Proportions
SiO2	64.02	64.14	-0.1200	GD	0.6563
TiO2	1.09	0.52	0.5719	QTZ	0.0912
Al2O3	15.38	15.37	0.0121	BIO	0.3394
Fe2O3	9.46	9.65	-0.1917	PLAG	1.8891
MnO	0.14	0.17	-0.0267	KSP	1.9254
MgO	3.18	2.52	0.6562	MG	0.0269
CaO	1.98	2.10	-0.1246		
Na2O	2.08	2.28	-0.1988		
K2O	2.58	2.63	-0.0461		
P2O5	0.09	0.24	-0.1495	GRAN = Y	
Total	100.00	99.62	Squared Residuals =		0.8893

G.2 Trace Elements

Trace element modelling was preformed using MODULUS ver. 2.21, an igneous petrogenetic computer program written by M.W. Knoper at New Mexico Tech. The program is written for use with LOTUS 1-2-3. Table G.2a is a print-out of the batch melting sub-program of MODULUS and uses equations set forth in Allegre and Minster (1978). Table G.2b is a similar spreadsheet from MODULUS for AFC. Equations for AFC are after Reagan et al. (1987). See Knoper (1990) for explanation of program and terms.

Table G.2a

	Non-Modal Equilibrium (Batch) PM Comment:				
	Givn Co	Calc Cl	Calc Cs	Bulk D	Bulk P
Na	15580	15507.	14691.4	0.9474	0.809
K	21584	43756.	17316.4	0.39575	0.6749
Rb	67	151.27	33.7117	0.22285	0.2665
Cs	0	NA	NA	0.1799	0.1795
Ca	14294	6712.3	15572.7	2.32	1.635
Sr	275	233.93	344.112	1.471	1.9848
Ba	880	1148.6	1301.76	1.13335	2.224
Th	0	NA	NA	0.065	0.0349
U	0	NA	NA	0.00932	0.00536
La	12	32.022	3.01489	0.09415	0.0647
Ce	0	NA	NA	0.078	0.0524
Nd	0	NA	NA	0.0589	0.0349
Sm	0	NA	NA	0.05979	0.02997
Eu	0	NA	NA	0.62	0.628
Tb	0	NA	NA	0.06818	0.02804
Yb	1.8	4.8101	0.40501	0.0842	0.0333
Lu	0	NA	NA	0.08068	0.02964
Y	45	126.13	9.03153	0.0716	0.0495
Ga	0	NA	NA	0	0
P	393	1310	0	0	0
Nb	18	32.472	10.5406	0.3246	0.2343
Ta	0	NA	NA	0.1706	0.0918
Zr	245	651.33	63.1795	0.097	0.0695
Hf	0	NA	NA	0.163	0.1345
Sc	54	51.692	46.2337	0.8944	0.4992
Ti	6594	10125.	4110.80	0.406	0.1825
V	187	60.841	210.846	3.4655	2.3065
Cr	83	7.3807	88.5362	11.9955	3.50031
Cu	0	NA	NA	1.345	0.9
Zn	0	NA	NA	1.345	0.9
Pb	0	NA	NA	0.577	1.064
Mg	0	NA	NA	2.3875	0.0125
Mn	0	NA	NA	0.96	0.02
Fe	0	NA	NA	0.42	0.07
Co	32	42.078	20.6426	0.49057	0.10031
Ni	72	49.983	58.5091	1.17057	0.10031

(NA = "not available", ERR = "error")

Intmd Partition Coefficients		
Mineral	Melt Mode	Source Mode
oli 1	0.0000	0.0000
opx 1	0.0000	0.0500
cpx 1	0.0000	0.0400
plg 1	0.3100	0.5700
amp	0.0000	0.0000
bio	0.0400	0.0500
ksp	0.3400	0.0800
gar	0.0000	0.0000
qtz	0.3000	0.1800
	0.0000	0.0000
crd	0.0000	0.0000
mgt 1	0.0100	0.0300
ilm 1	0.0000	0.0000
zir 1,3	0.0000	0.0000
aln	0.0000	0.0000
apa	0.0000	0.0000
sph	0.0000	0.0000
rut 1,2,4	0.0000	0.0000
	0.0000	0.0000
	0.0000	0.0000
	0.0000	0.0000
Total	1.0000	1.0000

System T-P-X	
1	T = 0
2	P = 0
3	M = 0
4	FM = 0
5	MgO = 0

M. F. Liquid
F = 0.300

M. F. Xtals
(1-F)= 0.700

0.23529
ksp

Table G.2b

Open-System AFC (DePaolo)
Comment:

	Givn Co	Calc Cl	Z	Bulk D	Givn Ci	Givn Ca
Na	0	NA	-0.1117	0.945	0	0
K	0	NA	0.32905	0.5703	0	0
Rb	0	NA	0.68141	0.2708	0	0
Cs	0	NA	0.66529	0.2845	0	0
Ca	0	NA	-2.3058	2.81	0	0
Sr	235	152.31	-2.1552	2.682	0	225
Ba	1150	1064.5	-0.4894	1.266	0	900
Th	0	NA	0.61494	0.3273	0	0
U	0	NA	0.9908	0.00782	0	0
La	28.7	33.339	0.47176	0.449	0	35
Ce	68.5	77.397	0.388	0.5202	0	65.7
Nd	35.9	39.096	0.21741	0.6652	0	35
Sm	6.5	7.0640	0.23905	0.6468	0	5.14
Eu	1.43	1.3336	-0.4723	1.2515	0	1.25
Tb	0.99	1.0586	0.14178	0.72948	0	0.92
Yb	3.55	4.0508	0.382	0.5253	0	4.5
Lu	0.603	0.6873	0.44296	0.47348	0	0.525
Y	0	NA	0.42588	0.488	0	0
Ga	0	NA	1	0	0	0
P	0	NA	0.29411	0.6	0	0
Nb	0	NA	-0.0457	0.8889	0	0
Ta	0	NA	0.13741	0.7332	0	0
Zr	0	NA	0.51270	0.4142	0	0
Hf	0	NA	0.51929	0.4086	0	0
Sc	0	NA	-1.0792	1.7674	0	0
Ti	0	NA	0.31105	0.5856	0	0
V	0	NA	-5.5958	5.6065	0	0
Cr	0	NA	-1.6287	2.2344	0	0
Cu	0	NA	-1.3529	2	0	0
Zn	0	NA	-1.6352	2.24	0	0
Pb	0	NA	0.28	0.612	0	0
Mg	0	NA	-2.0341	2.579	0	0
Mn	0	NA	-0.3141	1.117	0	0
Fe	0	NA	-6.1352	6.065	0	0
Co	0	NA	-3.1805	3.5535	0	0
Ni	0	NA	-3.11	3.4935	0	0

(NA = "not available", ERR = "error")

Felsc Partition Coefficients

Crystallizing Mineral	Mode
	0.0000
opx	0.0000
cpx	0.0000
plg	0.5700
amp	0.0000
bio	0.1000
ksp	0.0800
gar	0.0000
qtz	0.2224
	0.0000
crd	0.0000
mgt	0.0200
ilm	0.0000
zir 1,3	0.0010
aln	0.0001
apa	0.0060
sph	0.0005
rut 1,2,4	0.0000
	0.0000
	0.0000
	0.0000
Total	1.0000

System T-P-X

1	T =	0
2	P =	0
3	M =	0
4	FM =	0
5	MgO =	0

M. F. Liquid
F = 0.800

M. F. Xtals
(1-F)= 0.200

X = -0.176
Y = 0.000

Rate Ratios

Asm/Xtl=	0.150
Ext/Xtl=	0.000
Int/Xtl=	0.000

Appendix H
Chemistry of Granulites and Paragneisses
used in modelling

Table H.1 Chemistry of Post-Archean Felsic Granulites and their respective references. Refer to Fig. 26 for number of corresponding reference. All elemental concentrations are given in ppm.

	Ba	Sr	La	Yb
1. Maccarrone et al., (1983), fine-grained granulites.	702	199	---	---
2. Maccarrone et al., (1983), gneissic Al-granoblastites.	715	200	---	---
3. Fettes and Mendum, (1987),	603	234	---	---
4. Rudnick and Taylor, (1987), McBride, Aust.	743	213	24	5.5
5. Condie, (1990), unpublished compilation of Post-Archean felsic granulites.	---	---	16	2.5

Table H.2 Chemistry of Paragneisses used as assimilant, A, in Figs. 26 and 27. Data from Lanzirotti, 1988. All elemental concentrations are given in ppm.

	Ba	Sr	La	Yb
x (n=10)	882	250	31	4.5

Appendix I
Recommendations for further study

Radiometric dates for supracrustal rocks in the northern Wet Mountains is particularly lacking. A larger data base would more accurately constrain the different thermal and deformational events that pre- and postdate the the granitoid intrusions.

Geobarometry and geothermometry will be useful in unravelling the spatial, temporal, and chemical evolution of the 1.7 Ga group for all south-central Colorado.

O-isotope study to strengthen the argument for assimilation of metasedimentary and metavolcanic rocks.

References

Allegre, C.J. and Minster, J.F., 1978, Quantitative models of trace element behavior in magmatic processes. EPSL, vol. 38, p. 1-25.

Anderson, J.L, 1983, Proterozoic anorogenic granite plutonism of North America. GSA Memoir 161, p. 133-154.

Anderson, J.L., and Cullers, R.L., 1978, Geochemistry and evolution of the Wolf River batholith, a late Precambrian rapakivi massif in North Wisconsin, U.S.A.: Precambrian Research, v.7, p. 287-324.

Barker, F., (ed), **Trondhjemites, Dacites, and Metamorphic Rocks**, Dordrecht: D. Reidel, 1979.

Bickford, M.E., 1986, Geochronology of volcanic and plutonic rocks in the Gunnison, Salida, and Wet Mountains areas, central Colorado. *In*: Van Schmus, W.R. (ed), **International field conference on Proterozoic geology and geochemistry:** IGCP Project 215 and 217, p. 17-26.

Bickford, M.E., 1988, The accretion of Proterozoic crust in Colorado: Igneous, sedimentary, deformational, and metamorphic history. *In*: Ernst, W.G., (ed.), **Metamorphism and Crustal Evolution of the Western U.S.**: Prentice-Hall, New Jersey, p. 411-430.

Bickford, M.E., Cullers, R.L., Shuster, R.D., Premo, W.R., and Van Schmus, W.R., 1989a, U-Pb zircon geochronology of Proterozoic and Cambrian plutons in the Wet Mountains and southern Front Range, Colorado. *In*: Grambling, J.A., and Tewksbury, B.J. (eds), **Proterozoic geology of the southern Rocky Mountains**: GSA Special Paper 235, p. 49-64.

Bickford M.E., Shuster, R.D. and Boardman, S.J., 1989b, U-Pb geochronology of the Proterozoic volcano-plutonic terrane in the Gunnison and Salida areas, Colorado. *In*: Grambling, J.A., and Tewksbury, B.J. (eds), **Proterozoic geology of the southern Rocky Mountains**: GSA Special Paper 235, p. 33-47.

Blumenfeld, Phlippe, and Bouchez, Jean-Luc, 1988, Shear criteria in granite and migmatite deformation inthe magmatic and solid states. Jour. of Structural Geology, vol. 10, p. 361-372.

Bowen, N.L., and Tuttle, O.F., 1950, The system $NaAlSi_3O_3$-$KAlSi_3O_8$-H_2O. Jour. of Geol., vol. 58, p. 489-511.

Boyer, R.E., 1962, Petrology and structure of the southern Wet Mountains, Colorado. Geol. Soc. Am. Bull., vol. 73, p. 1074-1069.

Brock, M.R., and Singewald, Q.D., 1968, Geologic map of the Mount Tyndal quadrangle, Custer County, Colorado; U.S. Geological Survey Geologic Map GQ-596, scale 1:24000.

Brown, G.C., 1982, Calc-alkaline intrusive rocks: their diversity, evolution, and relation to volcanic arcs. *In*: Thorpe, R.S. (ed.). **Orogenic Andesites and Related Rocks**: pp. 437-462. Wiley, London.

Brown, G.C., Thorpe, R.S., and Webb, P.C., 1984, The geochemical characteristics of granitoids in contrasting arcs and comments on magma sources. J. Geol. Soc. London, vol. 141, p. 413-426.

Bryan, W.B., Finger, L.W. and Chayes, F., 1969, Estimating proportions in petrographic mixing equations by least-squares approximation. Science, vol. 163, p. 926-927.

Chappell, B.W. and White, A.J.R., 1974, Two contrasting granite types. Pacific Geol., vol. 8, p. 173-174.

Christman, R.A., Brock, M.R., Pearson, R.C., and Singewald, Q.D., 1959, Geology of thorium deposits of the Wet Mountains, Colorado--A progress report; U.S. Geological Survey Bulletin 1072-H, p. 491.

Condie, K.C., 1978, Geochemistry of Proterozoic granitic plutons from New Mexico, U.S.A.. Chemical Geology, vol. 21, p. 131-149.

Condie, K.C., 1982, Plate-tectonic model for Proterozoic continental accretion in the southwestern United States. Geology, vol. 10, p. 37-42.

Condie, K.C., and Budding, A.J., 1979, Geology and geochemistry of Precambrian rocks, central and south-central New Mexico. New Mexico Bureau of Mines and Mineral Resources Memoir 35.

Condie, K.C. and Knoper, M.W., 1986, Geology and origin of early Proterozoic rocks from the Gunnison area, central Colorado. *In*: Van Schmus, W.R. (ed), **International field conference on Proterozoic geology and geochemistry**: p. 3-16.

Cullers, R.L and Graf, J.L., 1984, REE in igneous rocks of the continental crust: Intermediate and silicic rocks-ore petrogenesis. *In*: Henderson, P. (ed), **Rare Earth Element Geochemistry**: p. 275-316.

Cullers R.L. and Wobus, R.A., 1986, Proterozoic framework of the southern Front Range and Wet Mountains, Colorado. *In*: Condie, K.C. and Van Schmus, W.R. (eds), **International field conference-Proterozoic geology and geochemistry, central Colorado**: p. 55-68.

DePaolo, D.J., 1981, Neodymium isotopes in the Colorado Front Range and crust-mantle evolution in the Proterozoic. Nature, v. 71, p. 193-196.

Dostal, J., Dupuy, C., Carron, J.P., Le Guen de Kerneizon, M. and Maury, R.C., 1983, Partition coefficients of trace elements: Applications to volcanic rocks of St. Vincent, West Indies. Geochim. Cosmochim. Acta, vol. 47, p. 525-533.

Drake, M.J. and Weill, D.F., 1975, Partition of Sr, Ba, Ca, Y, Eu^{+2}, Eu^{+3}, and other REE between plagioclase feldspar and magmatic liquid: An experimental study. Geochim. Cosmochim. Acta, vol. 39, p. 689-712.

Epis, C.R., Wobus, R.A., and Scott, G.R., 1979, Geologic map of the Black Mountain quadrangle, Fremont and Park Counties, Colorado. USGS Map I-1195, scale 1:62,500.

Fettes, D.J., and Mendum, J.R., 1987, The evolution of the Lewisian complex in the Outer Hebrides. *In:* Park, R.G., and Tarney, J. (eds), **Evolution of the Lewisian and comparable Precambrian high grade terrains.** Geol. Soc. London Special Paper, 27, p. 27-44.

Frey, F.A., Haskin, M.A., Betz, J., and Haskin, L.A., 1968, Rare earth abundances in some basic rocks. J. Geophys, Res, vol. 73, p. 6085-6098.

Fujimaki, H. and Tatsumoto, M., 1984, Partition coefficients of Hf, Zr, and REE between phenocrysts and groundmass. J. Geophys. Res., vol. 89, p. 662-672.

Govindaraju, K., 1989, Geostandards Newsletter, v. 13.

Gromet, L.P. and Silver, L.T., 1983, Rare earth element distributions among minerals in a granodiorite and their petrogenetic implications. Geochim. Cosmochim. Acta, vol. 47, p. 925-939.

Hamilton, W.B., 1981, Crustal evolution by arc magmatism. Royal Society of London Philosophical Transactions, ser. A, vol. 301, p. 279-291.

Hanson, G.N., 1978, Theapplication of trace elements to the petrogenesis of igneous rocks of granitic composition. EPSL, vol. 38, p. 26-43.

Harper, W.F., 1976, Structure of Precambrian metamorphic rocks west of the Ilse fault zone, Hardscrabble Mountain quadrangle, Colorado. Unpub. M.S. thesis, Louisiana State University, p. 101.

Harris, N.B.W., Pearce, J.A., and Tindle, A.G., 1986, Geochemical characteristic of collision-zone magmatism. *In* Coward, M.P. and Ries, A.C. (eds), **Collision Tectonics:** Geological Society Special Pub. No. 19, p. 67-81.

Hawkesworth, C.J., 1979, $^{143}Nd/^{144}Nd$, $^{87}Sr/^{86}Sr$, and trace element characteristics of magmas along destructive plate margins. *In* Atherton, M.P. and Tarney, J. (eds.) **Origin of Granite Batholiths: Geochemical Evidence:** p. 549-571.

Hedge, C.E., Houston, R.S., Tweto, O.L., Peterman, Z.E., Harrison, J.E., and Reid, R.R., 1986, The Precambrian of the Rocky Mountain Region; U.S. Geological Survey Prof. Pap. 1241-D.

Hildreth, W., 1981, Gradients in silicic magma chambers: implications for lithospheric magmatism. J. Geophys. Res., v. 86, p. 10153-10192.

Hoffman, P.F., 1988, United plates of America, the birth of a craton: Early Proterozoic assembly and growth of Laurentia: Annual Reviews of Earth and Planetary Sciences, v. 16, p. 543-603.

Huang, W., and Wyllie, P.J., 1975, Melting reactions in the system $NaAlSi_3O_8$-$KAlSi_3O_8$-SiO_2 to 35 kilobars, dry and with excess water. Jour. of Geol. vol. 83, p. 737-748.

Hyndman, D.W., 1985, **Petrology of Igneous and Metamorphic Rocks:** McGraw-Hill, New York, p. 466.

Irving, A.J., and Frey, F., 1984, Trace element abundances in megacrysts and their host basalts: Constraints on partition coefficients and megacryst genesis. Geochim. Cosmochim. Acta, vol. 48, p. 1201-1221.

Knoper, M.W., 1990a, Geochemistry of early Proerozoic supracrustal rocks, west-central Colorado: evidence for their petrogenesis and tectonic setting. PhD dissert., New Mex. Institute Mining and Tech., Socorro, NM.

Knoper, M.W., 1990b, MODULUS ver. 2.21--Petrogenetic computer program using LOTUS 1-2-3 (submitted for publication).

Knoper, M.W., 1990c, MIXFRA--A least-squares mixing computer program, (unpublished).

Knoper, M.W. and Condie, K.C., 1988, Geochemistry and Petrogenesis of Early Proterozoic Amphibolites, West-Central Colorado, USA. Chemical Geology, vol. 67, p. 209-225.

Lanzirotti, A., 1988, Geology and geochemistry of a Proterozoic supracrustal and intrusive sequence in the central Wet Mountains, Colorado. NMIMT unpublished M.S. thesis.

Lindstrom, D.J., and Korotev, R.L., 1982, TEABAGS: Computer programs for instrumental neutron activation analysis. J. Radioanal. Chem., vol. 70, p. 439-458.

Maaloe, S. and Wyllie, P.J., 1975, Water content of a granite magma deduced from the sequence of crystallization determined experimentally with water-undersaturated conditions. Contrib. Mineral. Petrol., vol. 52, p. 175-191.

Maccarrone, E., Paglionico, A., Piccarreta, G., and Rottura, A., 1983, Granulite-amphibolite facies metasediments from Calabria, Southern Italy: their protoliths and the processes controlling their chemistry. Lithos, vol. 16, p. 95-111.

Maniar, P.D., and Piccoli, P.M., 1989, Tectonic discrimination of granitoids. Geol. Soc. Am. Bull., v. 101, p. 635-643.

Miller C.F. and Mittlefehldt, D.W., 1982, Depletion of light rare-earth elements in felsic magmas. Geology, vol. 10, p. 129-133.

Nash, W.P. and Crecraft, H.R., 1985, Partition coefficients for trace elements in silicic magmas. Geochim. Cosmochim. Acta, vol. 49, p. 2309-2322.

Nelson, B.K., and DePaolo,D.J., 1985, 1700-Myr greenstone volcanic successions in southwestern North America and isotopic evolution of the Proterozoic mantle. Nature, v. 312, p. 143-146.

Noblett, J.B., Cullers, R.L., Bickford, M.E., 1987, Proterozoic Crystalline rocks in the Wet Mountains and Vicinity Central Colorado: In New Mexico Geological Society Guidebook, 38th Field Conference, p. 73-82.

Norrish, K., and Chappel, B.W., 1977, An accurate X-ray fluorescence spectrographic method for the analysis of a wide range of geologic samples. Geochim. Cosmochim. Acta, vol. 33, p. 67-76.

Norrish, K., and Hutton, J.T., 1969, X-ray fluorescence spectrometry: *In* Zussman, J. (ed.) **Physical Methods in Determinative Mineralogy, London**: Academic Press.

Paterson, S.R. and Tobisch, O.T., 1988, Using pluton ages to date regional deformation: Problems with commonly used criteria. Geology, vol. 16, p. 1108-1111.

Paterson, S.R., Vernon, R.H., and Tobisch, O.T., 1989, A review of criteria for the identification of magmatic and tectonic foliations in granitoids. Jour. of Structural Geology, vol. 11, p. 349-363.

Pearce, J.A., 1975, Basalt geochemistry used to investigate past tectonic environments on Cyprus. Tectonophysics, vol. 25, p. 41-67.

Pearce, J.A., 1982, Trace element characteristics of lavas from destructive plate boundaries. *In* Thorpe. R.S. (ed.), **Andesites**, New York: John Wiley & Sons, p. 525-548.

Pearce, J.A., Harris, N.B.W., and Tindle, A.G, 1984, Trace element discrimination diagrams for the tectonic interpretation of granitic rocks. Journal of Petrology, vol. 25, p. 956-983.

Pitcher, W.S., 1983a, Granite type and tectonic environment. *In*: Hsu, K. (ed.), **Mountain Building Process**: p. 19-40. Academic Press, London.

Pitcher, W.S., 1983b, Granite: typology, geological, environmental and melting relationships. *In*: Atherton and Gribble (ed.), **Migmatites, melting and metamorphism**, p. 277-287. Shiva Publishing Limited, Cheshire, United Kingdom.

von Platen, H., 1965, Kristallisation granitischer Schmelzen. Contrib. Mineral. Petrol., vol. 11, p. 334-381.

Reagan M.K., Gill, J.B., Malavzssi, E., and Garcia, M.O., 1987, Changes in magma composition at Arenal volcano, Costa Rica, 1968-1985: Real-time monitoring of open-system differentiation. Bull. of Volc., vol. 49, p. 415-434.

Reed, J.C., Bickford, M.E., Premo, W.R., Aleinikoff, J.N., and Pallister, J.S., 1987, Evolution of the early Proterozoic Colorado province: Constraints from U-Pb geochronology. Geology, vol. 15, p. 861-865.

Reuss, R.L., 1974, Precambrian quartzite-schist sequence in Wilson Park, Fremont County, Colorado. Mountain Geologist, vol. 11, p. 45-58.

Rudnick, R.L., and Taylor, S.R., 1987, The composition and petrogenesis of the lower crust: A xenolith study. J. Geophys. Res., vol. 92, p. 13981-14005.

Scott, G.R., 1977, Reconnaissance geologic map of the Canon City quadrangle, Fremont County, Colorado. USGS Map MF-892, scale 1:24,000.

Scott, G.R., Taylor, R.B., Epis, R.C. and Wobus, R.A., 1978, Geologic map of the Pueblo 1 X 2 quadrangle, south-central Colorado: USGS, Map I-1022, scale 1:250,000.

Sekine, T., and Wyllie, P.J., 1982, Phase relationships in the system KAlSiO4-Mg2SiO4-SiO2-H2O as a model for hybridization between hydrous siliceous melts and peridotite. Contrib. Mineral. Petrol., v. 79, p. 368-374.

Shand, S.J., 1951, **Eruptive Rocks**, Murby and Co., London.

Smith, D.A., 1977, **Colorado mining: A photographic history;** p. 101.

Stacey, J.S., and Hedlund, D.C., 1983, Lead-isotopic compositions of diverse igneous rocks and ore deposits from southwestern New Mexico and their implications for early Proterozoic crustal evolution in the western United States. Geol. Soc. Am. Bull., vol. 94, p. 43-57.

Sun, S.S., 1980, Lead isotopic study of young volcanic rocks from mid-ocean ridges, ocean islands and island arcs. Phil Trans. R. Soc. Lond., vol. A297, p. 409-445.

Taylor, R.B., 1974, Neogene tectonism in south-central Colorado, in Curtis, B.F., ed., Cenozoic history of the southern Rocky Mountains. GSA Memoir 144, p. 211-226.

Taylor, R.B., Scott, G.R., Wobus, R.A., and Epis, R.C., 1975a, Reconnaissance Geologic Map of the Royal Gorge Quadrangle, Fremont and Custer Counties, Colorado; U.S. Geological Survey Miscellaneous Investigation Map I-869.

Taylor, R.B., Scott, G.R., Wobus, R.A., and Epis, R.C., 1975b, Reconnaissance Geologic Map of the Cotopaxi 15-minute Quadrangle, Fremont and Custer Counties, Colorado; U.S. Geological Survey Miscellaneous Investigation Map I-900.

Taylor, R.B., Scott, G.R., and Wobus, R.A., 1975c, Reconnaissance Geologic Map of the Howard Quadrangle Central Colorado; U.S. Geological Survey Miscellaneous Investigation Map I-892.

Taylor, S.R., and McClennan, S.M., 1985, **The Continental Crust: Its Composition and Evolution.** Blackwell, Oxford.

Tuttle, O.F., and Bowen, N.L., 1958, Origin of granite in the light of experimental studies in the system $NaAlSi_3O_8$-$KAlSi_3O_8$-SiO_2-H_2O. GSA Memoir 74.

Tweto, O., 1975, Laramide (late Cretaceous-Early Tertiary) Orogeny in the Southern Rocky Mountains, in Curtis, B.F., ed., Cenozoic history of the Southern Rocky Mountains. GSA Memoir 144, p. 1-44.

Tweto, O., 1987, Rock units of the Precambrian basement in Colorado. U.S. Geological Survey Prof. Paper 1321-A, p. 1-59.

Van Schmus, W.R., and Bickford, M.E., 1981, Proterozoic chronology and evolution of the midcontinent region, North America. *In*: Kroner, A., (ed.), **Precambrian plate tectonics**: Amsterdam, Elsevier, p. 261-293.

Watson, E.B., 1980, Some experimentally determined zircon/liquid partition coefficients for the REE. Geochim. Cosmochim. Acta, vol. 44, p. 895-897.

Weaver, C.E. and Tarney, 1984, Empirical approach to estimating the composition of the continental crust. Nature vol. 310, p. 575-677.

White, A.J.R., 1979, Sources of granitic magmas. GSA Abst. Prog., vol. 11, p. 539.

White, E.W. and Johnson, G.G., 1970, X-Ray absorption wavelengths and two-theta tables. American Society for testing and material-Data series DS 37A, 2nd ed., p. 293.

Whitney, J.A., 1975, The effects of pressure, temperature and X_{H2O} on phase assemblage in four synthetic rock compositions. Joun. of Geol., vol. 83, p. 1-31.

Whitney, J.A., 1988, The origin of granite: The role and source of water in the evolution of granitic magmas. Geol. Soc. Am. Bull. vol. 100, p. 1886-1897.

Wickham, S.M., 1987, The segragation and emplacement of granitic magmas. Jour. Geol. Soc. London, 144: 281-297.

Winchester, J.A., and Floyd, P.A., 1976, Geochemical magma type discrimination application to altered and metamorphosed basic igneous rocks. EPSL, vol. 28, p. 459-469.

Winkler, H.G.F., 1979, **Petrogenesis of Metamorphic Rocks**, 5th ed., New York: Springer-Verlag, p.283-339.

Wobus, R.A., Epis, R.C.,and Scott, G.R., 1976, Reconnaissance Geologic Map of the Cripple Creek-Pikes Peak Area, Teller, Fremont, and El Paso Counties, Colorado; U.S. Geological Survey Miscellaneous Field Studies Map MF-805.

Wobus, R.A., Epis, R.C.,and Scott, G.R., 1979, Geologic Map of the Cover Mountain Quadrangle, Fremont, Park and Teller Counties Colorado; U.S.Geological Survey Geologic Quadrangle Map I-1179.

Wobus, R.A., Chase, R.B., Scott, G.R., and Taylor, R.B., 1985a, Reconnaissance Geologic Map of the Cooper Mountain Quadrangle, Fremont County, Colorado; U.S. Geological Survey Miscellaneous Field Studies Map MF-1762.

Wobus, R.A., Chase, R.B., Scott, G.R., and Taylor, R.B., 1985b, Reconnaissance Geologic Map of the Phantom Canyon Quadrangle, Fremont County, Colorado; U.S. Geological Survey Miscellaneous Field Studies Map MF-1764.

Wood, D.A., 1979, A variably veined sub-oceanic upper mantle--Genetic significance for mid-ocean ridge basalts from geochemical evidence. Geology, vol. 7, p. 499-503.

Wyllie, P.J., 1977, Crustal anatexis: an experimantal review. Techtonphysics, v. 43, p. 41-71.

This thesis is accepted on behalf of the faculty of the Institute by the following committee:

Adviser

Aug 28th, 1990
Date